UC San Diego
UC San Diego Electronic Theses and Dissertations

Title
Cardiac Interstitial Cell Fate in Embryonic and Neonatal Microenvironments

Permalink
https://escholarship.org/uc/item/52b4b75v

Author
Wang, Bingyan Jessica

Publication Date
2019

Supplemental Material
https://escholarship.org/uc/item/52b4b75v#supplemental

Peer reviewed|Thesis/dissertation

UNIVERSITY OF CALIFORNIA SAN DIEGO

SAN DIEGO STATE UNIVERSITY

Cardiac Interstitial Cell Fate in Embryonic and Neonatal Microenvironments

A dissertation submitted in partial satisfaction of the
requirements for the degree

Doctor of Philosophy

in

Biology

by

Bingyan Jessica Wang

Committee in charge:

       University of California San Diego

           Professor Åsa Gustafsson
           Professor Deborah Yelon

       San Diego State University

           Professor Mark A. Sussman, Chair
           Professor Sanford I. Bernstein
           Professor Robert W. Zeller

2019

The Dissertation of Bingyan Jessica Wang is approved, and it is acceptable in quality and form for publication on microfilm and electronically:

_____

_____

_____

_____

Chair

University of California San Diego

San Diego State University

2019

DEDICATION

I would like to dedicate this dissertation to my late Grandpa, Professor Ma Zongxiang, who was the most respectful scholar and role model in my life. You taught me how to solve problems, and more importantly, how to ask questions. You never stopped believing in me in my pursuit of higher education. You are the reason for who I am today.

TABLE OF CONTENTS

LIST OF ABBREVIATIONS

AM   Amniochorionic membrane

AzG   Azami-Green

BF   Bright Field

c-Kit   Tyrosine-protein kinase Kit or CD117

cCIC   c-Kit$^+$ cardiac interstitial cell

CIC   Cardiac Interstitial Cell

CICs^{TCR} c-Kit$^+$ CICs isolated from Tg:TCR heart

CPC   Cardiac Progenitor Cell

cTnI   Cardiac Troponin I

cTnT   Cardiac Troponin T

dpi   Days post-injection

E   Embryonic day#

EB   Embryoid body

ECM   Extracellular Matrix

EMT   Epithelial-mesenchymal transition

ESC   Embryonic Stem Cell

Ex/Em   Excitation/Emission

FACS   Fluorescence activated cell sorting

FUCCI   Fluorescence Ubiquitination-based Cell Cycle Indicators

GFP   Green fluorescent protein

HNA   Human Nuclear Antigen

hpi	Hours post-injection
ICM	Inner cell mass
IPC	Internal positive control
IUT	*in utero* transplantation
IVC	Inferior vena cava
LV	Left Ventricle
LVAD	Left Ventricular assist device
MI	Myocardial Infarction
mKO	monomeric Kusabira Orange
nTg	Non-transgenic
P	Postnatal day#
pHH3	Phosphorylated Histone H3
SM22α	Smooth muscle 22 α
SMA	Smooth muscle actin
SMC	Smooth Muscle Cell
SMMHC	Smooth muscle myosin heavy chain (also known as MYH11)
TCR	Tri-color Reporter
tdTmt	Tandem Tomato, tdTomato
TE	Trophectoderm
TenC	Tenascin C
Tg	Transgenic
TPM	Tropomyosin

TUNEL   Terminal deoxynucleotidyl transferase dUTP nick end labeling

Vim   Vimentin

vWF   von Willebrand Factor

αMHC   Alpha Myosin Heavy Chain

LIST OF FIGURES

LIST OF TABLES

LIST OF SUPPLEMENTAL VIDEOS

ACKNOWLEDGEMENTS

First and foremost, I would like to express my sincere gratitude to my mentor, Dr. Mark A. Sussman, for his continues support and guidance. The complete trust and freedom you gave me through the years to do "whatever I want" allowed me to be creative and rigorous. I am grateful for the opportunity you provided for me to grow as a scientist.

I would like to thank my committee members, Dr. Sanford Bernstein, Dr. Robert Zeller, Dr. Åsa Gustafsson, and Dr. Deborah Yelon. Your guidance, invaluable input, and expertise is greatly appreciated. I am honored to have you as part of my committee.

I would like to acknowledge the Rees-Stealy Research Foundation, American Heart Association, and Inamori Foundation for financial support of my research. I would also like to extend my thanks to SDSU Biology Department and Joint-Doctoral Program, as well as Genomics Core and Animal Facility.

To all past and present Sussman lab personnel I have encountered through the years, thank you for being part of Sussmaniacs and making our workplace a joyful environment. I enjoyed working with you and I learned so much from all of you. Special thanks to Dr. Roberto Alvarez Jr., for his expertise in embryo manipulation and for paving the groundwork for this dissertation. Dr. Natalie Gude, thank you for being the wonder woman of the lab, you will always have my admiration of your wisdom and expertise. Megan Monsanto and Natalia Navarro, thank you for being my mental support and for your belief in me, it is my true luck to have both of your accompany along this journey. To my undergraduate interns Alvin Muliono and Sharon Sengphanith, your presence and

endless curiosity have been the day to day motivation for my work. I am so lucky to have known all of you.

And finally, I would like to thank Timothy Engle, for always being there for me. You've witnessed all my tears in this journey and you could always find a way to cheer me up. Thank you for being in my life.

Chapter 1, in part, is taken in part as it appears in *Circulation Research*, 2018. Mechanisms of Cardiac Repair and Regeneration. Broughton KM*, Wang BJ*, Firouzi F, Khalafalla F, Dimmeler S, Fernandez-Aviles F, Sussman MA. The dissertation author was a co-primary author and investigator of this review article [1].

Chapter 2, in full, is has been submitted for publication of the material as it may appear in publication. Adaptation Within Embryonic and Neonatal Heart Environment Reveals Alternative Fates for Adult c-Kit[+] Cardiac Interstitial Cells. Bingyan J. Wang, Roberto Alvarez Jr., Alvin Muliono, Sharon Sengphanith, Megan M. Monsanto, Joi Weeks, Roberto Sacripanti, and Mark A. Sussman. The dissertation author was the primary author and investigator of this manuscript [2].

Chapter 3 is presented in this dissertation as an alternative model and primary cell source for cardiac interstitial cell fate study of Chapter 2. I would like to acknowledge Dr. Roberto Alvarez Jr. for his extensive work in designing and establishing the Tg:TCR mouse line. Chapter 3, in full, will be prepared for submission. (Tentative title) Transgenic Triple Color Reporter Mouse as a Valuable Lineage Tracing and Cell Fate Model for Cardiomyocytes, Endothelial Cells, and Smooth Muscle Cells. Bingyan J. Wang, Roberto Alvarez Jr., Sharon Sengphanith, Alvin Muliono, David Ebeid, Carolina Esquer, and Mark

A. Sussman. The dissertation author is the primary author and investigator of this manuscript as of December 2019.

Education

2019	Doctor of Philosophy in Biology, University of California San Diego and San Diego State University
2013-2015	Teaching Assistant, San Diego State University
2011-2013	Research Assistant, California State University, Los Angeles
2011	Master of Science, California State University, Los Angeles
2004	Master of Science, Delft University of Technology
2002	Bachelor of Science, Beijing Technology and Business University

Publications

Wang BJ, Alvarez R, Muliono A, Sengphanith S, Monsanto MM, Weeks J, Sacripanti R, Sussman MA. Adaptation Within Embryonic and Neonatal Heart Environment Reveals Alternative Fates for Adult c-Kit+ Cardiac Interstitial Cells. bioRxiv. 2019:758516.

Monsanto MM, **Wang BJ**, Ehrenberg ZR, Echeagaray O, White KS, Alvarez R, Fisher K, Sengphanith S, Muliono A, Gude NA, Sussman MA. Enhancing Myocardial Repair with CardioClusters. bioRxiv. 2019:759845.

Lampert MA, Orogo AM, Najor RH, Hammerling BC, Leon LJ, **Wang BJ**, Kim T, Sussman MA, Gustafsson ÅB. BNIP3L/NIX and FUNDC1-mediated mitophagy is required for mitochondrial network remodeling during cardiac progenitor cell differentiation. Autophagy. 2019 Jul;15(7):1182-1198. doi: 10.1080/15548627.2019.1580095. Epub 2019 Feb 22. PubMed PMID: 30741592; PubMed Central PMCID: PMC6613840.

Broughton KM, Khieu T, Nguyen N, Rosa M, Mohsin S, Quijada P, **Wang BJ**, Echeagaray OH, Kubli DA, Kim T, Firouzi F, Monsanto MM, Gude NA, Adamson RM, Dembitsky WP, Davis ME, Sussman MA. Cardiac interstitial tetraploid cells can escape replicative senescence in rodents but not large mammals. Commun Biol. 2019;2:205. doi: 10.1038/s42003-019-0453-z. eCollection 2019. PubMed PMID: 31231694; PubMed Central PMCID: PMC6565746.

Korski KI, Kubli DA, **Wang BJ**, Khalafalla FG, Monsanto MM, Firouzi F, Echeagaray OH, Kim T, Adamson RM, Dembitsky WP, Gustafsson ÅB, Sussman MA. Hypoxia Prevents Mitochondrial Dysfunction and Senescence in Human c-Kit+ Cardiac Progenitor Cells. Stem Cells. 2019 Apr;37(4):555-567. doi: 10.1002/stem.2970. Epub 2019 Jan 30. PubMed PMID: 30629785; PubMed Central PMCID: PMC6588544.

Chandran S, Suggs JA, **Wang BJ**, Han A, Bhide S, Cryderman DE, Moore SA, Bernstein SI, Wallrath LL, Melkani GC. Suppression of myopathic lamin mutations by muscle-specific activation of AMPK and modulation of downstream signaling. Hum Mol Genet.

2019 Feb 1;28(3):351-371. doi: 10.1093/hmg/ddy332. PubMed PMID: 30239736; PubMed Central PMCID: PMC6337691.

Alvarez R Jr*, **Wang BJ***, Quijada PJ, Avitabile D, Ho T, Shaitrit M, Chavarria M, Firouzi F, Ebeid D, Monsanto MM, Navarrete N, Moshref M, Siddiqi S, Broughton KM, Bailey BA, Gude NA, Sussman MA. Cardiomyocyte cell cycle dynamics and proliferation revealed through cardiac-specific transgenesis of fluorescent ubiquitinated cell cycle indicator (FUCCI). J Mol Cell Cardiol. 2019 Feb;127:154-164. doi: 10.1016/j.yjmcc.2018.12.007. Epub 2018 Dec 18. PubMed PMID: 30571978; PubMed Central PMCID: PMC6588545.

Kim T, Echeagaray OH, **Wang BJ**, Casillas A, Broughton KM, Kim BH, Sussman MA. In situ transcriptome characteristics are lost following culture adaptation of adult cardiac stem cells. Sci Rep. 2018 Aug 13;8(1):12060. doi: 10.1038/s41598-018-30551-1. PubMed PMID: 30104715; PubMed Central PMCID: PMC6089936.

Gude NA, Firouzi F, Broughton KM, Ilves K, Nguyen KP, Payne CR, Sacchi V, Monsanto MM, Casillas AR, Khalafalla FG, **Wang BJ**, Ebeid DE, Alvarez R, Dembitsky WP, Bailey BA, van Berlo J, Sussman MA. Cardiac c-Kit Biology Revealed by Inducible Transgenesis. Circ Res. 2018 Jun 22;123(1):57-72. doi: 10.1161/CIRCRESAHA.117.311828. Epub 2018 Apr 10. PubMed PMID: 29636378; PubMed Central PMCID: PMC6192707.

Broughton KM*, **Wang BJ***, Firouzi F, Khalafalla F, Dimmeler S, Fernandez-Aviles F, Sussman MA. Mechanisms of Cardiac Repair and Regeneration. Circ Res. 2018 Apr 13;122(8):1151-1163. doi: 10.1161/CIRCRESAHA.117.312586. Review. PubMed PMID: 29650632; PubMed Central PMCID: PMC6191043.

Sacchi V, **Wang BJ**, Kubli D, Martinez AS, Jin JK, Alvarez R Jr, Hariharan N, Glembotski C, Uchida T, Malter JS, Yang Y, Gross P, Zhang C, Houser S, Rota M, Sussman MA. Peptidyl-Prolyl Isomerase 1 Regulates Ca2+ Handling by Modulating Sarco(Endo)Plasmic Reticulum Calcium ATPase and Na2+/Ca2+ Exchanger 1 Protein Levels and Function. J Am Heart Assoc. 2017 Oct 10;6(10). doi: 10.1161/JAHA.117.006837. PubMed PMID: 29018025; PubMed Central PMCID: PMC5721875.

Monsanto MM, White KS, Kim T, **Wang BJ**, Fisher K, Ilves K, Khalafalla FG, Casillas A, Broughton K, Mohsin S, Dembitsky WP, Sussman MA. Concurrent Isolation of 3 Distinct Cardiac Stem Cell Populations From a Single Human Heart Biopsy. Circ Res. 2017 Jul 7;121(2):113-124. doi: 10.1161/CIRCRESAHA.116.310494. Epub 2017 Apr 26. PubMed PMID: 28446444; PubMed Central PMCID: PMC5555597.

Monsanto MM*, **Wang BJ***, Sussman MA. Synthetic MSC? Nothing Beats the Real Thing. Circ Res. 2017 May 26;120(11):1694-1695. doi: 10.1161/CIRCRESAHA.117.310986. PubMed PMID: 28546347; PubMed Central PMCID: PMC5555396.

Liu N, **Wang BJ**, Broughton KM, Alvarez R, Siddiqi S, Loaiza R, Nguyen N, Quijada P, Gude N, Sussman MA. PIM1-minicircle as a therapeutic treatment for myocardial

infarction. PLoS One. 2017;12(3):e0173963. doi: 10.1371/journal.pone.0173963. eCollection 2017. PubMed PMID: 28323876; PubMed Central PMCID: PMC5360264.

Alvarado E, Yousefelahiyeh M, Alvarado G, Shang R, Whitman T, Martinez A, Yu Y, Pham A, Bhandari A, **Wang B**, Nissen RM. Wdr68 Mediates Dorsal and Ventral Patterning Events for Craniofacial Development. PLoS One. 2016;11(11):e0166984. doi: 10.1371/journal.pone.0166984. eCollection 2016. PubMed PMID: 27880803; PubMed Central PMCID: PMC5120840.

Quijada P, Hariharan N, Cubillo JD, Bala KM, Emathinger JM, **Wang BJ**, Ormachea L, Bers DM, Sussman MA, Poizat C. Nuclear Calcium/Calmodulin-dependent Protein Kinase II Signaling Enhances Cardiac Progenitor Cell Survival and Cardiac Lineage Commitment. J Biol Chem. 2015 Oct 16;290(42):25411-26. doi: 10.1074/jbc.M115.657775. Epub 2015 Aug 31. PubMed PMID: 26324717; PubMed Central PMCID: PMC4646189.

Wang B, Doan D, Roman Petersen Y, Alvarado E, Alvarado G, Bhandari A, Mohanty A, Mohanty S, Nissen RM. Wdr68 requires nuclear access for craniofacial development. PLoS One. 2013;8(1):e54363. doi: 10.1371/journal.pone.0054363. Epub 2013 Jan 22. PubMed PMID: 23349862; PubMed Central PMCID: PMC3551808.

Honors and Awards

2018-2019   University Graduate Fellowship, San Diego State University
2018-2020   American Heart Association Predoctoral Fellowship
2018   ISHR Early Career Investigator Travel Award, Halifax, Canada
2017-2018   Inamori Fellowship, San Diego State University
2015-2018   Rees-Stealy Research Fellowship, San Diego State University

Scientific Presentations

2018 Cardiac Progenitor Cell Fate in Embryonic and Neonatal Environments. AHA Scientific Sessions. Chicago, IL.
2018 Cardiac Progenitor Cell Fate in Embryonic and Neonatal Environments. ISHR. Halifax, NS, Canada.
2017 Lineage Contribution of Adult c-Kit+ Cardiac Progenitor Cells in Embryonic and Neonatal Development. Abstract for oral presentation. American Heart Association Scientific Sessions. Anaheim, CA..
2017 Lineage Contribution of Adult c-Kit+ Cardiac Progenitor Cells in Embryonic and Neonatal Development. Alternative Muscle Club. La Jolla, CA.
2017 Cardiac Progenitor Cell Lineage Tracing During Embryonic Cardiomyogenesis. Abstract for poster presentation. Basic Cardiovascular Sciences Conference. Portland, OR.
2017 Cardiac Progenitor Cell Lineage Tracing During Embryonic Cardiomyogenesis. Abstract for poster presentation. 36th Annual Meeting of the North America Section, ISHR. New Orleans, LA.

2011   Exploring the Roles of Wdr68 and Dyrk1b in Muscle Differentiation. The 23th Annual CSU Program for Education and Research in Biotechnology. Anaheim, CA.
2010   Exploring the Roles of Dyrk1b and Wdr68 in Development and Differentiation. The 9th International Zebrafish Conference. Madison, WI.

Professional Experience

2013-2019   Doctoral Candidate, San Diego State University
2016-2019   Graduate Assistant, Mark Sussman Laboratory, SDSU
2013-2015   Graduate Teaching Assistant, Cell and Molecular Biology
2012-2013   Lecturer (part-time), Animal Biology, Cal State L.A.
2009-2013   Research Assistant / Lab manager, Robert Nissen Lab, Cal State L.A.
2008-2011   Master's student, Cal State L.A.
2002-2004   Master's student, TU Delft, Netherlands

ABSTRACT OF THE DISSERTATION

Cardiac Interstitial Cell Fate in Embryonic and Neonatal Microenvironments

by

Bingyan Jessica Wang

Doctor of Philosophy in Biology

University of California San Diego, 2019
San Diego State University, 2019

Professor Mark A. Sussman, Chair

Cardiac interstitial cells (CIC) perform essential roles in myocardial biology through preservation of homeostasis as well as response to injury or stress. Studies of murine CIC biology reveal remarkable plasticity in terms of transcriptional reprogramming and ploidy state with important implications for function. Despite over a decade of characterization and *in vivo* utilization of adult c-Kit$^+$ CIC (cCIC), adaptability and functional responses upon delivery to adult mammalian hearts remain poorly understood. Limitations of characterizing cCIC biology following *in vitro* expansion and adoptive transfer into the adult heart were circumvented by delivery of the donated cells into early

cardiogenic environments of embryonic, fetal, and early postnatal developing hearts. These three developmental stages were permissive for retention and persistence, enabling phenotypic evaluation of *in vitro* expanded cCICs after delivery as well as tissue response following introduction to the host environment. Embryonic blastocyst environment prompted cCIC integration into trophectoderm as well as persistence in amniochorionic membrane. Delivery to fetal myocardium yielded cCIC perivascular localization with fibroblast-like phenotype, similar to cCICs introduced to postnatal P3 heart with persistent cell cycle activity for up to 4 weeks. Fibroblast-like phenotype of exogenously transferred cCICs in fetal and postnatal cardiogenic environments is consistent with inability to contribute directly toward cardiogenesis and lack of functional integration with host myocardium. In contrast, cCICs incorporation into extra-embryonic membranes is consistent with fate of polyploid cells in blastocysts. These findings provide insight into cCIC biology, their inherent predisposition toward fibroblast fates in cardiogenic environments, and remarkable participation in extra-embryonic tissue formation.

CHAPTER 1

Current Field of Myocardial Repair and Regeneration

INTRODUCTION

Myocardial repair and regeneration is an important area of research motivated by increasing occurrence and expanding distribution of heart failure and cardiac-related diseases. Desperate unmet need for novel interventional strategies to treat cardiovascular disease prompted the rapid implementation of clinical approaches to promote myocardial regeneration and repair, but outcomes thus far have been modest at best. This Chapter is to provide a review on how the field has matured from an academic perspective and to provide an overview of the fundamentals that shape perceptions and guide my research directions.

Lower vertebrates

Zebrafish (*Danio rerio*) and other teleost fish are able to regenerate portions of their heart after injury, thus making it a robust and major cardiac regeneration model organism known to date. Zebrafish heart presents a prototypic two-chambered vertebrate heart, with a single atrium and ventricle, which pumps venous blood to ventral aorta leading to gill arches for oxygenation to occur, and from where the blood is distributed to the rest of the body [3]. Adult zebrafish heart can fully regenerate within 2 months after surgical removal of ~20% ventricular myocardium. Immediately following resection surgery, a large clot of erythrocytes form in the wound in order to seal bleeding from the ventricular lumen, and the organ sustains sufficient contractile force to continue to drive circulation. The erythrocyte accumulation that seals the apex matures into a fibrin-rich milieu about 2-4 days postamputation (dpa) that clears erythrocytes [4]. At this initial stage of cardiac repair, undifferentiated progenitor cells localize at the apical edge of existing

myocardium, forming the blastema that undergo differentiation and contribute to cardiomyocytes with increased mitotic capacity [5]. In contrast to fibrosis and scarring response that is seen in mammalian and amphibian hearts after cardiac injury, the zebrafish heart only displays small collagen deposits which later extend into fibrin clot. However, the fibrin clot does not extend to scar tissue during the cardiac repair in zebrafish. Instead, the fibrin clot is gradually replaced by newly formed cardiac myofibers into a contiguous wall of compact muscle establishment at 10-30 myocytes width [5]. BrdU pulse-chase experiments revealed that cardiomyocyte mitoses peak at 14 dpa, and are limited to the most epicardial layer of the ventricular-apical region. Surrounding epicardial tissue rapidly expands into a new epithelial cover for the exposed myocardium and supplies a subpopulation of epicardial cells to undergo an epithelial-to-mesenchymal transition (EMT) to revascularize the myocardial tissue [5]. By 60 dpa, the size and shape of ventricle appear grossly normal as well as the contractile properties of beating hearts. After ventricular resection, zebrafish only appears less active and shows less coordinated swimming during the first week. After 1 week of recovery, the activity and behavior of surgery zebrafish are indistinguishable from sham control animals [4,6].

Different injury approaches to mediate zebrafish cardiac injuries have been described to yield distinct outcomes of myocardial regeneration, highlighting the heterogeneity of regenerative response in different injury models. Cryocauterization (CC), also known as cryoinjury (CI), has been used as an alternative procedure that closely models the pathophysiological process of coronary artery ligation that is used in rodent and larger mammal models. In this model, a liquid nitrogen-cooled copper probe is placed

directly in contact with the ventricle for a few seconds in order to induce approximately 25% of ventricular damage [7]. In contrast to ventricular resection model, cryoinjury induces massive cell death and necrosis during the initial weeks following injury. A massive scar is also observed in the injured area, which resembles the process of mammalian ventricular remodeling after acute myocardial infarction (MI). The fibrotic tissue is subsequently degraded and replaced by functional cardiac tissue. Although cardiac function and coronary vasculature are completely recovered by 130 days post-injury, the regenerated heart is not completely morphologically restored, as arrhythmic ventricular contraction and a thickened ventricular wall are seen in surviving animals The delayed recovery is likely due to the need to remove necrotic tissue caused by cryoinjury prior to regenerative responses taking place (González-Rosa et al. 2011).

A double transgenic system has been described to facilitate inducible cell type-specific genetic ablation in zebrafish [9]. In this transgenic Z-CAT fish (zebrafish cardiomyocyte ablation transgenes), cardiomyocyte-specific Cre recombinase under the *cmlc2* promoter drives the expression of a cytotoxic DTA (diphtheria toxin A chain) gene, which can cause more than 60% cardiomyocyte death throughout the heart upon a single injection of 4-hydroxytamoxifen (4-HT) administration [9]. This massive cardiomyocyte loss does not affect zebrafish survival but causes lethargy, gasping, reduced exercise capacity, and severe stress hypersensitivity, which are classic behavior signs of cardiac failure that are not seen after ventricular resection. These signs can be reversed within several days, concomitantly with rapid regeneration of ventricular cardiomyocytes. By 30 days post injury, ventricles are fully muscularized with minimal scarring and restored function [9].

Recently, hypoxia-induced cardiac injury models in zebrafish were also developed and applied as a more closely mimics of cardiac ischemic injury [10,11]. In these models, hypoxia was induced either by phenylhydrazine-induced anemia treatment, or by perfusion of Argon/CO_2 gas in water. A hypoxia/reoxygenation treatment was also applied to recapitulate ischemia/reperfusion injury in mammals. Cardiac oxidative stress, inflammation, cardiomyocyte death and proliferation were evidenced, accompanied by initial decrease in ventricular function followed by full recovery [10,11].

Cardiac regeneration studies have not been limited to zebrafish. *Giant danio*, a cyprinid family species closely related to zebrafish, has been reported to be able to regenerate myocardial tissue after ventricular damage caused by cautery injury [12]. However, the regeneration occurs at a lesser extent in comparison to zebrafish, where necrotic tissue remains part of the ventricle after 60 days [12]. Another cyprinid, the goldfish (*Carassius auratus*), is also able to replace a cauterized region of the ventricular myocardium by myocardial tissue within 6 weeks [13]. Unexpectedly, medaka (*Oryzias latipes*), another teleost model species, could hardly regenerate its heart tissue after ventricular resection [14]. Persistence of fibrotic scar, lack of vascularization, and minimal cardiomyocyte proliferation were observed during 60 days post-amputation [14].

Mammals

In contrast to lower vertebrates, cardiac regeneration capacity is limited and insufficient to restore normal cardiac function. There are fundamental differences between mammalian and fish heart anatomy as well as cardiac biology. Mammalian heart is a four-chambered, double circulation system with two pumping units work in series at

a high-pressure load [15]. Mammalian cardiomyocytes withdraw from cell cycle and become binucleated shortly after birth, while zebrafish cardiomyocytes are mononucleated and retain proliferative potential throughout life [16].

Before septation, embryonic mammalian heart shows anatomical similarities to two-chambered single-circulation adult zebrafish heart. Intriguingly, the mechanisms underlying cardiac regeneration in fish are conserved in fetal and neonatal mammalian heart. Using genetically determined mosaicism, an X-linked cardiomyocyte-lethal mutant gene was conditionally expressed and induced massive cardiomyocyte loss in heterozygous knockout female embryos due to random X inactivation [17]. These fetal hearts were able to restore approximately 50% of lost cardiac tissue, resulting in a fully functional heart, revealing an impressive regenerative capacity of the fetal heart [17].

Neonatal mouse heart regeneration has been elucidated in several studies and injury models[18–23]. Neonatal mice at P1 can fully regenerate their hearts within three weeks with minimal scarring after surgical removal of up to 15% of the apex of left ventricle [19,24]. The regenerated ventricular apex has normal systolic function 2 months after surgery. The reparative response is similar to those seen in zebrafish heart regeneration. At 1 day post-resection, a large blood clot is formed to seal the entire apex and it is associated with a robust inflammatory infiltration to the injury site. Gradual resorption of this apical blood clot is observed at later time points followed by its replacement by normal myocardial tissue [20]. Genetic fate mapping indicated that the majority of cardiomyocytes within the regenerated tissue originated from preexisting cardiomyocytes [20]. By 21 dpa, the entire apical defect was fully replaced by

cardiomyocyte and vascularization is restored in the regenerated ventricular apex [24].

However, this regenerative capacity is lost by one week, where apical resection of P7 mice fail to regenerate, coinciding with the developmental window when rodent cardiomyocytes begin to lose their proliferative potential [19,23,25]. This study carefully identified a time window immediately after birth when the mammalian heart mounts a robust regenerative response [24].

To establish how the neonatal mouse heart responds to ischemic injury, an MI model by permanent ligation of the left anterior descending (LAD) coronary artery was incorporated in P1 mice [26].Myocardial necrosis was evidenced at day 3 after MI, followed by a marked decline in left ventricular systolic function at day 4. However, within 3 weeks, neonatal mice were able to launch a regenerative response that restored 95% of the infarcted myocardium, associated with neovascularization that restored perfusion to the infarcted myocardium. Little to no fibrotic scar was detectable at 3 weeks post infarction, except a small fibrotic tissue immediately surrounding the suture site remains due to the persistence of anatomical barrier by the ligature [26]. Importantly, no signs of systolic dysfunction were apparent at 9 months of age, suggesting a long-term sustained cardiac function [26]. Similarly, direct experimental evidence for neonatal heart regeneration has been reported in mice in other injury models including cryoinfarction and clamping [26–28]. These findings in neonatal mice are strikingly concordant with myocardial regeneration capacity of newborn rats at 4-7 day-old following burn injury [29]. Necrotic tissues were completely removed by 14 days after operation when newly formed myocardial fibers can be seen. Bundles of myocardial fibers formed during the period of regeneration, however,

incompletely replaced the scar by 75 days [29]. Collectively, these findings suggest that the neonatal mammalian heart has a robust cardiac regeneration capacity following multiple forms of tissue damages, but this potential is maintained only during a transient time window and disappears briefly after birth.

The evidence of cardiac regeneration in fish and neonatal rodents after cardiac injury inspired studies on whether human neonatal hearts can functionally recover after cardiac injury. A recent study reported a case of severe MI and cardiac damage in a newborn infant, with subsequent complete cardiac recovery observed within weeks which led to long-term normal heart functions [30], providing solid evidence of complete functional heart recovery in human. A long-term myocardial scarring follow-up report showed that children underwent corrective heart surgeries for congenital heart malformations dramatically improved ventricular function and rarely showed any scar tissue [31]. This finding also extends the time window of myocardial cells mitosis in human infants from 9 months to 12 years of age [31]. However, the extent of the enormous regenerative potential of growing children's hearts and its time dependency are yet to be understood [31–33]. Collectively, these data suggest that, similar to neonatal rodents, young human hearts may also have intrinsic regenerative capacity to repair myocardial damage and the underlying mechanism in rodents might be potentially translational to human.

Numerous studies have been reported using various adult mammalian models during the past decades, including mice, rats, swine, etc [34–36]. A recent report carried out a large-scale investigation of myocardial repair in non-human primates using *Cynomolgus*

monkeys [37]. However, to this date, cardiac regeneration is very limited in adult mammals and possible translational mechanisms are still yet to be explored (Figure 1.1).

Cardiomyogenesis

The loss of cardiomyocytes is considered as the primary cause of impaired heart function. Cardiomyocyte proliferation is believed to be the primary mechanism of heart regeneration in lower vertebrates [38]. In zebrafish, new cardiomyocytes are created at 14 days post ventricular amputation as assessed by BrdU incorporation, and the severed ventricle can be restored with a new wall of muscle within a month [4,16]. For decades, mammalian cardiomyocytes are described as having progressive loss of mitotic activity as the heart grows into maturity and are believed to be permanently withdrawn from the cell cycle [25,39]. However, accumulative evidences in recent studies revealed proliferative capability of cardiomyocytes occurring in mammalian heart after birth and during adult life [40–42]. Within the first week of postnatal life, neonatal mouse heart can fully regenerate after partial surgical resection, and this regenerative response was characterized by cardiomyocyte proliferation [24,43]. Neomyogenesis is unique to neonatal heart repair, as this critical feature is lost after postnatal day 7 and in the adult mouse heart [24,27,44]. Beyond perinatal persistence of cardiomyocyte cell cycle activity, a myocyte proliferation burst at postnatal day 15 has been reported [43]. This proliferation during preadolescence adds ~500,000 cardiomyocytes to the mouse heart, representing a total 40% cardiomyocyte numbers increase, and establishes the final number of cardiomyocytes in the murine heart [43]. In humans, evidence for cardiomyocytes mitosis and cytokinesis in young humans has been reported [41]. During first year of life, mitotic cardiomyocytes assessed

by H3P-positivity contribute to 0.04% of total cardiomyocytes present at birth, and this percentage drops to 0.009% in a 20 year-old young adult heart [41]. This study demonstrated that cell cycle activity remains detectable in a normal human heart at up to 20-year of age. Using ^{14}C-based birth-dating technique, the annual turnover rate of cardiomyocytes is calculated to be 1.9% in a young adolescent heart and 1% in adult hearts [45]. This rate further decreases to 0.45% at age of 75. Amazingly, at age of 50, only 55% of the cardiomyocytes remain from birth, while 45% are generated later in life [45,46]. It has become clear that adult mammalian heart is not a terminally differentiated organ, although the duration and extent of proliferation remain extremely limited. Understanding the mechanism of cardiomyocyte proliferation and cell cycle arrest is fundamental to develop strategies to stimulate cardiomyocyte turnover and to promote cardiac regeneration.

Source of new cardiomyocytes

Two primary hypotheses of cell source that contribute to new cardiomyocyte formation are from resident stem and progenitor cell pool differentiation, and from pre-existing cardiomyocytes dedifferentiation followed by cell cycle re-entry.

Recent lineage tracing studies by genetic fate mapping indicate that the vast majority of new cardiomyocytes formed during zebrafish heart regeneration is primarily driven by pre-existing cardiomyocytes [22,47,48]. In both studies, a 4-hydroxy-tamoxifen (4-OH) inducible Cre/*lox* approach was used to generate transgenic lines in which CreER is driven by *cmlc2* and the newly formed cardiomyocytes were visualized by EGFP signal after excision of *lox*P-flanked stop sequences. Tamoxifen administration was used to

10

prelabel nearly all cardiomyocytes prior to injury. Following apical resection, new cardiomyocytes were also found to express EGFP, which indicates their adopted lineage is derived from pre-existing cardiomyocytes [47,48]. Specifically, the gene product of *polo-like kinase 1* (*plk1*) was shown to be an essential component of cardiomyocyte proliferation during heart regeneration [47]. Embryos pre-treated with Plk1 inhibitor cyclapolin 9 drastically lost the regeneration capacity due to a significant decrease in the number of BrdU-positive mitotic cardiomyocytes [47]. A subpopulation of cardiomyocytes within the ventricular wall were found to activate the regulatory sequences of *gata4*, a gene required for cardiomyogenesis during embryonic development, that contribute substantially to local muscle regeneration by proliferation [6,48]. Collectively, this evidence leads to the idea that pre-existing cardiomyocytes are the predominant source mechanism for heart regeneration in zebrafish [6].

To determine the lineage of origin of neonatal mouse heart, similar fate-mapping study was employed with tamoxifen-inducible lacZ reporter mice under control of αMHC promoter [24]. The percentage of lacZ-positive cells remains similar between sham and resected hearts, indicating that new myocytes arose from a resident αMHC-positive lineage rather than from a progenitor cell population [6,24].

By all accounts, resident cardiomyocyte mitotic activity remains a rare event in late postnatal and adult mice, and degree of myocardial regeneration from preexisting cardiomyocytes is functionally insignificant [49,50]. A fate-mapping study combining 2 different pulse-chase approaches concluded that preexisting cardiomyocytes are the primary source of cardiomyocyte replacement after injury [51]. A fate-mapping study

combining two different pulse-chase approaches was launched by pre-labeling resident cardiomyocytes with stable isotope and tamoxifen inducible GFP, and cardiomyocyte labeling during normal aging or after myocardial infarction is then assessed [51]. The percentage of labeling should decrease if the source of new myocytes is from non-myocyte as this would dilute the pre-existing GFP positive population. The ratio of GFP labeled cardiomyocyte in this system indeed declined from 79% to 67% at the border zone after myocardial injury, but the new cardiomyocytes generated were predominantly GFP+, leading to a conclusion that division of pre-existing cardiomyocytes is the dominant source of cardiomyocyte replacement after injury[21,51,52]. An *in vivo* clonal analysis and fate mapping at single-cell level based on the mosaic analysis with double markers (MADM) model revealed that αMHC-expressing cardiomyocytes are the origin of postnatal cardiomyogenesis, although the generation is found to be very rare [46]. A recent study employed an instant lineage tracing strategy, in which only 48-hour instant-chase was allowed upon tamoxifen administration on Kit-CreER fluorescent reporter mice. This short time window should not be enough time to complete all episodes of biological processes from recombination induction to fully differentiated new cardiomyocytes. Thus, the detection of fluorescent positive cardiomyocytes within such a short time window is more likely to be generated from pre-existing cardiomyocytes rather than derived from stem cells through lineage conversion [53]. All of these genetic lineage-tracing studies have in common is that, the extent of cardiomyocyte formation from pre-existing cardiomyocyte pool is a rare event that occurs only at a low rate in adult mammalian heart [22,46,49,53]. Therefore, understanding the endogenous regenerative mechanism limited by

cardiomyocyte proliferation, signal transduction, and other underlying cellular mechanisms may shed lights on potential therapeutic strategies.

Cardiomyocyte mitosis during the first year of life in humans contributes to 0.04% of total cardiomyocytes present at birth and this drops to 0.009% in a 20-year-old young adult heart as assessed by phospho-Histone3 immunolabeling [41]. Annual human cardiomyocyte turnover rates over lifespan are calculated to be 1.9% (adolescent), 1% (middle age), and 0.45% (old age), and by age 50 the cardiomyocytes remaining from birth are $\approx$55% [45]. There are clearly substantial limitations of endogenous regenerative mechanisms from cardiomyocytes in the adult mammalian heart. Although the adult mammalian heart possesses an extremely limited capacity for cardiomyocyte renewal, understanding the mechanism(s) of cardiomyocyte proliferation and cell-cycle arrest are fundamental to develop strategies to stimulate turnover and promote cardiac regeneration.

Cardiomyocyte dedifferentiation and proliferation are well known in lower vertebrates (e.g., zebrafish and newts [47,54,55]) as the primary mechanism of heart regeneration [4], but the early postnatal mammalian cardiomyocytes also capable of considerable plasticity. Cardiomyocyte dedifferentiation changes in structural and fetal protein expression levels and is a primary cellular response in response to stresses such as atrial fibrillation and hibernating myocardium [56,57]. Molecular mechanism(s) of cardiomyocyte dedifferentiation and proliferation involve epigenomic reprogramming with downregulation of cardiac structure and function genes as opposed to induction of cell-cycle reentry and proliferation genes [58]. Dedifferentiation increases in human and mouse cardiomyocytes treated with osteopontin (OSM [oncostatin M], a member of the IL-6

13

inflammatory cytokines) [59] as well as P130 and retinoblastoma protein [60]. Despite these initial observations, cardiomyocyte dedifferentiation in the adult mammalian heart remains a rare and inefficient process, with poorly understood underlying molecular mechanisms requiring further characterization.

Self-renewing, clonogenic, and multipotent cardiac stem cells (CSCs) have been extensively studied as a potential source to promote myocardial repair and regeneration through direct engagement with tissue as well as indirect actions to activate endogenous myocardial cells in studies of mice, rats, dogs, swine, and humans [61–67]. CSC-derived from postnatal hearts expresses stem cell surface markers (c-Kit/Sca-1) and stem cell phenotypic function (clonogenicity/sphere formation ability) [62,68,69]. Activation by environmental stimuli such as infarction injury prompts CSCs that normally reside in cardiac niches to divide, migrate, undergo lineage commitment, and mitigate pathological damage [70]. CSCs lineage determination in the adult mammalian heart demonstrate the presence of Ca^{2+} oscillations as well as Numb, α-adaptin, and Notch-1 signaling as regulators of symmetrical versus asymmetrical division that influence fate decisions [71,72]. Asymmetrical division of CSCs leading to lineage commitment is promoted by ATP released from dying cells that increases $Ca2^+$ oscillations through the IP3 pathway in the endoplasmic reticulum [73]. Bone marrow-derived cells have also been intensively assessed for capacity to mediate myocardial repair and regeneration as documented in many basic and clinical studies [74–81]. c-Kit+ bone marrow cells injected directly into the local injury site exhibit lineage commitment toward myocytes and vessels, mitigating damage from coronary artery disease [75]. Bone marrow-derived mesenchymal stromal

14

cells function in myocardial regeneration and survive primarily by influencing resident cardiac cells. Mesenchymal stromal cell-mediated cytokine release regulates cardiac cells behavior through multiple signaling pathways [82,83]. Observation of male bone marrow–derived progenitor cells transplanted into female hearts and found as cardiomyocytes with Y-chromosomes raised the possibility of progenitor cells differentiated into cardiac cells [84]. Bone marrow cells migrate to the damaged tissue (facilitated through cytokines paracrine system) led to a significant magnitude of myocardial remodeling and functional repair [77,78]. However, outcomes of multiple clinical trials involving treatment of heart failure patients with bone marrow derived cells has settled into a consensus of safe, albeit very modest, improvements in myocardial structure and function. Overall, the poor retention and survival of these and other adoptively transferred stem cell types into damaged myocardium remains a major limitation for clinical implementation.

Molecular Regulation of Proliferation, Cell Cycle, and Commitment

Genetic triggers for cell cycle reactivation to drive cardiomyocyte mitosis in the adult heart have been advanced as potential therapeutic targets for heart regeneration. For example, Hippo-Yap signaling is critical for cell intrinsic regulation of cardiomyocyte proliferation. Hippo-deficient mouse embryos develop cardiomegaly with robust cardiomyocyte proliferation and potentiated canonical Wnt/β-catenin signaling [85,86]. Loss of cardiac-specific Yap and Taz (cKO) impairs heart development and knockout mice suffer progressive dilated cardiomyopathy [87,88]. Yap-cKO neonatal hearts failed to regenerate after MI at P2, displayed extensive fibrotic infarct scar and deleterious loss of

15

healthy myocardium, whereas control mice effectively recovered from resection challenge [88]. Constitutive Yap activation in adult heart significantly enhanced cardiac regeneration, improved cardiac function, and promoted cardiomyocyte proliferation by 2.5-folds after infarction challenge [87,88]. Regenerative activity of Yap is partially associated with stimulating insulin-like growth factor (IGF), phosphorylation of Akt, and inhibition of GSK3β which could enhance β-catenin nuclear recruitment [86,88].

Additional molecular candidates for regulation of cardiomyocyte proliferation include Meis1 and neuregulin (Nrg1). Meis1 is a homeodomain transcription factor essential for normal cardiogenesis and embryonic hematopoiesis. Meis1 deletion in adult hearts increased number of cardiomyocytes prompted to enter cell cycle with concomitant increases in cytokinesis, while Meis1 cardiomyocyte overexpression induced premature cell cycle arrest in neonatal hearts [18]. Inhibitory actions of Meis1 upon proliferation are hypothetically mediated through transcriptional activation of CDK inhibitors p15, p16, and p21 [18,89]. Nrg1 purportedly induces mature mononucleated cardiomyocyte cell division through ErbB4/ErbB2 receptor leading to enhanced myocardial regeneration [90,91]. Transient induction of constitutively active ErbB2 may trigger cardiomyocyte dedifferentiation and proliferation upon MI, followed by redifferentiation and regeneration [90,92]. Administration of recombinant Nrg1 rescues cardiomyocyte depletion in pediatric heart disease and stimulates generation of new myocardium in neonatal mice after injury [93]. Cardiomyocyte cell cycle re-entry stimulated by rNrg1 administration in human infants with congenital heart disease at < 6 months of age could provide therapeutic opportunity for treatment prior to surgical repair for developmental defects [93]. Despite such intriguing

observations, relevance of these types of molecular intervention candidates for adult human myocardium remains both questionable and unknown, as studies were predominantly performed in the context of postnatal or developing myocardium that exhibits increased cardiomyocyte proliferative plasticity similar to lower vertebrates.

Multiple additional paracrine factors and associated signal transduction pathways contribute in the process of myocardial repair. For example, FGF is essential for recruitment of receptors and coordinating epicardial and myocardial activities into regenerating muscle, improving angiogenesis and myocyte survival in acutely injured mammalian hearts [94]. FGF induces downstream PI3 activity correlated with cardiac mitosis during development that is blunted by p38 MAPK. Inhibition of p38 induces DNA synthesis and G2/M transition in cardiomyocytes, acting synergistically with FGF1 signaling mediated by PI3K and Akt [94,95]. Thyroid hormones (THs) regulate diverse developmental processes as both hyper- and hypothyroid conditions detrimentally impact upon myocardial growth and maturation. Tri-iodo-L-thyronine (T3) serves as the primary driver of maturation and suppresses proliferation of near-term fetal ovine cardiomyocytes *in vitro* [96] by upregulating p21 and downregulating cyclin D1 [96,97]. Preadolescent T3 surge in mice coincides with a brief cardiomyocyte proliferative burst mediated by IGF-1/Akt pathway that may dictate binuclear cardiomyocyte number [43].

During cardiac regeneration, fibroblasts can play an important role, via myofibroblast trans-differentiation through WNT signaling pathway. Stress fiber formation and contractile proteins expression are the hallmarks of fibroblast trans-differentiation [98]. Several attempts at genetically engineered induction of fibroblast differentiation into

cardiomyocytes and cardiac progenitor cells using defined regulatory factors such as selected miRNAs or JAK inhibitor I tout the possibility of *in vivo* trans-differentiation of cardiac fibroblasts into cardiomyocytes through cellular reprogramming [99–102]. However, extrapolation of any of these putative mechanisms in service of therapeutically relevant regeneration in the human (or large animal) context remains dubious due to low conversion efficiency and will require further exploration.

Fundamental biological differences between lower vertebrates and humans remain problematic for extrapolation of findings to promote myocardial repair and regeneration. For example, centrosomes of cardiomyocytes in rat hearts disassemble shortly after birth but remain intact in adult zebrafish and newts [103]. Loss of centrosome integrity in postnatal cardiomyocytes coincides with cell-cycle arrest, revealing a potential mechanism underlying the post-mitotic state of mammalian adult cardiomyocytes [103]. Mps1 protein kinase is a mitotic checkpoint kinase in cell cycle regulation via its function in centriole assembly and centrosome duplication in mouse and human cells [104]. In zebrafish, Mps1 mutants fail to regenerate and restore ventricular wall, instead, the injured heart developed large connective-tissue scars 3 weeks after ventricular resection, suggesting a critical cell-cycle regulatory role of Mps1 in proliferation [6,104]. Similarly, inhibition of the cell-cycle regulator Plk1 drastically inhibited the heart regeneration in zebrafish, resembling the regeneration perturbation seen in zebrafish Mps1 mutants in zebrafish. This inhibition was not due to increased cardiomyocyte apoptosis, but primarily was from loss of mitotic cardiomyocytes [47,105].

Despite decades of targeted and focused efforts the adult mammalian cardiomyocyte remains remarkably refractory to molecular interventions intended to promote re-entry into cell cycle and proliferation. Clearly, neonatal and lower vertebrate myocardium is a very different molecular and cellular milieu for manipulation of cardiomyocyte proliferation relative to the adult mammalian heart [106]. Although research continues to identify novel and provocative avenues for influencing cardiomyocyte proliferation, the implementation of any such maneuvers in any therapeutic context continues to be hampered by low efficiency and debatable reproducibility. Lastly, almost all experimental models involve use of lower vertebrate species and relatively young animals, both of which are problematic for translational relevance to the aged human population most likely to require regenerative therapy. Indeed, the reparative potential of myocardium inexorably declines over time and is clearly impaired in aged individuals at the time and place where it is most needed by several intractable factors as described in the following section.
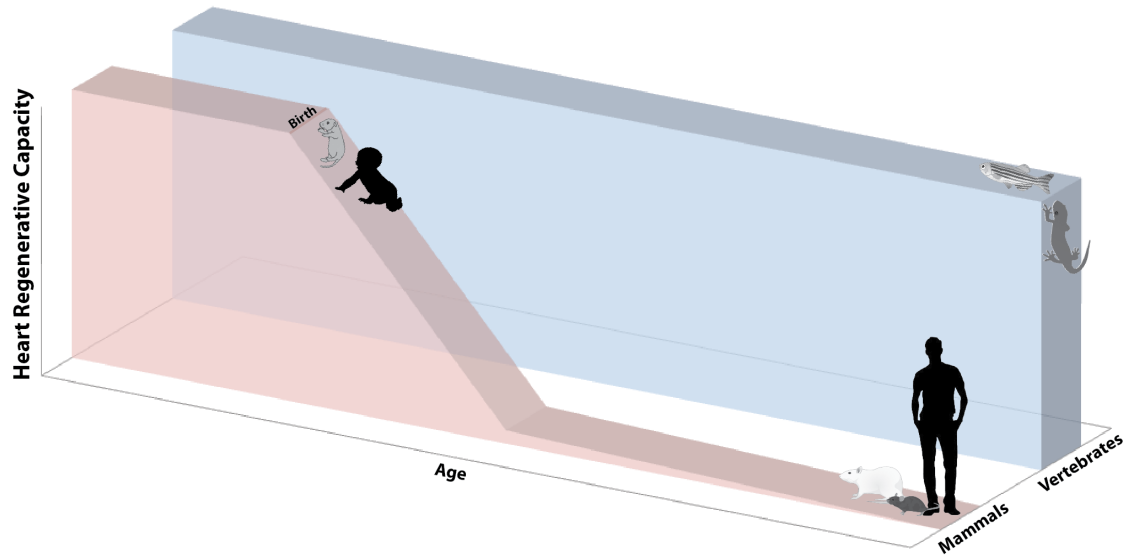
Figure 1.1 Heart regeneration capacity is lost in adult mammals

Vertebrates (*e.g.* zebrafish, axolotl) are able to fully regenerate their hearts thorough their life. Neonatal mammals (*e.g.* mouse, human) can partially regenerate their heart, however this capacity is lost in adult mammals. Height or bricks indicates regeneration potential.

SUMMARY

Remarkable progress has been made in a little over a decade since the revolutionary concept was advanced that the human heart is not a postmitotic organ incapable of regeneration and repair. Tissue regeneration and organ repair documented and accepted for several lower vertebrate species in the laboratory setting prompted researchers to ponder whether such processes could be recapitulated in the mammalian setting. The once universally held dogma of the mammalian heart as a postmitotic organ without regenerative potential was crushed by an avalanche of new research. Although none could argue that the process in adult mammals was as efficient as in several lower vertebrates, some provocative parallels were advanced between early pre- and postnatal development and retention of regenerative capacity. Thus, a primary focus of research continues to concentrate on what is present in the nascent developing myocardium that is lost on maturation into early adulthood. Concurrently, devotees of regenerative species that retain the capability for myocardial repair throughout life are keen to identify those molecular and cellular mechanisms preserved in lower vertebrates that disappear (or become latent) in mammals. Molecular control of cellular behavior seems to be the key, but regulation of cellular regenerative potential in vivo has proven to be far more nuanced and challenging. Progress has been frustratingly slow to deliver efficacious translational solutions to impact human health, but it is important to recognize that the concept of mammalian myocardial regeneration debuted shortly after the turn of the century and has provided a wealth of return on investment with expanding knowledge and innovative approaches. The pressure for deliverables has been intense, leading to clinical testing

21

that some have dubbed as premature and of questionable value. However, conclusions drawn from experience in the clinical arena are quite contrary to the view of skeptics and demonstrate not only safety but also modest (albeit variable) efficacy. These initial forays into treatment also have highlighted theoretical and practical challenges that need to be conquered to improve on pioneering cell therapy trials. The future belongs to optimists who recognize and acknowledge limitations of current approaches while promoting their view that if we can all agree that regeneration occurs, no matter how inefficiently, then we should stop debating relevance for cardiac biology and concentrate instead upon improving the process and outcome.

Chapter 1, in part, is taken in part as it appears in Circulation Research, 2018.

Mechanisms of Cardiac Repair and Regeneration. Broughton KM*, Wang BJ*, Firouzi F,

Khalafalla F, Dimmeler S, Fernandez-Aviles F, Sussman MA. The dissertation author was

a co-primary author and investigator of this review article [1].

CHAPTER 2

Adaptation Within Embryonic and Neonatal Heart Environment Reveals Alternative

Fates for Adult c-Kit$^+$ Cardiac Interstitial Cells

INTRODUCTION

Myocardial homeostasis is maintained by dynamic interaction on multiple levels between cardiomyocytes and the cardiac interstitial cell (CIC) population. Decades of study reveals CICs as a heterogeneous collection of cell types that defy simple categorization, due in part to their fluid adaptability in response to development, aging, acute injury, and chronic stress [107–109]. Parsing out CIC subtypes with specific markers such as periostin or Tcf21 has merged with the more impartial and nuanced approach of transcriptomic profiling at the single cell level [110–112]. Appreciation for the complexity of CIC biological properties continues to grow, as does recognition that environmental influences exert profound control over CIC phenotypic characteristics and functional activities.

Studies of CIC biology often rely upon assessments performed using populations expanded by *in vitro* cell culture for various reasons of sample yield, manipulability, and of course simplification compared to challenges of the myocardial milieu *in vivo* [49,68,69,113,114]. Such studies provide tremendous insights but also are limited by inescapable aspects of cell culture adaptation, natural selection *ex vivo* for robust proliferative cell subsets, and multiple choices for conditions of experimental design. Collectively, these variables contribute to the wide range of interpretations and published literature for CIC biology that has been extensively reviewed [110,115–117]. Moreover, a plethora of selected subpopulations of *in vitro* expanded CICs have been intensively studied for cardioprotective and reparative potential upon reintroduction into pathologically injured myocardium for over a decade [68,118,119], but consequences of cell

culture environment upon CIC properties in terms of reshaping population characteristics or individual cellular functional capabilities remains relatively unstudied and poorly understood. Typically, such cultures involve two dimensional (2D) monolayer growth and serial passaging to obtain sufficient numbers of cells for treatments [120–123]. Such 2D culture conditions promote reprogramming toward a common shared transcriptional profile, even between CIC subpopulations enriched by selection for unrelated markers as well as comparisons between multiple donor sources [111,124,125]. Taken further, our group found that relatively short-term 2D cell culture for five serial passages results in loss of cell-specific identity markers and increased homogeneity in a CIC subpopulation enriched for c-Kit+ expression (cCIC) compared to correspondingly selected freshly isolated cells by single cell RNA-Seq transcriptional profiling [125]. Findings such as these support the contention that CIC isolation and propagation conditions exert profound influences upon biological and functional properties, consistent with our recent reports of hypoxic culture conditions antagonizing mitochondrial dysfunction and senescence in human cCICs [122] as well as tetraploid conversion of murine cCICs [126]. Surprisingly, despite irrefutable evidence of alterations following *in vitro* expansion of primary CIC isolates, there are essentially no studies to document the extent of such changes as permanent or transient and whether CICs undergo another round of phenotypic and functional adaptation following reintroduction to their native environment of *in vivo* myocardium.

A major impediment to assessing re-adaptation of cultured CICs following delivery to host adult myocardium is poor retention and persistence of the donated cell population [127–130] . Although employing augmented approaches to embed CICs offers some

improvement over direct injection to recipient myocardium, bioengineering solutions involving injectable gels or cultured patches severely limits direct interaction between exogenously introduced CICs and host myocardium. Furthermore, delivery to pathologically injured myocardium further stresses the CIC population already coping with dramatic changes in environmental conditions. For example, host immune-mediated reaction to pathologic injury including CIC delivery prompts a powerful inflammatory response involving cytotoxic action. Indeed, developing myocardium exhibits stage-specific permissivity for incorporation of introduced or migrating cells [107,131]. Therefore, we reasoned that assessment of cultured cCIC adaptation following reintroduction to myocardial tissue *in vivo* would be facilitated by delivery to early developmental stages characterized by cardiogenic activity and negligible inflammation.

Permissive conditions present in embryonic tissue or an early stage developing heart allows for engraftment and persistence of injected cCICs, then followed in subsequent days to weeks for determination of phenotypic characteristics exhibited by both exogenously introduced cells as well as host reaction to their presence. In this Chapter, three distinct developmental stages of embryonic (E3.5), fetal (E15.5), and postnatal (P3) were chosen for introduction of cCICs. Results demonstrate engraftment and long-term persistence of cCICs including exclusion from the inner cell mass of pre-implantation blastocysts. Additionally, cCICs display negligible adaptability and functional plasticity following delivery to cardiogenic fetal or postnatal hearts. These findings implicate *in vitro* expansion as a primary determining factor in cCIC adaptability and provide novel insight regarding cCIC biology.

MATERIALS AND METHODS

All animal protocols and studies were approved by the review board of the Institutional Animal Care and Use Committee at San Diego State University.

Mouse cCIC isolation and fluorescence engineering

CICs were isolated from 8-week old FVB/J mice by enzymatic dissociation (Collagenase II, 460U/mL, Worthington, LS004174) of the whole heart on a Langendorff apparatus (Radnoti, 158831) as previously described [123]. Following myocyte depletion, Lin$^-$CD45$^-$c-Kit$^+$ cCICs were obtained by removing lineage$^+$ and CD45$^+$ fraction using lineage depletion Kit (Miltenyi, 130-110-470) and CD45 Microbeads (Miltenyi, 130-052-301), followed by c-Kit$^+$ cCICs enrichment (Miltenyi, 130-091-224) by magnetic-activated cell sorting (MACS). Cells were expanded in growth media [DMEM/F12 (Gibco, 11330032) supplemented with 10% ES-FBS (Gibco, 16141079), 10ng/mL basic FGF (BioPioneer, HRP-0011), 20ng/mL EGF (Sigma-Aldrich, E9644), 1X ITS (Lonza, 17-838Z), 10ng/mL LIF (BioPioneer, SC-041-2), and 1X (Gibco, 10378016)] and passaged every 2-3 days to maintain at a confluency of ≤40%. Cultured cCICs were transduced with lentiviral PGK-mCherry construct at MOI of 5 and puromycin selected to stably express mCherry fluorescence. cCICs used in mCherry experiments were isolated from two male mice, and cCICs used in FUCCI experiments were isolated from four mice (2 males + 2 females).

Embryoid body formation

For cell aggregation, 2.75 x 10^6 cCICs were plated in 5mL EB medium [KnockOut DMEM (Gibco 10829-018) supplemented with 15% KnockOut Serum Replacement (Gibco 10828-028), 0.1mM MEM Non-Essential Amino Acids Solution (Gibco 11140-050),

1X GlutaMAX-I (Gibco 35050-079)] in low-attachment petri-dish for 4 days at 37ºC, 5% CO_2. For mesoderm induction, cCIC-EBs were transferred to AF-coated tissue culture dish in EB medium supplemented with 10% ES-FBS to allow attachment overnight, followed by mesodermal induction media [IMDM (Gibco, 31980030) and Ham's F12 (HyClone, SH30026.01) supplemented with 5ng/mL Activin A (Peprotech, 120-14E), 0.5ng/mL BMP4 (Peprotech, 120-05ET), 5ng/mL human VEGF (Peprotech, 100-20) and 1X Pen/Strep (Gibco, 15140163)] for 24 hours, cardiac induction media [StemPro-34 SFM medium (Gibco, 10639011) supplemented with 2mM L-glutamine (Gibco, 25030081), 0.5mM Ascorbic acid (Sigma-Aldrich, A4403-100MG), 5ng/mL human VEGF, 10ng/mL human basic FGF, and 50ng/mL human FGF10 (Peprotech, 100-26)] for 7 days. Subsequently, cells were washed twice in cold PBS and fixed in 1% PFA for immunocytochemistry. For protein lysates, cell pellets were collected before mesodermal induction and at the end of cardiac induction.

Histology and Immunofluorescence staining

Mice were heparinized (Sigma-Aldrich H3393, 10Unit/g) by intraperitoneal injection and euthanized at harvest time points. For animals younger than 14 days, euthanasia was carried out by anesthetization on ice followed by decapitation. For animals at 14 days and older, euthanasia was carried out by isoflurane overdose followed by cervical dislocation. Hearts were perfused with PBS and 1% paraformaldehyde (PFA) before removal from thoracic cavity, followed by fixation in 1% PFA immersion overnight at 4ºC. Fixed hearts were dehydrated in 30% sucrose in PBS overnight at 4ºC, then in OCT+30% Sucrose mix at 1:1 ratio, before mounting in NEG50 and frozen on dry ice.

Frozen sections were cut at 20μm thickness and collected onto Superfrost glass slides. Sections were allowed to dry for 48 hours prior to storage at -20°C.

Following equilibrium at RT for 5min and brief rehydration in PBS, frozen tissue sections were incubated in permeabilization solution (0.1% Triton X-100, 0.1M Glycine, 1% BSA in PBS) for 30 minutes at RT, then blocked in blocking solution [10% Donkey Serum (Millipore, S30-100mL), 0.1M Glycine, 1% BSA in PBS] for 1 hour at RT. Cells grown and fixed in chamber slides were permeabilized for 15 minutes and blocked for 1 hour prior to antibody staining. Following blocking, samples were incubated overnight in primary antibodies at 4°C (see dilutions in Table 2.2), washed in PBS, and incubated in secondary antibodies (1:100) for 90 minutes at RT. All samples were counterstained with DAPI (Sigma-Aldrich D9542, 0.1μg/mL) and mounted in VectaShield and imaged by Leica SP8 confocal microscopy.

Immunoblotting

At time of harvesting, cells were washed twice in cold PBS and lysed in RIPA buffer (Thermo, 89901) with freshly added proteinase inhibitor and phosphatase inhibitors cocktails (Sigma P0044, P8340, P5726) for 30min on ice with intermittent vortexing. Cell lysates were then centrifuged for 10min at 11 000g at 4°C to remove insoluble debris. Supernatants were quantified with Bradford assay (ThermoFisher, 23236) and 20μg lysates were run on 4-12% Bis-Tris protein gels (Invitrogen, NP0335BOX) and transferred onto PVDF membrane (Millipore, IPFL00010), followed by blocking in 10% Non-fat dry milk (Lab Scientific) for 1 hour at RT. Primary antibodies (see dilutions in Table S1) were

incubated overnight at 4ºC and secondary antibodies (1:1 000) for 90min at RT. Immunoblots were scanned with LI-COR Odyssey Clx system.

Quantitative RT-PCR

Total RNA was isolated using Quick-RNA Miniprep kit (Zymo Research, R1055) following manufacturer's protocol. RNA concentration was determined using NanoDrop 2000 spectrophotometer (ThermoFisher) and normalized to 500ng for cDNA synthesis by iScript cDNA synthesis kit (BioRad, 170-8891). 6.5ng cDNA was used for each qPCR reaction using iQ SYBER Green (BioRad, 170-8882) on a CFX Real-Time PCR thermocycler (BioRad). Primers and sequences used in this study are listed in Table 2.3. Ct values were normalized to *Actb* and analyzed by ΔΔCt method relative to ESCs.

Generation of mouse chimera: blastocyst isolation, injection, and uterine transfer

Superovulated FVB/J females at 4-5 weeks of age were mated with FVB/J males overnight. The next morning, mating was confirmed by vaginal plug, and mated females (0.5 days post-coitum, dpc) were euthanized by cervical dislocation for collection of zygotes from oviduct. Zona pellucida was removed by briefly digestion in hyaluronidase. Alternatively, 3.5dpc females were euthanized and uterine horns were flushed with M2 media (Millipore, MR-015-D) for collection of morula. Zygote and morula were both collected in M2 and cultured in pre-equilibrated KSOM media bubbles (Millipore, MR-106-D) under mineral oil immersion (Sigma, M8410) at 37ºC (5% CO_2, humidified) until blastocyst injection.

For blastocyst injection, cultured cCICs were trypsinized and pelleted in growth media supplemented with 1X HEPES (Gibco, 15630080). Approximately 8-12 cells were

injected into each blastocyst. Following injection, blastocysts were washed in M2 and allowed to recover in KSOM for 30min before uterine transfer. Approximately 15-20 blastocysts were transferred into the uterus of 2.5dpc pseudopregnant recipient B6/CBA females mated with vasectomized Swiss Webster males. Alternatively, 20-25 blastocysts were transferred into the uterus of 0.5dpc pseudopregnant B6/CBA females. FVB/J background GFP[+]ESCs were used as chimera generation control.

Whole-mount blastocyst immunostaining and 3D reconstruction

CIC-injected blastocysts were incubated in pre-equilibrated KSOM media for 48 hours at 37°C (5% CO_2, humidified). Post-injection blastocysts at 24hpi and 48hpi were fixed in 1% PFA overnight at 4°C. Blastocysts were washed in PBST (PBS + 0.1% Tween-20), incubated in 0.1% Triton X-100, 1% BSA, 0.1M Glycine, 10% Donkey Serum in PBST for 30min at RT. Primary antibodies (see dilutions in Table S1) were incubated overnight at 4°C and secondary antibodies (1:100) were incubated for 1.5 hours at RT. DAPI was added to last PBST washes to stain nuclei. All washes and incubations were performed in liquid bubbles under mineral oil immersion. Following staining, blastocysts were gradually transferred from PBST to 20%, 50%, 70% glycerol, and mounted in 80% glycerol. Z-stack series scanning was performed using Leica SP8 confocal microscopy (63X) at 5μm interval depth. Three-dimensional reconstruction videos were generated using Leica LAS X analysis software.

in utero transplantation (IUT)

Timed pregnant FVB/J female inbred mice were anesthetized with ketamine/xylazine according to body weight at 10μL/g. Uterine horns were exteriorized

through a short ventral midline incision at lower abdomen. Cells were delivered using a microcapillary needle with the appropriate volume of cell suspension at approximately 5 000 cells per embryo into pericardial space. After injection, the uterine horns were gently placed back into the abdomen and the maternal abdominal muscle and peritoneum were closed by surgical adhesive. Following recovery, two buprenorphine doses (0.2μg/body weight g) were given every 12 hours as analgesia. At 2dpi, dams were euthanized by isoflurane overdose followed by cervical dislocation. Embryos were dissected out of uteri in cold PBS and fixed in 1% paraformaldehyde immersion at 4°C overnight.

FUCCI constructs and expression

The FUCCI system consists of two chimeric proteins, mKO-Cdt1 and AzG-Geminin, which oscillate reciprocally during the cell cycle, labeling the nuclei in G1 phase orange and those in S/G2/M phases green[132]. During G1/S transition, both probes are present, resulting in a yellow fluorescence (overlaid green and red); during the brief gap between M and G1 phases, neither probe is present and fluorescence is absent. Oscillation between red, yellow, or green signals tracks cell cycle status [42,132] (Figure 2.8a). FUCCI lentiviral plasmids were generated as previously described[42]. For FUCCI expression, cCICs were transduced with lentiviral PGK-Cdt1-mKO and PGK-Gem-AzG constructs at MOI of 2.5 of each construct and sorted for mKO$^+$/AzG$^+$ double positivity by flow cytometry (BD, Canto).

Postnatal intramyocardial cell delivery

FVB/J Neonates were anesthetized by hypothermia on ice for 1-3min until immobile. Anesthesia was maintained by placing pups on an ice filled petri-dish

throughout the procedure. Peristernal thoracotomy was performed by making a small incision at the fourth intercostal space. Intercostal muscles were separated by blunt lateral dissection in order to facilitate access to the heart. After expanding the fourth intercostal space, the apex was gently stabilized using curved forceps. With gentle pressure on the abdomen, hearts can be exteriorized and stabilized with microforceps without damaging myocardium. Cells were delivered via a flame pulled glass capillary needle (opening diameter ~50μm, calibrated by hemocytometer) with tangential angle into myocardium and titrated volume was injected by mouth pipetting (Sigma, A5177). Approximately 5 000 - 10 000 cells were delivered in a total of 2.5μL via three injection sites tangential to the LV apex region. After injection, the heart was returned to the thoracic cavity, and the muscle and skin incision was closed using surgical adhesive (Meridian, Surgi-lock 2oc). Post-injection pups were warmed up rapidly on a heating pad for several minutes until recovery (body color turns pink and spontaneous movement), followed by mixing the pups with dam's bedding in order to reduce chances of cannibalization. Post-op pups were returned to the dam and littermates as soon as possible and maternal acceptance was monitored. The whole surgical procedure should be complete within 10 minutes to minimize the time spent separated from the mother and to improve survival. At 7, 14, 21, 28dpi, injected hearts were collected and washed twice in cold PBS, followed by fixation in 1% paraformaldehyde at 4ºC overnight.

Myocardial infarction and intramyocardial injection

Myocardial infarction and intramyocardial injection were carried out as previously described [133] on FVB/J strain mice. Briefly, the heart was popped out through the fourth

intercostal space and the left anterior descending artery (LAD) was permanently ligated at the second distal branching point using 7-0 silk suture. Following LAD ligation, three injections were delivered (Harvard Apparatus, Hamilton infusion pump) at the border zone surrounding the blanching area at a tangential angle parallel to myocardial wall, in order to ensure intramyocardial cell delivery. A total of 100 000 cells/10μL were injected per heart at three injection sites. Following injection, the heart was immediately placed back into the intrathoracic space and the muscle and skin were closed by surgical adhesive.

Cardiac cell disassembly and quantification

Post-injection hearts were enzymatically disassembled into single cell suspension and subjected to flow cytometry for fluorescence-based cell count. For neonates, postop pups at 2hpi and 48hpi were heparinized and anesthetized on ice. Anesthesia was maintained by hypothermia in a Petri dish filled with ice during surgical procedure. Perfusion and digestion was performed following a modified protocol as previously described [134]. Briefly, the heart was digested (Collagenase II, 460U/mL) by continuous perfusion through LV apex with the aortic arch clamped (5min at 1mL/min). The digested tissue was then triturated and transferred into a 15mL conical tube for subsequent digestion for 15-30min in 37°C water bath with agitation. All cell suspension was filtered through a 75μm cell strainer to exclude cardiomyocytes and tissue debris. The flow through was pelleted by centrifugation at 350g for 10min. Cell pellets were then resuspended in 500μL PBS/0.5%BSA and subjected to flow cytometry count.

For quantitative analysis from adult heart injection, cardiomyocytes must be removed due to their rod-shape and large cell size exceeding the capacity of flow-

cytometer. Only the non-myocyte population was used for cell count. Non-myocytes were obtained from post-MI hearts at 48hpi. As described in cCIC isolation method, post-op hearts were enzymatically digested (Collagenase II, 460U/mL) on a Langendorff apparatus (12-18min at 1mL/min), triturated, and filtered through 100μm cell strainer to remove undigested debris. The supernatant was then sequentially filtered through a 40μm and a 30μm cell strainer. The flow-through containing all non-myocytes was pelleted by centrifugation at 350g for 10min. Cell pellets were then resuspended in 1mL PBS/0.5%BSA and subjected to flow cytometry count.

Flow Cytometry

Single cell resuspension was analyzed using a BD FACSCanto instrument. Cells digested from Sham (uninjected) hearts were used to exclude auto-fluorescence disturbance, and cultured cCICs expressing mCherry fluorescence were used as positive gating to establish fluorescence levels. All cells from neonatal hearts were analyzed. A recorded volume of 100-200μL cell suspension from adult interstitial cells were analyzed, and the whole heart cell count was calculated based on volumetric ratio relative to 1mL initial cell suspension. Flow cytometry data were analyzed by FlowJo software (BD Biosciences).

Echocardiography

Echocardiography was performed using Vevo2100 (Visual Sonics) system from LV parasternal long and short axis at heart rate range of 500-550 beats/min. Ejection fraction (EF) and Fractional Shortening (FS) were determined by off-line analysis. Age-matching unoperated mice were used as baseline controls.

Masson's Trichrome staining

Masson's trichrome staining was performed using Trichrome stains kit following manufacturer's protocol (Sigma-Aldrich, HT15). Briefly, frozen tissue sections re-hydrated in PBS for 5min and post-fixed in 10% formalin for 1 hour at RT, followed by fixation in Bouin's solution overnight at RT. Next day, sections were washed in water and subjected to a series of staining in Weigert's Iron Hematoxylin Solution for 5min, Biebrich Scarlet-Acid Fuchsin for 5min, Phosphotungstic / Phosphomolybdic Acid Solution for 5min, Aniline Blue Solution for 5min, and 1% Acetic Acid for 2min with washes in deionized water in between. Finally, sections were gradually dehydrated through alcohol and cleared in Xylene for 3min before mounting in Permanox. All images were scanned by Leica DMIL600 microscope using xy stage tilescan and automatically stitched by Leica LAS X analysis software.

Cell Death Detection

TUNEL assay was performed using *in situ* cell death detection Kit (Roche 11684795910) following manufacturer's protocol. Briefly, frozen tissue sections were re-hydrated in PBS for 5min at RT, post-fixed in 4% paraformaldehyde in PBS for 20min, and permeabilized in 0.1% Triton X-100, 0.1% sodium citrate for 2min at 4ºC. Following a brief wash in PBS, samples were incubated in TUNEL reaction mixture (Label solution + Enzyme solution, 9:1) for 1 hour at 37ºC. Samples were then washed in PBS, mounted in VectaShield, and scanned using a Leica SP8 confocal microscope.

Ploidy quantification

Following euthanasia, mouse sperm was collected from vas deferens and maintained in PBS/0.5%BSA on ice. Bone marrow cells (BMC) were collected from femur flushed with PBS/0.5%BSA using a 27-gauge needle and filtered through 30μm cell strainer to remove debris. Cultured cCICs were trypsinized and pelleted at 300g for 5min. Cells were then stained with Sytox Green (Invitrogen, S7020, 1μM) for 15 min at RT before subjected to flow cytometry analysis. Unstained cells of each cell type served as negative gating controls. Ploidy comparison was established using sperm as haploid and BMC as diploid control using FlowJo software.

Alternatively, sperm, BMC, and cCIC suspensions were manually mixed and cytospun (Thermo, Cytospin 4) for 3min at 800rpm with low acceleration onto a poly-D-Lysine coated slide. Cells were then fixed in 1% PFA for 20min at RT, stained with DAPI for 5min at RT, following by three PBS washes to remove excess staining. cCIC nuclei were identified by mCherry fluorescence, BMC nuclei were identified by mCherry negativity, and sperm nuclei were identified by unique fishhook-like nuclear morphology. Nuclear DAPI signals were scanned by z-series spanning entire nucleus at 1μm interval using Leica SP8 confocal microscopy. Z-projection was reconstructed with sum intensity by ImageJ. Nuclear intensity was quantified by nuclear volume tracing using ImageJ and presented as arbitrary units (A.U.).

Human CIC isolation and culturing

Left ventricular wall tissue biopsies were obtained from patients undergoing left ventricular assist device (LVAD) implantation. Human CICs (hCICs) were isolated from

adult heart biopsies obtained from consenting patients during Left Ventricular Assistant Device (LVAD) implantation as previously described [135]. All procedures are consistent with Institutional Review Board (IRB) approval following NIH guidelines for human subject research. Briefly, biopsy tissue was enzymatically digested (Collagenase II, 500U/mL), minced, and magnetically sorted for c-Kit$^+$ positivity (Miltenyi, 130-091-332). hCICs were maintained and propagated in F12 Ham's media supplemented with 10% ES-FBS, 5mU/mL human erythropoietin (Sigma-Aldrich, E5627), 10ng/mL human recombinant basic FGF (BioPioneer, HRP-0011), 0.2mmole/L L-glutathione (Sigma-Aldrich, 66013-256), and 1% PGS.

Statistical Analysis

All data were presented as mean ± SEM and analyzed by GraphPad Prism 5.0b with unpaired student t test, two-tailed. A *p* value < 0.05 was considered statistically significant.

RESULTS

Mesodermal potential maintained by cCIC in vitro

cCICs were genetically modified to stably express mCherry fluorescent protein by lentiviral infection, with expanded cCICs exhibiting spindle-shaped morphology in culture (Figure 2.1a; 97.6% mCherry[+]). Robust expression of *c-Myc, Gata3, Gata6,* and *Gata4* mRNAs relative to Embryonic Stem Cells (ESCs) is evident by quantitative PCR (Figure 2.1b). Spontaneous aggregation into 3D embryoid body spheres (EBs) in suspension culture is commonly used to study ESC differentiation potential [69,136], and culture expanded cCICs similarly aggregate into clusters (Figure 2.1c). The mesodermal origin of cCIC [15] is consistent with increased expression of the mesoderm marker SM22 alpha (SM22α), whereas endoderm (α-Fetoprotein, AFP) and ectoderm (βIII-Tubulin, TUJ1) markers remained undetectable before and after aggregation of cCICs into EB-like clusters to promote differentiation (Figure 2.1d). cCICs uniquely express SM22α but not AFP shown by confocal microscopy immunolabeling (Figure 2.1e). In addition to mesoderm potential, a majority of mesodermal induced cCICs express the cardiac fibroblast marker vimentin (Vim), consistent with fibroblast origin (Figure 2.1f). Collectively, these findings portray cCIC in culture as mesodermal-lineage derived cells with characteristic fibroblast-associated marker expression.

Extra-embryonic tissue integration of cCIC in preimplantation blastocysts

Chimeras blastocyst formation following cell injection is used as a stringent assessment for testing stem cell pluripotency [137,138]. Adult multipotent cells may harbor properties similar to ESCs allowing for chimera formation when injected into blastocysts

[139–141]. At the blastocyst stage, a small number of blastomeres develop into the pluripotent ICM that will later give rise to all three germ layers of the embryonic body for normal somatic and germ-line contribution. The rest of the blastomere differentiates into TE that will later give rise to extra-embryonic tissues and support embryonic development [137,138]. Therefore, cCICs were delivered into murine blastocysts that were subsequently cultured *ex vivo* for 24-48 hours post-injection (hpi; Figure 2.2). Presence of injected cCICs was directly visualized by expressed mCherry fluorescence without immunolabeling. Injected cCICs persist in the blastocoel, inner cell mass (ICM), and trophectoderm (TE) of blastocysts at 24hpi (Figure 2.2b-d, arrowheads, Supplemental Video 2.1). Spindle-shaped morphology of *in vitro* cCIC was observed in hatching blastocysts at 48hpi (Figure 2.2e, Supplemental Video 2.2). Coupling between cCICs and blastocyst cells is revealed by presence of tight junctions (Figure 2.2f, ZO1, arrowheads) shared with neighboring host trophoblasts (CDX2) but rarely with the inner cell mass (ICM; Oct3/4) (Figure 2.2g). cCIC location among the monolayer TE ring immediately adjacent to trophoblasts was visualized by confocal optical sectioning of cCIC nuclei (Figure 2.2h-i). cCIC anchoring among trophoblasts in the preimplantation chimeric blastocyst suggests extra-embryonic tissue integration, assessed by surgical transfer of chimeric blastocysts into pseudopregnant females. Following the anticipated extra-embryonic pattern, cCICs mosaically integrate predominantly in chorionic lamina of the amniochorionic membrane (AM) opposite from squamous amniotic epithelium (Laminin+) at 10 days post-injection (dpi; E13.5, Figure 2.2j-l). In contrast, absence of cCICs from the inner cell mass of developing embryonic tissue was exhaustively evaluated without a single positive finding

(n=253), whereas embryo chimerism was readily observed with a frequency of 19.2% using ESC as a control cell (n=10/52; Table 1, Figure 2.3). Therefore, although cCICs possess sufficient functional capacity for extra-embryonic tissue integration they are unable to participate in embryonic chimerism.

Fetal myocardium retains cCIC at perivascular regions

Efficient chimeric competency relies on pairing donor cell autonomous developmental timing with host organ developmental stages [142–144]. In other words, synchronizing degree of stemness/commitment of CICs with the developmental timing of recipient hearts is critical for successful chimera formation and possible long-term cell retention. CICs are thought to be required during cardiogenesis, therefore the matching stages of CICs may lie during post-implantation stages from primitive streak formation at E7.5 and onwards during embryonic heart formation. Empirical testing of *in utero* transplantation (IUT) into pericardial space of approximately 5 000 cCICs in a time course ranging from E7.5-E16.5 (data not shown) revealed the optimal prenatal stage for engraftment and persistence was E15.5 (Figure 2.4a). Assessment of cCIC fate performed 2 days after *in utero* delivery revealed persistence at multiple intracardial and pericardial locations (Figure 2.4b, arrowheads), particularly at perivascular regions around tricuspid aortic valve (Figure 2.4c, Ao). Retained cells were also found in extra-cardiac tissues within the vicinity of thoracic cavity including thymus, lung, diaphragm, and skeletal muscle (Figure 2.5a-e). Embedded cCICs are negative for cardiogenic lineage markers von Willebrand Factor (vWF) (Figure 2.4b, Ao), SMA (Figure 2.4c, Ao), Desmin (Figure 2.4d, Ao, RV, IVS) and the M-phase marker phospho-histone H3 (Figure

2.5f). However, cCICs in perivascular regions express the fibroblast marker vimentin (Figure 2.4e, green). Consistent with previous observations from blastocyst chimeras, fetal AM incorporated cCICs in a mosaic pattern (Figure 2.4f-g), confirming functional capacity of cCIC contribution to extra-embryonic tissues. Thus, the prenatal cardiogenic environment allows for engraftment and persistence of injected cCICs that do not contribute directly towards cardiogenesis but instead maintain a fibroblast-like phenotype.

Neonatal myocardium allows for long-term persistence of cCICs

Empirical testing for intramyocardial injection of approximately 5 000 cCICs in a time course ranging from P0 to P5 (data not shown) revealed the optimal postnatal stage for engraftment and persistence was P3 (Figure 2.6a). Assessment of cCIC fate performed every 7 days until 28 days post-injection (dpi) revealed several distinct features depending upon the time point examined. Patches of mCherry+ cCICs were found within the left ventricular (LV) myocardium at 7dpi with spindle-shaped morphology aligned along host myocardium (Figure 2.6b). Consistent with cCIC phenotype in the fetal heart (Figure 2.6c-d), cCICs in the postnatal myocardium lack expression of cardiac lineage markers for smooth muscle (SMA) or cardiomyocytes (Desmin) at 7dpi (Figure 2.6b-c). Tenascin C (TenC) accumulates in myocardium surrounding persisting cCICs at 7dpi indicative of extracellular matrix (ECM) remodeling response (Figure 2.6d). Patches of cCICs remain in LV myocardium at 14dpi (Figure 2.6e) that form ZO1-associated tight junctions with neighboring host myocardium (Figure 2.6f). Although cCICs intercalate between resident myocytes, the expression of markers for cardiogenic lineage remains absent at 14dpi (Figure 2.6g). Following cCIC fate at 21 and 28dpi showed persistence

at the LV apex region, although cell number was diminished relative to levels at 7 and 14dpi (Figure 2.6h,k). Endogenous mCherry tag fluorescence grew dim at these later time points, requiring immunolabeling to amplify the signal for confocal imaging. Surviving cCICs maintain proximity to cardiomyocytes as well as fibroblast-associated vimentin expression at 21dpi (Figure 2.6i-j). However, a week later at 28dpi the spindle-shape morphology of remaining cCICs becomes increasingly indistinct as distance from cardiomyocytes increases (Figure 2.6l-m). Primary conclusions from postnatal injections of cCICs are 1) remarkable persistence for at least 28dpi, and 2) cell marker expression consistent with fibroblast lineage in the absence of any cardiogenic commitment.

Multiple factors contribute to cCIC persistence in postnatal hearts

Extended persistence in the postnatal heart (Figure 2.6) led to experiments focused upon determining underlying mechanisms of cCIC retention and survival. Three distinct considerations were evaluated: 1) early retention after delivery, 2) ongoing cell cycle activity of engrafted cCICs, and 3) cCICs long term survival and host inflammatory response.

First, early retention following delivery was assessed with injection of 5 000 cCICs into a P3 heart. Percentages of cCICs retained in the neonatal heart at 2 and 48hpi were 36.2±17.0% (1,812±848) versus 33.4±6.2% (1,674±535) as measured by enzymatic digestion followed by flow cytometry for mCherry+ cells (Figure 2.7a-b). To contextualize the retention of cCICs in the neonate, comparative analysis was undertaken following established protocols from our group of 100 000 cells injected intramyocardially at the time of challenge into the infarct border zone of adult (P90) mice [123]. In comparison,

percentage of cCICs retained in the adult infarcted heart at 48hpi was significantly lower at 5.2±1.0% (5,192±954; *P < 0.0001*) (Figure 2.7c) verifying higher fractional initial cell retention in neonatal versus a pathologically injured adult heart.

Second, cell cycle activity of cCICs retained in the postnatal heart was assessed using Fluorescence Ubiquitination-based Cell Cycle Indicator (FUCCI) labeling [42,132] (Figure 2.8a). The FUCCI system consists of two chimeric proteins, mKO-Cdt1 and AzG-Geminin, which oscillate reciprocally during cell cycle, labeling the nuclei in G1 phase orange and those in S/G2/M phases green[132]. During G1/S transition, both probes are present, resulting in a yellow fluorescence (overlaid green and red); during the brief gap between M and G1 phases, neither probe is present and no fluorescence is expressed[132]. Therefore, oscillation between orange and green signals can faithfully track cell cycle status and circumvent the limitation of proliferation markers (Figure 2.8a). CICs were transduced with FUCCI lentiviruses (CIC^{FUCCI}) to employ AzG and mKO oscillation. Only AzG$^+$/mKO$^+$ double positive cells were FACS sorted to ensure that the transduced cells were capable of expressing both FUCCI constructs (Figure 2.8b). To demonstrate cell cycle dynamic of CIC^{FUCCI}, we compared pHH3 and FUCCI dual-fluorescence expression in CIC^{FUCCI} *in vitro*. Proliferating CIC^{FUCCI} stably expressing AzG and mKO are shown in Figure 2.8c-f, whereas pHH3 only labeled cells in M phase (Figure 2.8d-f, white arrows), and failed to label cells that are in G1/S or S/G2 transitions (Figure 2.8d, yellow arrow, AzG$^+$/mKO$^+$/pHH3$^-$; Figure 2.8f, green arrow, AzG$^+$/mKO$^-$/pHH3$^-$). Collectively, FUCCI dual-fluorescence can overcome the limit of pHH3 and faithfully label cycling cells even when they are not in M phase. CICs^{FUCCI} were intramyocardial injected into P3 hearts and

engraft CIC^FUCCI cell cycle status was analyzed by native fluorescence of AzG and mKO. Engrafted cCIC^FUCCI exhibit both AzG and mKO2 fluorescence consistent with G1/S transition (AzG$^+$/mKO2$^+$) as well as G1 phase (AzG$^-$/mKO2$^+$) at 7 and 14dpi (Figure 2.9a-f). In comparison, by 21dpi, the majority of cCICs are AzG$^-$/mKO2$^+$ with only a few AzG$^+$/mKO2$^+$ (Figure 2.9g-i). Thus, cCICs delivered to the postnatal heart undergo cell cycle activity that diminishes between 14 to 21dpi.

Third, cCIC survival and host inflammatory response was evaluated by TUNEL assay and co-immunostaining with the apoptotic marker cleaved caspase-3 (CC-3). Apoptotic activity was absent from cCICs negative for both TUNEL and cleaved caspase-3 (Figure 2.10a-b). Similarly, necrotic marker TNFα$^+$ detected in injection site did not colocalize with remaining cCICs (Figure 2.10c). Inflammatory T lymphocytes (CD3$^+$) infiltrates were undetectable at engrafted cCIC sites at 14dpi (Figure 2.10d), but were found surrounding sparse cCICs at peri-epicardial region at 18dpi (Figure 2.10e). Summing up findings related to persistence, initial retention is improved by cCICs delivery to postnatal hearts where cell cycle activity after engraftment is maintained and cell death avoided, although the maturing host immune response likely antagonizes persistence weeks after initial delivery.

Neonatal cardiac structural and functional development are not compromised by cCIC persistence

Long-term engraftment and persistence of injected cCICs had minimal impact upon host myocardial structure and function assessed by histologic and echocardiographic analyses. Fibrotic remodeling in the region of injected cCICs was not

markedly elevated from normal tissue at 21dpi, with minimal deposition within the apical-pericardial region at 28dpi by Masson's Trichrome staining (Figure 2.11a). cCIC-injected hearts were structurally indistinguishable from PBS-injected control hearts, with gross morphology and myofibril arrangement at injection site, border zone, and remote zone comparable at 28dpi by cardiac Troponin I (cTnI) immunolabeling (Figure 2.11b). Consistent with negligible impact of cCIC delivery upon myocardial structure, ejection fraction (EF) and fractional shortening (FS) were comparable between hearts receiving cCICs and uninjected age-matched controls (Figure 2.11c-d). Collectively, these results demonstrate negligible impairment of myocardial structure or function consequential to cCIC persistence.

Polyploid DNA content of cCIC consistent with extra-embryonic membrane localization following blastocyst injections

Developing embryos are comprised exclusively of diploid cells, whereas tetraploid cells are depleted from the epiblast lineage by mid-gestation stage, excluded from the inner cell mass, and instead reside among the trophoblast layer, contributing to extra-embryonic membranes [145,146]. The extra-embryonic membrane localization of blastocyst-injected cCICs is consistent with tetraploid DNA content of *in vitro*-expanded cCIC [126]. Tetraploid (*4n*) content of cCICs used for this study was confirmed by nuclear DNA content and larger nuclear size compared to sperm (haploid, *1n*) or bone marrow cells (BMC, diploid, *2n*) by flow cytometry and microscopy-based nuclear intensity quantification (Figure 2.12a-c). Thus, we posit that tetraploid exclusion during early embryonic development accounts for the extra-embryonic membrane localization of cCIC

blastocyst injections (Figure 2.12d), demonstrating phenotypic characteristics consistent with limited multipotentiality.

Human CICs in permissive mouse embryos.

Similar to mouse CICs (mCICs), a population of c-Kit[+] CICs were previously identified in adult human heart and were shown to be beneficial in cardiac repair [135,147,148]. The generation of human-mouse interspecies chimera has been experimentally validated with other multipotent human stem cell types, which yielded unequivocal lineage contribution evidence [142]. For example, human iPSC derived multipotent somatic neural crest (NC) cells can functionally integrate into postgastrulation mouse embryos and contribute to NC-associated melanocyte lineage in coat pigmentation [149]. Although interspecies chimera production can be extremely difficult and a rare event to expect, hCIC-mouse chimera could create a feasible experimental system to study hCIC engraftment in a developmentally permissive host environment *in vivo*. Therefore, we aimed to test hCIC engraftment in murine embryonic and neonatal hosts. hCICs were isolated from human cardiac explant obtained during implantation of left ventricular assist device (LVAD). Following isolation, hCICs were culturally expanded, fluorescently tagged with FUCCI constructs, and sorted for mKO/AzG double positivity (Figure 2.13a). Following blastocyst injection, hCICs were found to be retained within the host murine blastocyst by 24hpi, and engrafted into host TE by 48hpi (Figure 2.13b-c). Unlike mCICs, hCICs were not found to be integrated into AM 10dpi, shown by negative immunostaining of human nuclear antigen (HNA) (Figure 2.13d-e). No hCIC was detected in the embryo proper from 11 surviving human-mouse injected embryos (Table 2.1). When delivered

intramyocardially into neonatal mouse heart at P3, hCICs were able to remain active in the cell cycle by 2dpi (Figure 2.13f-g). Collectively, these data revealed that hCICs can recapitulate mCIC's engraftment capability and cell fate in permissive murine recipients.

DISCUSSION

Biological activities of CIC continue to defy simple categorization, due in part to the heterogeneous nature of the population as well as inherent plasticity of individual cells[150,151]. CICs participate in all aspects of myocardial biology from development to maturation, homeostasis to aging, and acute injury to chronic remodeling[107–109]. Regulatory functions of CICs in critical aspects of cardiac biology have spawned multiple approaches to influence their properties and activity with the goal of promoting beneficial action and mitigating maladaptive influences. After more than a decade of intensive investigation using various CICs expanded *ex vivo* to promote myocardial repair [68,118,119] much still remains unknown about adaptation of the cells, particularly with respect to culture conditions or reintroduction to intact myocardium. Even for the extensively characterized cCIC subpopulation, phenotypic properties and changes experienced by culture expanded cells upon reintroduction to a myocardial environment remain largely unknown. Heightened awareness of profound biological changes exerted by limited *ex vivo* culture expansion upon cCICs including transcriptional reprogramming[125] and ploidy alteration[126] emphasized the need to evaluate responsiveness of cCICs to myocardial exposure.

Marginal retention and subsequently poor survival of cCIC injected into adult myocardial tissue is a widely accepted limitation that hampers assessment of cellular biological activities occurring over several days to weeks. The strategy for overcoming this obstacle with *ex vivo* modifications to enhance cCIC engraftment and persistence with concomitant improvements in outcomes has been pursued by our group[123,148,152] and

50

others[153–155]. Many attempts have been made to enhance long-term cell retention, including genetic engineering the donor cells with protective or proliferative molecules [147,148], combinatory delivery with other stromal supportive cell types or adhesive materials [153,154], and repeated dose of cell injections following cardiac injury [155]. All of these efforts gained encouraging yet marginal improvements by primarily focusing on improving the cells, with minimal attention paid to the recipient microenvironment. In all of these models, donor cells were often delivered into pathologically damaged hearts where they encountered with inflammation, cell death, autophagy, vascular dysfunction, and loss of extracellular matrix support [156]. In the heart, CICs reside within a specific stem cell niche, a complex and dynamic microenvironment that directly regulates cell behavior and function during development [157]. In damaged heart, this essential regulation is severely compromised due to chronic inflammation and progressive myocardial deterioration, making it a non-permissive environment for CICs to stick [158]. As a consequence of this hostile microenvironment, transplanted CICs were immediately challenged with compromised cell survival and engraftment. Limited follow up studies can be performed on transplanted cells due to this rapid cell loss, making it almost impossible to interpret cell contribution.

In addition, such "unnatural" solutions to enhance cCIC engraftment and persistence deviate from widely employed methodologies relying upon serial passaging of cells in standard culture conditions without manipulation of environmental conditions or molecular properties [121–123,155]. In the absence of interventions to enhance persistence, an alternative concept is to deliver cCIC to a myocardial environment possessing

conditions that promote retention, growth, survival, and possibly integration. Following this alternative strategy, delivery of cCIC to cardiogenic fetal and neonatal environments should allow for prolonged presence and tracking to assess phenotypic adaptation. Precedents for this concept involving embryonic stem cell chimeras[137,138,142,143,153,159] or fate-mapping of cells introduced into cardiogenic environments [160,161] demonstrate that early developmental stages are particularly suited for assessing pluripotency and cellular plasticity. Thus, three distinct stages of embryonic, fetal, and neonatal development were used to interrogate phenotypic adaptation of cultured cCICs, which provided 4 weeks cell retention and made the direct phenotypic characterization possible.

Embryogenesis is a spatiotemporally exquisite process. Rapid and dynamic cell migration, differentiation, and apoptosis occur at all times. At the blastocyst stage, a small number of blastomeres develop into the pluripotent inner cell mass that gives rise to all three germ layers of the embryonic body for normal somatic and germ-line contribution. The rest of the blastomere differentiates into trophectoderm giving rise to extra-embryonic tissues and supporting embryonic development [137,138]. Exclusion from the inner cell mass (origin of future embryo proper) and integration into trophectoderm (origin of future amniotic membrane) demonstrates a novel facet of cCIC biology (Figure 2.12d). Our results are partially in congruence with a previous report where cell-fusion induced tetraploid hybrid cells contributed to chimera placenta after blastocyst injection [162]. Interestingly, tetraploid hybrids from fibroblast or neural stem cells with ESCs were further shown to differentiate into three germ layers *in vitro* and give rise to somatic tissues of embryo proper *in vivo* while maintaining tetraploid chromosome composition during

chimera development [163,164]. Cultured murine cCICs acquire tetraploid DNA content with serial passaging and override cellular senescence [126]. Therefore, in contrast to the previously reported tetraploid hybrids, our CICs spontaneously become tetraploid without the need of fusion with ESCs, therefore do not carry the required ESCs properties for embryo proper contribution. Indeed, the tetraploid nature of cCICs (Figure 2.12) likely accounts for the mechanism behind engraftment into trophectoderm and amniotic membrane integration (Figure 2.2 and Figure 2.4), since embryo chimerism by blastocyst injection requires karyotypic normalcy of donor stem cells[137]. Tetraploid exclusion from the embryo and polyploidy of extra-embryonic membranes are fundamental biological properties of development[145,146]. Presence of c-Kit+ cells in murine amniotic fluid and in the amnion [165] presents a potential permissive milieu to host transplanted cCICs and a possible mechanism for amniotic membrane engraftment. Similar to findings reported here, extra-embryonic membrane contribution for pluripotent human ES cells follows introduction into murine blastocysts [166]. Intriguing commonality of cardioprotective action from infarction injury shared between cultured cCIC [121,123,147,148,155] and trophoblast-derived stem cells isolated from E3.5 blastocysts [167] suggest additional biological similarities may exist between these cell types. Clearly, incorporation of cCIC into extra-embryonic membranes following blastocyst injection demonstrates E3.5 to be a permissive environment for investigation of cCIC biological adaptation.

Unlike extra-embryonic tissue integration observed in blastocysts, cCICs adopt fibroblast-associated phenotypic traits in prenatal and neonatal hearts (Figure 2.4 and Figure 2.6). Mixed engraftment in multiple sites including cardiac, noncardiac, and extra-

embryonic locations in the prenatal E15.5 environment demonstrates amniotic membrane is still permissive for cCIC engraftment. Furthermore, the developing fetus now tolerates presence of tetraploid cCIC, but without preferential myocardial localization or expression of cardiogenic markers. Instead, persistent cCIC show vimentin expression consistent with fibroblast phenotypic characteristics (Figure 2.4e). It is worth mentioning that the engraftment we observed in neonatal injections was unlikely to be a result of cell fusion events, because the engrafted CICs often appeared in large clusters (ranging from 100-500μm), and the likelihood that hundreds of cell fusion events occurring at the same time and the same location is unexpected. CICs were extensively applied in animal models to treat cardiac injury and gained significant reparative improvement [68,121,123], but their direct contribution to cardiac repair has been questioned. A recent transcriptomic analysis of cell culturing consequences revealed that identity characteristics and heterogeneity in freshly isolated cells are decreased or lost after *in vitro* culturing, accounting for the compromised reparative potential of CICs [125]. Clearly, donated cCIC lack inherent multipotential capacity for direct contribution as tissue-specific cell types within the host, presumably due to loss of identity-markers consequential to *in vitro* culture expansion [125]. Therefore, the microenvironmental impact is critical for CICs.

To date, how CICs interplay with the niche components remains unclear. Many studies suggest that CIC's protective function is mediated primarily through paracrine effects, including secretion of protective signaling and recruitment of endogenous regenerative cells [168–170]. According to this paracrine theory, the local cardiac environment plays a crucial role for proper signal transduction and cell behavior, as well as ECM

mediated cell-cell communication. This intercellular interaction with ECM harbors essential mechanical cues that can lead to systemic and physiological input [165]. The 4-week long-term engraftment observed in neonatal heart opens an adequate time window that allows detailed studies on paracrine effects of CICs and on environmental cues surrounding engrafted CICs with spatiotemporal dynamics. Comparing permissive neonatal hearts versus non-permissive adult heart environments may lead to insights on improving CIC survival and cardiac repair. For example, Bmp can induce cardiac marker Nkx2.5, but maintaining Nkx2.5 expression requires blocking of BMP signaling[15]. Transient BMP inhibition enhances differentiation of c-Kit$^+$ cardiac neural crest progenitors into spontaneously beating EBs [107]. Therefore, a possible approach of ultimate CIC retention and integration may rely on restricting BMP signaling at its lowest gradient. With findings of *in vivo* correlation between c-Kit and BMP activity, damaged host myocardium can be transiently fine-tuned to regulate BMP activity pre-transplantation to coordinate with CICs survival, engraftment, and long-term differentiation. Together, this study paves a way for future studies of environmental influence on plasticity of CICs in the recipient heart.

Efficient chimeric competency relies on pairing donor cell autonomous developmental timing with host organ developmental stages [142–144], a synchrony which is absent when donated cCIC are met with fetal or neonatal environments. Although cCIC fail to demonstrate multipotential commitment, the neonatal environment does allow for long term persistence. Following interaction between cCICs and the developing myocardial environment for weeks after delivery revealed several novel biological

adaptations from both the donated cells as well as the host tissue. This study was designed to follow cell engraftment of exogenous CICs isolated from adult mammalian hearts, whereas previous c-Kit[+] cell lineage tracing models all centralized on endogenous CIC source using transgenic mouse models [107,171,172]. These studies failed to account for the inherent differences between endogenous cells and exogenous cells, with the latter requiring *in vitro* culture manipulation and expansion before transplantation. Despite the difference in cell source, our data is in agreement with a recent publication, which reported that non-myocyte and myocyte segregation occurs at a narrow developmental time window between E10.5 and E11.5, and no non-myocyte to myocyte conversion was observed in later fetal or neonatal stages[131]. Indeed, no direct cardiomyocyte commitment was observed in our engraftment assays at either E15.5 or P3; both timings are later than the segregation window. While we chose to study CICs, our approach is not limited to CICs or the heart, and can be applied to tracking any transplanted cell types tagged by unique fluorescence in other organs. Therefore, information in this study can be used towards lineage tracing of any exogenous cell sources.

The time course of four weeks from a postnatal to early adult heart yielded distinct features correlating concurrent myocardial maturation with cCIC adaptation. Although cell tracking and quantitation of persistence *in situ* can present methodological challenges, these issues were circumvented by following fluorescently-tagged cells in frozen tissue sections to preserve native fluorescence and enable direct visualization without immunostaining. Furthermore, direct fluorescence visualization of FUCCI readouts allowed monitoring of cCIC cell cycle progression in host myocardium. From the outset

when cCIC delivery occurs at the optimal P3 time point, the reparative capacity of the postnatal heart that is present at P1-P2 has largely been lost, coinciding with cardiomyocyte exodus from cell cycle and increases in local ECM stiffness [19,24,173]. Comparable phenotypic traits with cCIC previously found in the fetal context include expression of vimentin but lack of cardiac lineage markers. Innate tissue reaction to the persistence of cCIC at 7dpi is likely represented by accumulation of tenascin C, an ECM component associated with wound healing responses [174–176]. The neonatal myocardium remains permissive for the exogenous cCICs, not only for initial retention (Figure 2.7), but also for ongoing cell cycle activity (Figure 2.9) and survival (Figure 2.10). Engrafted cCICs are well tolerated by the host myocardium up through two weeks after delivery (14dpi), after which withdrawal from cell cycle progression, arrival of adaptive immune CD3+ T cells (Figure 2.10d-e), and diminished morphologic features (Figure 2.6l-m) heralds decline of the donated cCIC population. Persistence by cell fusion in neonatal injections is unlikely since cCICs often appear in large clusters (ranging from 100-500μm), and numerous simultaneous cell fusion events all occurring at the same location would be unprecedented. Cell death due to inflammation, apoptosis, or necrosis is a major cause for post-injection cell loss [177], but scant evidence of these processes in donated cCIC (Figure 2.10) is consistent with their prolonged persistence in the postnatal heart.

Persistence of injected cCIC in neonatal hearts for up to 4 weeks (28dpi) is remarkable given longstanding issues of retention and engraftment in the adult heart. Donated cells are typically lost shortly after delivery with engraftment rates below 5-10% by 24hpi and less than 2% by 48hpi [127–130]. In comparison, initial cCIC engraftment of

36.2±17.0% at 2hpi remained high at 33.4±6.2% by 48hpi in neonatal injections (Figure 2.7). Moreover, histological analyses at the 4 week termination point for the study showed foci of remaining cCICs without fibrotic remodeling, preservation of local cardiomyocyte myofibrillar organization, and negligible impact upon myocardial structure (Figure 2.11). Cardiac function in juvenile mice that matured with engrafted myocardial cCIC possess contractile function indistinguishable from uninjected normal control mice at one month of age (Figure 2.11). Cell tracking and quantification of transplanted cells are challenging after injection. Various approaches have been employed for cell detection in animal models, most of which relied on indirect tracking methods and required post-experimental calculation to obtain cell number. One common method is delivering male CICs into female recipients and following Y-chromosome fluorescence *in situ* for donor cell tracking [129,155]. To determine number of cells retained, real-time PCR-based quantification of a male-specific gene *Rbmy* was used for analysis[128]. Additionally, bioluminescence based imaging, PET, and MRI scans were also commonly used for cell tracking and quantification [178]. All of these approaches require additional experimental steps and are limited with only indirect read-out for cell retention, not to mention that cell morphology and *in situ* analysis are often inapplicable when applying these methods. In this study, we tracked fluorescence tagged cells in frozen tissue sections, in which the native fluorescence was well preserved and readily imaged without immunostaining. Our data provided direct and unambiguous visualization of cell retention *in situ*. With the additional benefit of FUCCI system, the direct fluorescence visualization allowed monitoring of CIC cell cycle progression in host myocardium. For quantification purpose, counting cells

directly through flow cytometry provided a straightforward comparison of cell retention between permissive and non-permissive recipients. Together, using neonatal hearts for CIC engraftment is reliable and feasible method for direct cell tracking and cell counting. Our findings with neonatal cell injections bode well for proposed postnatal and pediatric cell therapy treatments for cardiomyopathy [179–182] where engraftment, persistence, and survival of donated cells should be significantly higher than in adults. The prevailing theory for mechanism of action in cell therapy involves paracrine effects including secretion of protective molecules and activation of endogenous reparative processes[168–170] facilitated by higher retention and persistence of injected cells in the neonatal heart consistent with our results. However, the human heart requires years to fully mature and specific developmental stages and mechanisms for optimal donor cell retention remain to be determined.

Looking ahead, conclusions from this study confirm the influence of microenvironments upon cell fate as well as limited multipotentiality remaining a consideration when using *ex vivo* expanded adult-derived stem cells. Developing hearts and blastocysts are permissive environments for long-term persistence of cCIC, with differential fate outcomes influenced by host tissues. cCIC fate was directed toward fibroblast or extra-embryonic membrane phenotypes. Neonatal hearts developing into adolescence with persistent cCICs were comparable to normal uninjected hearts in terms of myocardial maturation, structure, and contractile performance. Our study represents (to our knowledge) the first demonstration of significant cCIC retention and long-term persistence in a natural damage-free environment. The neonatal heart can therefore

serve as an *in vivo* platform for future studies intended to assess cCIC biological activity and the spatiotemporal dynamics of host myocardium undergoing development and remodeling with exogenously introduced cells.

Table 2.1 Generation of chimeric mice

Cell Source	# of blastocysts transferred	# of embryos	% Viability	# of chimeras	% chimerism	Extent of donor cell contribution to embryo proper
mCIC	1,055	253	24.0%	0	0	None
hCIC	151	11	7.39%	0	0	None
mESC (control)	123	52	42.3%	10	19.2%	Heart, Epidermis, Liver, Somites, Intestines
Total	**1,329**	**316**	**23.78%**	**0**		

Table 2.2 List of Antibodies

Name	Vendor/Catalogue	Dilution
AFP	R&D AF5369	1:100, 1:400 (IB)
CD3	Abcam, ab11089	1:100
CDX2	Abcam, ab157524	1:100
Cleaved Caspsase-3	Cell Signaling, 9661	1:100
cTnI	Abcam, ab56357	1:100
Desmin	Abcam, ab15200	1:100
HNA	Abcam, ab191181	1:100
Laminin	Abcam, ab11575	1:100
mCherry	ThermoFisher, M11217	1:200
Oct3/4	Santa Cruz Biotech, sc-5279	1:25
pHH3 (S10)	Abcam, ab47297	1:100
SM22α	Abcam, ab14106	1:100, 1:500 (IB)
SMA	Sigma Aldrich, A5228	1:100
TenC	RND, MAB2138	1:100
TNFα	Santa Cruz Biotech, sc-52746	1:100
TPM	Sigma Aldrich, T2780	1:100
TUJ	Sigma, T8660	1:400 (IB)
Vimentin	ThermoFisher, PA1-16759	1:200
Vinculin	Sigma, V9131	1:1,000 (IB)
vWF	Dako, A0082	1:200
ZO1	ThermoFisher, 617300	1:50

Table 2.3 List of Primers

| Gene	Forward 5'-3'	Reverse 5'-3'
Oct4	CCAGGCAGGAGCACGAGTGG	GAGAACGCCCAGGGTGAGCC
Klf4	CCTCCCACGGCCCCCTTCAA	ATCTTGGGGCACATGCGCGG
Nanog	AGGCTGCGGCTCACTTCCTTC	AGTCTGGCTGCCCCACATGGA
c-Myc	ACCACCAGCAGCGACTCTGAAG	GGGTGCGGCGTAGTTGTGCT
Nkx2.5	GGCTTTGTCCAGCTCCACT	CATTTTACCCGGGAGCCTAC
Gata4	CCATCTCGCCTCCAGAGT	CTGGAAGACACCCCAATCTC
Gata3	GCCTGCGGACTCTACCATAA	AGGATGTCCCTGCTCTCCTT
Gata6	TACACAAGCGACCACCTCAG	TGTAGAGGCCGTCTTGACCT
Actb	CTCTGGCTCCTAGCACCATGAAGA	GTAAAACGCAGCTCAGTAACAGTCCG
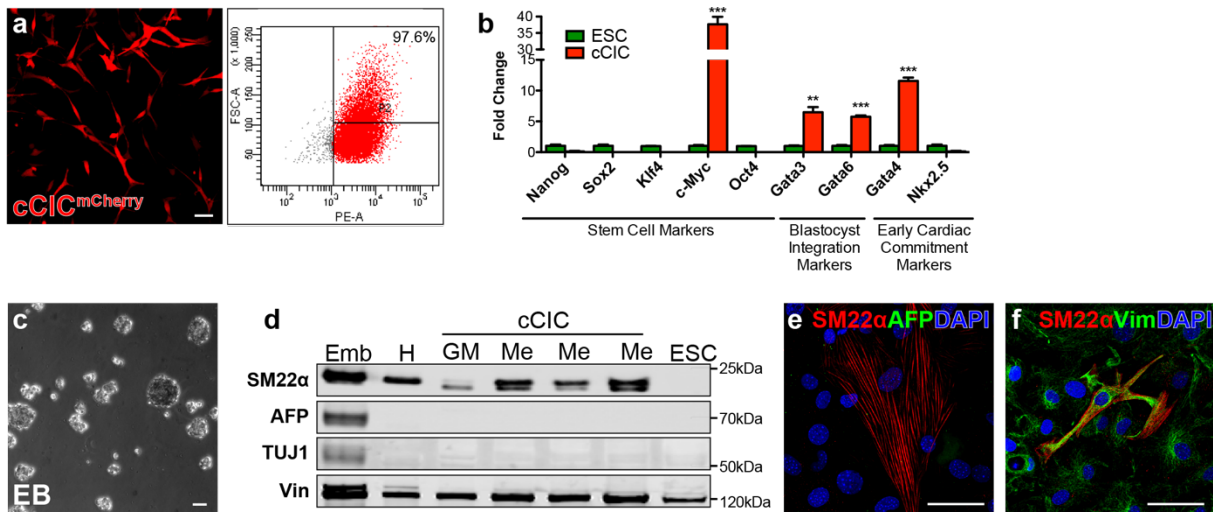
Figure 2.1 Mesodermal potential maintained by cCIC in vitro

(a) Morphology of cCICs isolated from adult heart with lentiviral engineered mCherry fluorescence, flow cytometry plot shows 97.6% cells are mCherry+. (b) Gene expression comparison of stem cell markers, blastocyst integration markers, and early cardiac commitment markers between cCICs and ESCs by qRT-PCR. Mean ± SEM, **P <0.01, ***P<0.0001 vs. ESC, n=4. Unpaired student t test, two-tailed. (c) Morphology of embryoid bodies (EBs) formed by cCICs at day 4 (n = 4). (d) Immunoblotting showing cCICs display mesodermal potential after differentiation for 7 days. Emb: E10.5 whole embryo lysate. H: P30 adult heart. GM: growth media, undifferentiated. Me: Mesoderm induction, differentiated. SM22α: Smooth muscle 22α, mesoderm. AFP: α-Fetoprotein, endoderm. TUJ1: βIII Tubulin, ectoderm. Vin: Vinculin, loading control. (e) Immunostaining showing cCICs are positive for SM22α and negative of AFP expression after 7-day mesodermal induction. (f) Immunostaining showing majority of cCICs express Vim (Vimentin), myofibroblast marker. Scale bar, 50*µ*m.
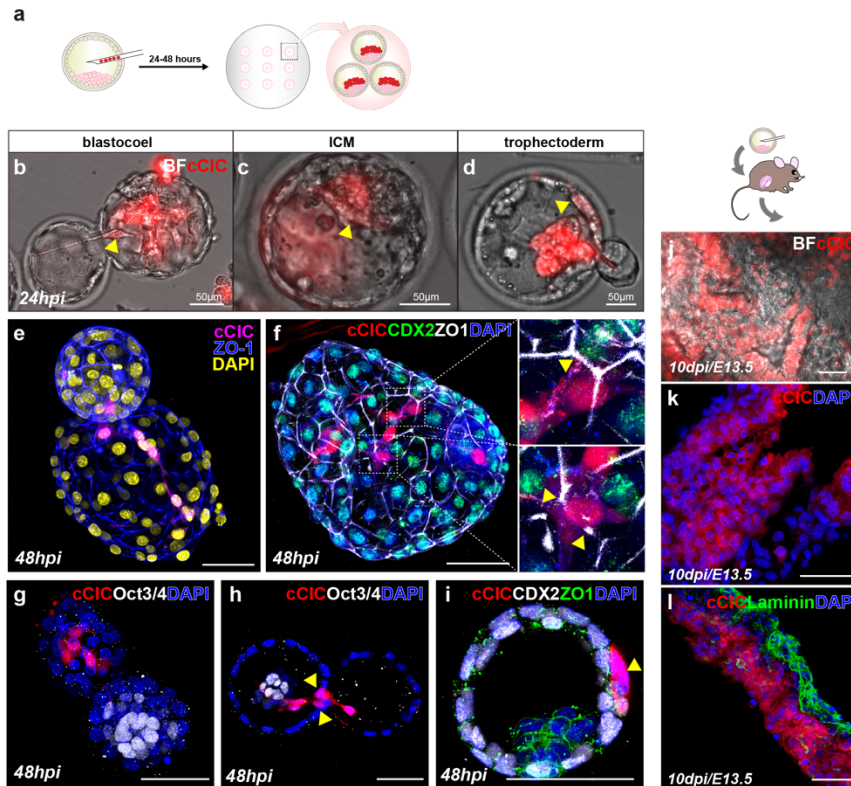
Figure 2.2 cCICs integrate into preimplantation blastocysts and adopted extra-embryonic fate

(a) Schematic of blastocyst injection and *ex vivo* incubation for 24-48 hours. (b-d) At 24hpi, injected cCICs were retained in blastocoel (b, n = 6/11), ICM (c, n = 2/11), and trophoblast (d, n = 8/11). ICM, inner cell mass. See also supplementary online Video 1. (e) At 48hpi, whole-mount immunostaining of injected blastocyst showing cCICs anchored with host cells and spread out as spindle morphology in a hatching blastocyst blastocoel. See also supplementary online Video 2. (f) Left, whole-mount immunostaining of injected blastocyst showing cCICs sharing tight junction (ZO1, white) with host trophectoderm layer (CDX2, green). Right, higher magnification of boxed area. Arrowheads: ZO1 junctions. (g) Immunostaining of ICM marker Oct3/4 (white) showing cCICs do not integrate into ICM. (h) A longitudinal optical section showing nuclei (arrowheads) of cCICs located at trophectoderm layer. (i) Higher magnification of transverse optical section showing cCICs (arrowhead) integrated among nuclei (DAPI, blue) of trophoblasts (CDX2, white), sharing tight junctions (ZO1, green). (j) After uterine transfer into pseudopregnant female, cCICs were detected in a mosaic pattern in extra-embryonic membrane from a chimeric embryo from blastocyst injection at 10dpi/E13.5. (k) Fluorescent scanning of a frozen sectioned extra-embryonic membrane showing mosaic cCICs integration. Nuclei, DAPI, blue. (l) Immunostaining of Laminin showing integrated cCICs localized to the opposite side of epithelial layer of extra-embryonic tissue. Laminin, green. Scale bar, 50μm.
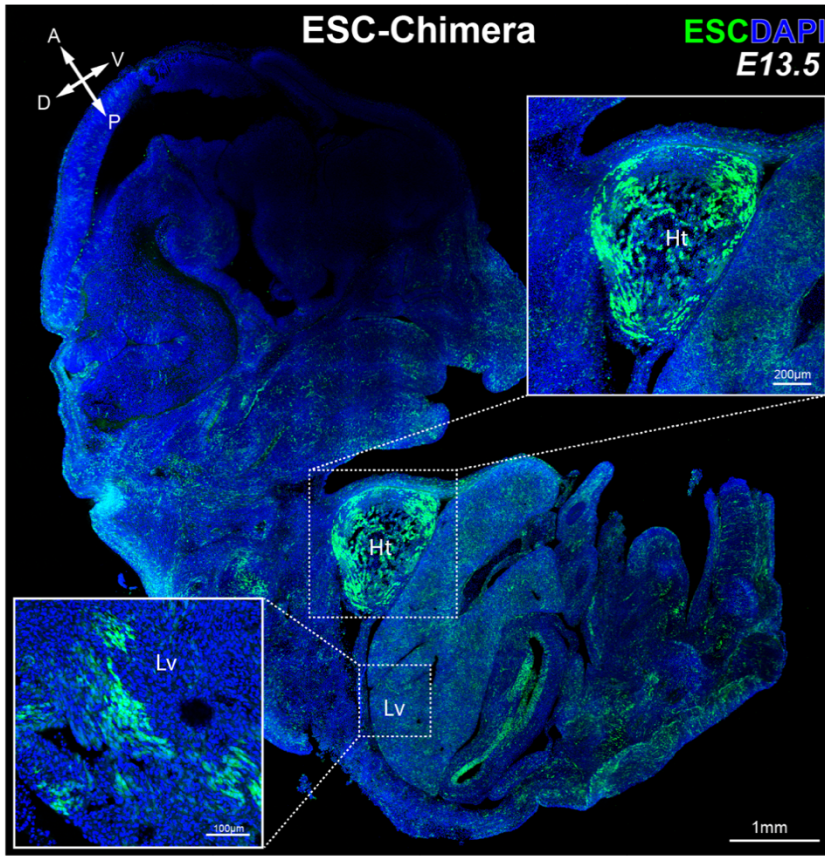
Figure 2.3 Chimera generation by ESCs

E13.5 ESC-Chimera with mosaic ESC-GFP integration pattern. Insets: high magnification of indicated organs. H: heart. Lv: Liver. Cross arrows: anatomical plane. A: anterior, P: posterior, D: dorsal, V: ventral. n = 10/52. Scale bar, 1mm.
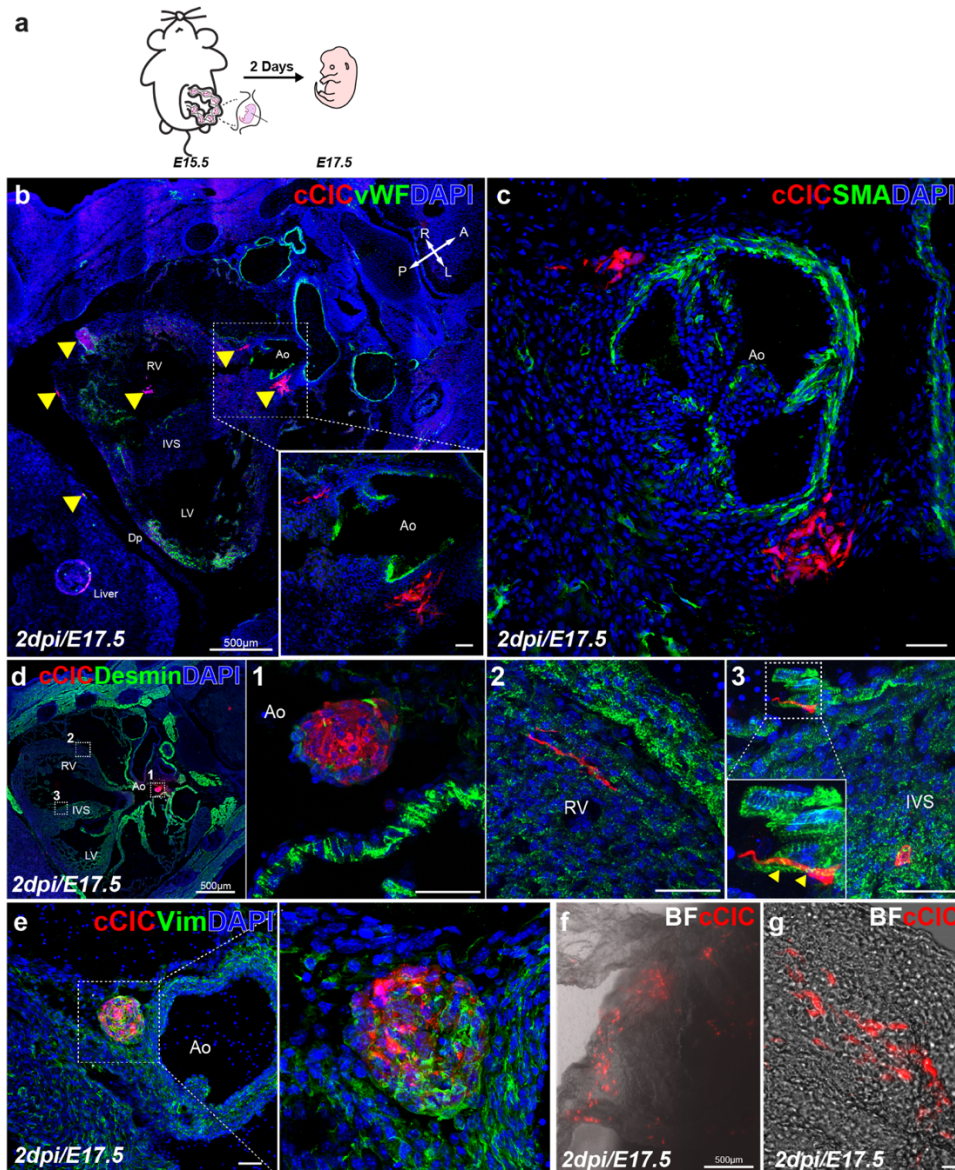
Figure 2.4 cCICs maintained fibroblast-like phenotype and integrated in extra-embryonic membrane following in utero transplantation (IUT)

(a) Schematic of IUT in E15.5 embryos and sample collection at E17.5 (2dpi). (b) Clusters of cCICs are scattered in the heart and nearby extracardiac tissues (arrowheads) (n=4/6). Inset, higher magnification of boxed area. vWF, von Willebrand factor, green. Ao, aorta. LV, left ventricle. IVS, interventricular septum. Cross arrows: indicate anatomical axis: A, anterior. P, posterior. L, left. R, right. (c) Clusters of cCICs at peri-aortic valve region. SMA, smooth muscle actin, green. (d) Immunostaining of cardiomyocyte lineage marker Desmin, boxed area shown in higher magnification in 1 Ao, 2 RV, 3 IVS. (e) Vim staining of a cluster of cCICs showing fibroblast lineage at perivascular region. Vim, Vimentin, green. (f-g) cCICs were detected in extra-embryonic membrane from IUT injected embryo at 2dpi. BF, Bright field. (n = 6/6). Scale bar, 50µm or as indicated.
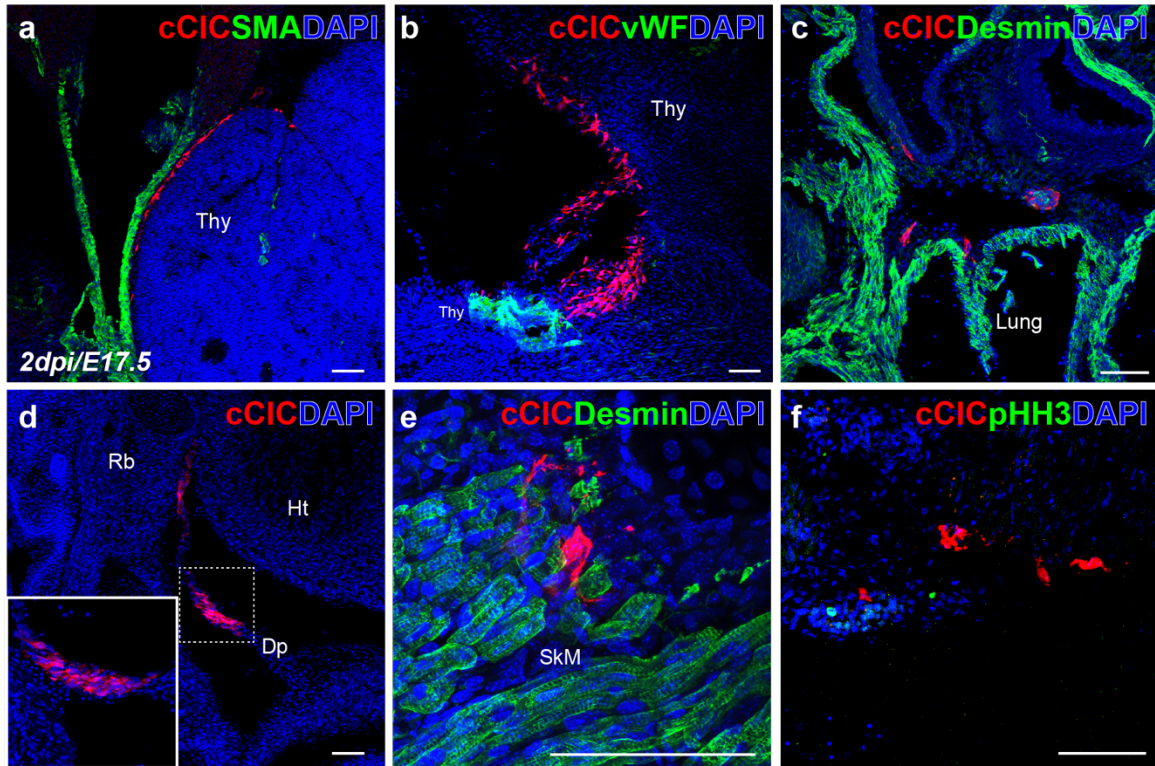
Figure 2.5 IUT delivered cCICs are detected in extracardiac tissues

(a, b) cCICs were found along Thymus. Thy, thymus. (c) cCICs distributed within lung. (d) cCICs integrated into and aligned within diaphragm. (e) cCICs integrated among skeletal muscle. Dp, diaphragm. Ht, heart. Rb, ribs. SkM, skeletal muscle. (f) Immunostaining of proliferation marker Phospho-Histone H3 (pHH3, green) showing cCICs remaining in vicinity of the heart are not in M phase at 2dpi. n = 4/6. Scale bar, 100μm.

Figure 2.6 Neonatal myocardium allows for long-term persistence of cCICs

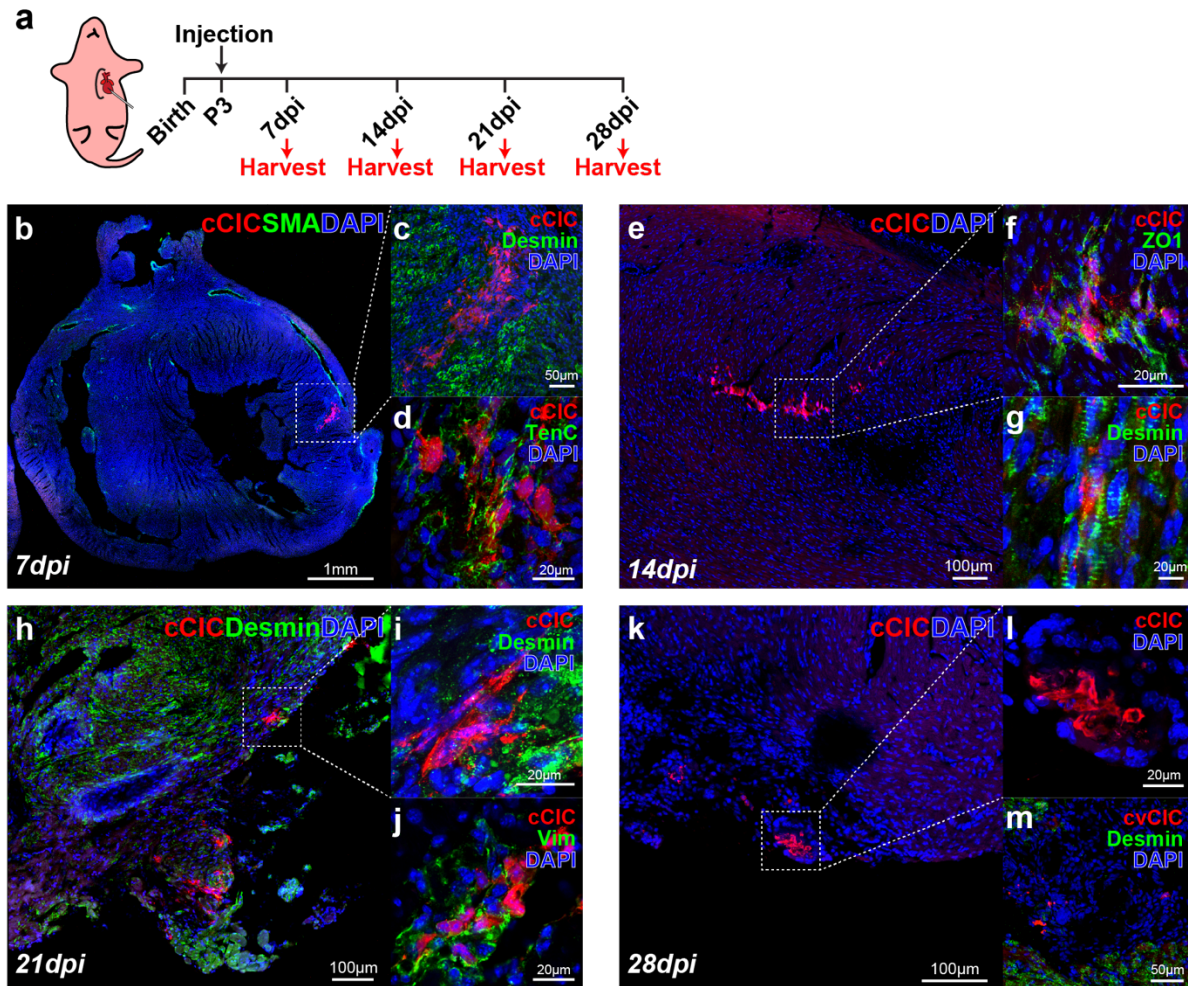(a) Schematic of neonatal injection at P3 and sample collection at 7-day interval for 28 days. (b) Tilescan showing cCICs are retained as patches within left ventricular (LV) wall at 7dpi (n = 5/5). (c) Zoom in of boxed area in (b) showing cCICs do not colocalize with cardiomyocytes (Desmin, green) at 7dpi. (d) cCICs express TenC at early injection period. (e) Tilescan showing cCICs are integrated within LV wall at 14dpi (n = 6/6). (f) Zoom in of boxed area in (e) showing cCICs share tight junctions (ZO1, green) with resident neighboring host cells at 14dpi. (g) cCICs intercalated among resident cardiomyocytes (Desmin, green) at 14dpi. (h) Tilescan of cCICs persistence at LV apex area at 21dpi (n = 9/16). (i) Zoom in of boxed area in (h) showing cCICs spindle morphology and closely localized to neighboring cardiomyocytes (Desmin, green). (j) cCICs continue to express TenC at 21dpi. (k) Tilescan showing cCICs persist at LV apex area at 28dpi (n = 3/3). (l) Zoom in of boxed area in (k). (m) cCICs do not colocalize with cardiomyocytes (Desmin, green) at 28dpi. Scale bar, as indicated.

69
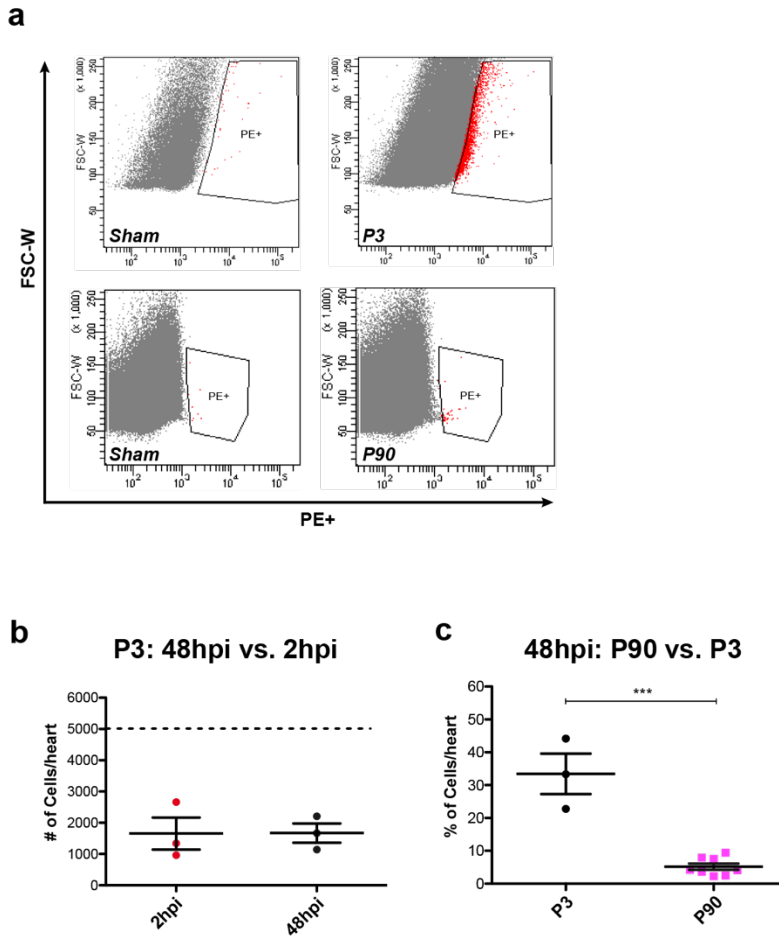
Figure 2.7 Comparison of cell retention between neonatal and adult heart recipient

(a) Representative flow cytometry dot plots of cCIC counts from P3 and P90 injections. Top: P3 injections at 2hpi. Bottom: P90 injections at 48hpi. (b) Number of injected cCICs detected at 2hpi and 48hpi per heart at P3. Dashed line: 5 000 cells injected per heart. Unpaired student t test, two-tailed (n = 3). (c) Percentage of injected cCICs detected at 48hpi per heart. P3: 5 000 cells injected per heart. P90: 100 000 cells injected per heart. Mean ± SEM, ***P <0.0001. Unpaired student t test, two-tailed (n = 3-8 hearts for each group).
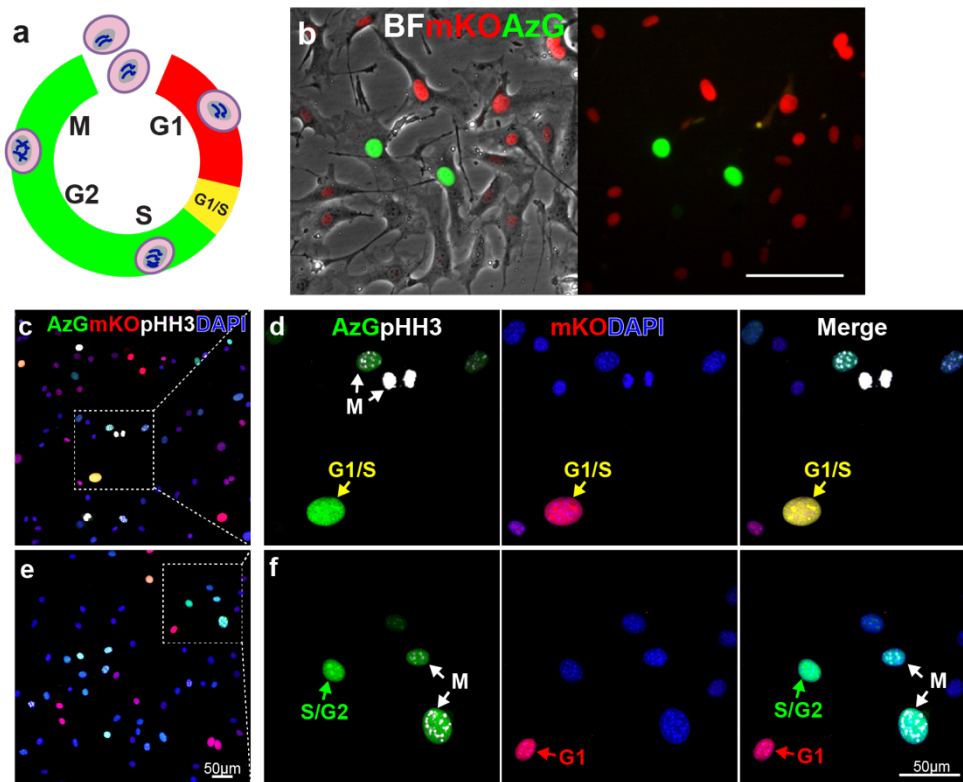
Figure 2.8 Validation of CIC^{FUCCI} in vitro

(a) Schematic of FUCCI fluorescence oscillation and cell cycle progression. (b) Morphology of FUCCI lentiviral engineered cCICs expressing mKO (G1 phase) and AzG (S/G2/M phases) fluorescence. BF, bright field. (c) CICs stably express Geminin-AzG (green) and Cdt-mKO (red) were immunostained with pHH3 (white), inset area is shown in B. (d) A cell in G1/S transition phase is AzG$^+$ and mKO$^+$ but pHH3$^-$ (yellow arrow), whereas a cell in M phase expresses pHH3$^+$/ AzG$^+$ (prophase) or pHH3$^+$ only (telophase) (white arrows). (e) representative image of a different area, inset is shown in D. (f) A cell in S/G2 transition phase is AzG$^+$ only (green arrow), where as a cell in G1 phase is mKO$^+$ only (red arrow).
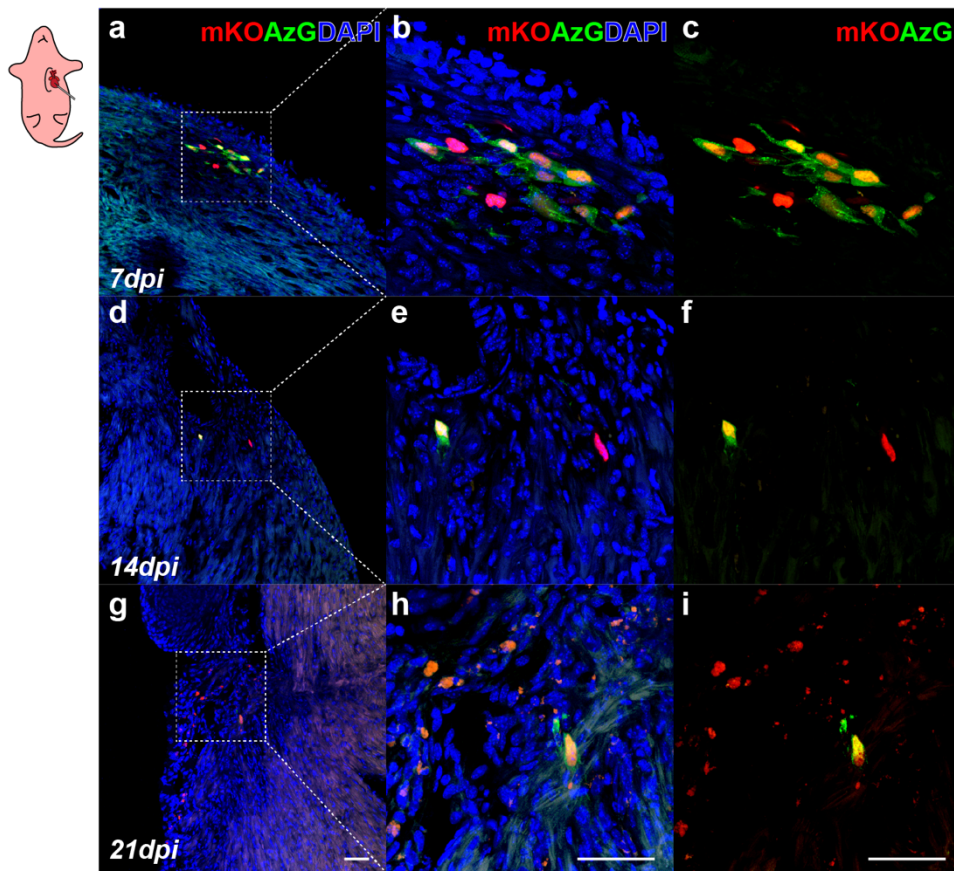
Figure 2.9 Engrafted cCICs remain active in cell cycle for up to 14 days revealed by FUCCI

(a-c) Following neonatal (P3) intramyocardial injection, the majority of cCICs express both mKO and AzG at 7dpi. Boxed area represented in (d, Merged) and (e, mKO and AzG) (n = 3). (d-f) cCICs are still proliferative at 14dpi indicated by AzG expression (green). Boxed area represented in (g, Merged) and (h, mKO and AzG) (n = 3). (g-i) Majority of retained cCICs not proliferative at 21dpi indicated mKO+ (red) AzG- expression (green). Boxed area represented in (j, Merged) and (k, mKO and AzG) (n = 3). Scale bar, 50μm.
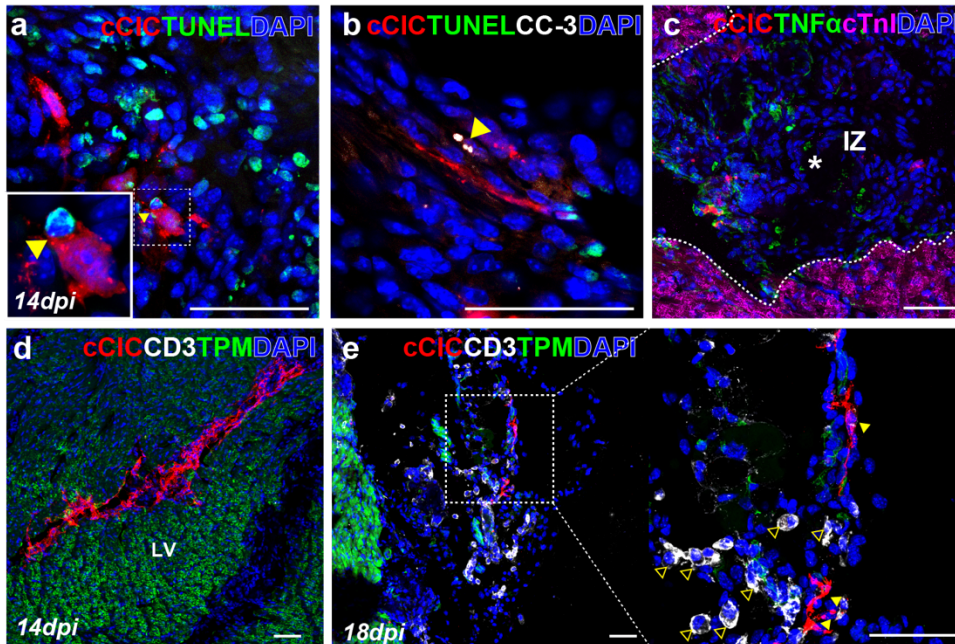
Figure 2.10 cCICs long term survival and host inflammatory response

(a) TUNEL staining showing cCICs do not express TUNEL (green) at 14dpi. Inset: high magnification of a cCIC adjacent to a TUNEL positive cell (arrowhead). (b) TUNEL (green) and Cleaved-Caspase 3 (CC3, white, arrowhead) immunostaining showing cCICs are negative of both apoptotic markers at 14dpi. n = 3. (c) cCICs do not colocalize with TNFα (green) in IZ (*). IZ, injection zone. (d) Immunostaining of CD3 showing no infiltrating T cells around engrafted cCICs at 14dpi. (e) A cluster of CD3+ T cells (arrowhead, clear) was detected surrounding cCICs (arrowhead, yellow) at peripheral region of epicardium at 18dpi. n = 3. Scale bar, 50µm.
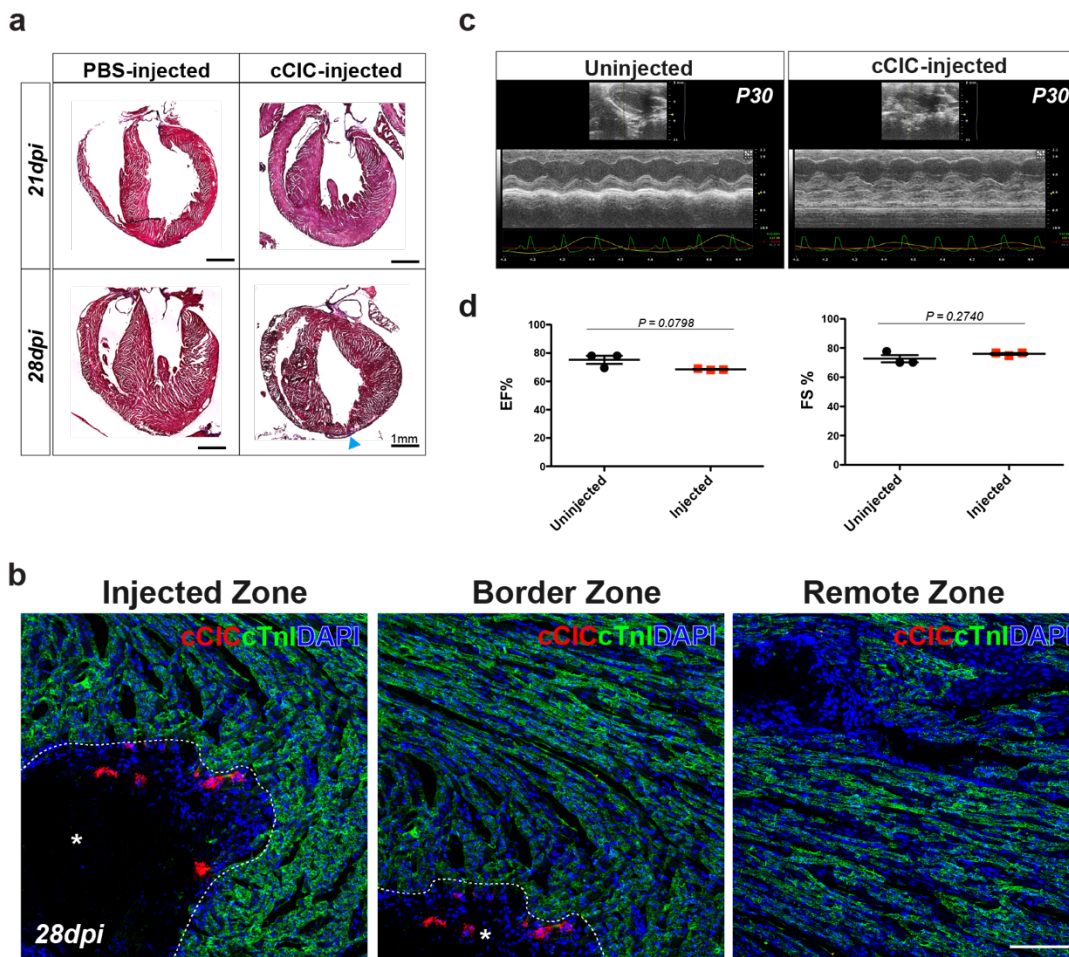
Figure 2.11 Neonatal cardiac structural and functional development are not compromised by cCIC persistence

(a) Masson's Trichrome staining of PBS-injected and cCIC-injected hearts at 21dpi and 28dpi. Small fibrotic area at 28dpi in LV apex (arrowhead). (b) Immunostaining of myocardium (cTnI) surrounding immediate injection zone (left, *), border zone (middle, *), and remote zone (right), showing structure of myocardium is morphologically normal at 28dpi. (c) Parasternal long-axis echocardiography at P30, showing injected hearts are comparable to sham operated animals. Left: Sham, uninjected. Right: cCIC-injected. (d) Cardiac physiological functions are comparable between injected and uninjected animals. EF, ejection fraction. FS, fractional shortening. Unpaired student t test, two-tailed (n = 3 hearts for each group). Scale bar, 100μm.
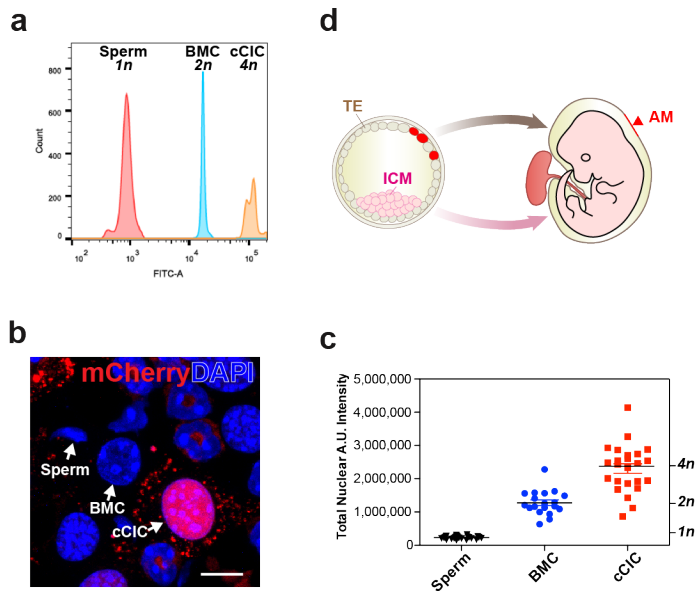
Figure 2.12 Polyploid DNA content of cCIC consistent with extra-embryonic membrane localization following blastocyst injections

(a) cCICs posess tetraploid (*4n)* DNA content relative to sperm (haploid, *1n*) and BMC (diploid, *2n*) as shown by flow cytometry. (b-c) cCICs tetraploidy confirmed by confocal microscopy relative to BMC and sperm. Left, nuclear morphology. Right, quantitation of DAPI intensity (n = 26 for sperms, n = 19 for BMCs, n = 24 for cCICs). (d) Cartoon model showing TE integrated cCICs (red) transitioning into patches in the AM (arrowhead), while ICM primarily give rise to embryo proper (light pink). TE: trophectoderm; ICM: inner cell mass; AM: amniochorionic membrane. Scale bar, 10μm.
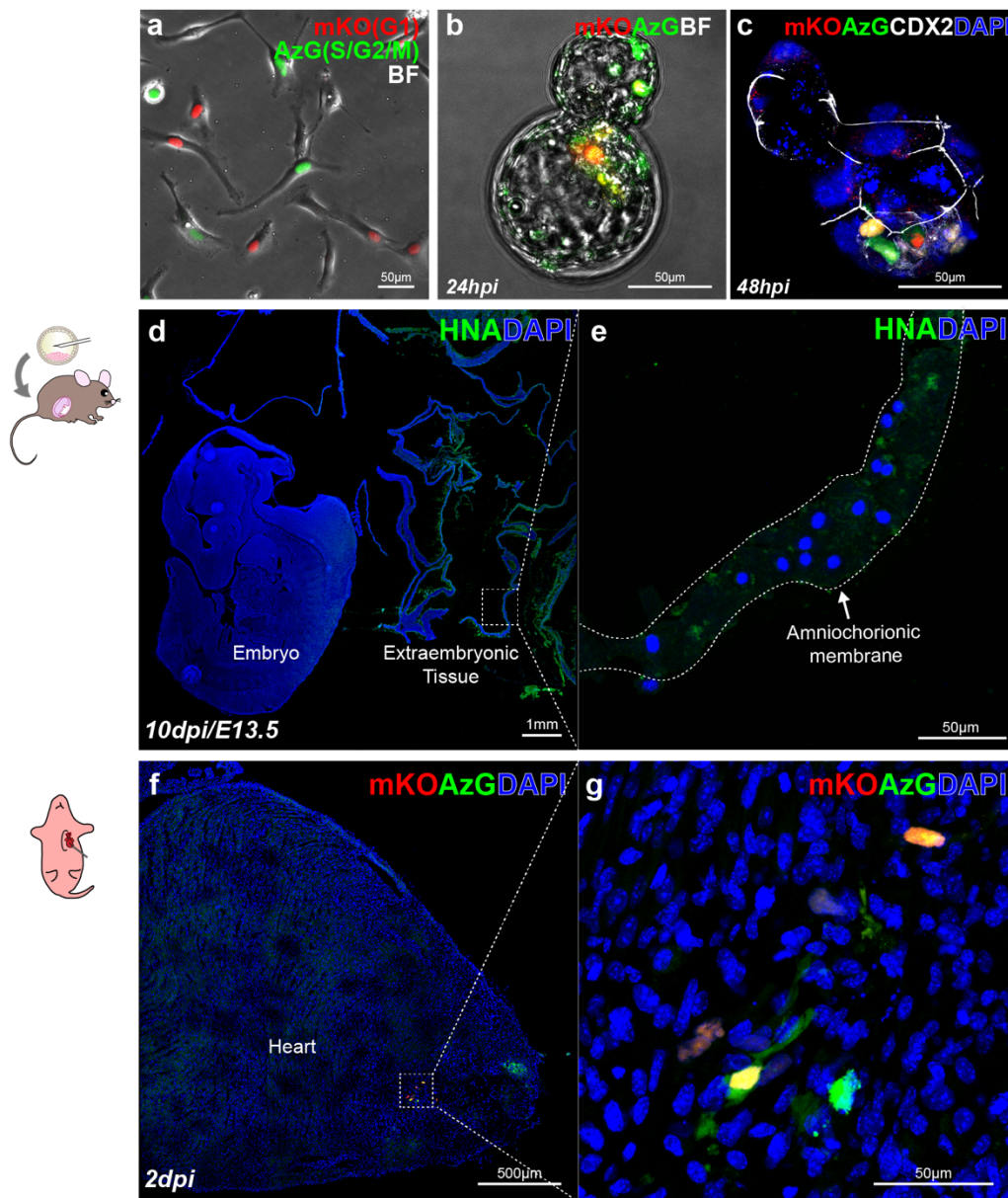
Figure 2.13 Human CICs (hCICs) in permissive mouse embryos

(a) Morphology of hCICs engineered with FUCCI lentivirus expressing mKO (red) and AzG (green). (b) At 24hpi, injected hCICs were retained in blastocyst expressing mKO (G1) and AzG (S/G2/M) fluorescence indicating their cell cycle status. (c) At 48hpi, whole-mount immunostaining of injected blastocyst showing hCICs retained in blastocyst surrounded by trophoblasts (CDX2, white) (n = 5). (d-e) HNA (green) immunostaining was not detected in hCICs injected mouse embryos or AMs at 10dpi (E12.5) (n = 2/2). Boxed area zoomed in (e). HNA, human nuclear antigen. (f-g) Sagittal section of neonatal heart showing hCICs detected from injection at P3, expressing both mKO and AzG as cell cycle indicators (n = 2/8). Boxed area zoomed in in (g).

SUPPLEMENTAL VIDEOS

Supplemental Video 2.1 Z-series of CICs ICM integration

Z-stack series of CICs retained in ICM and blastocoel by 24hpi. Z-size 100μm at 10μm interval. Red, native fluorescent of CICs. BF, bright field of blastocyst.

Supplemental Video 2.2 3D reconstruction of CICs anchoring in blastocyst

Three-dimensional reconstruction of whole-mount immunostaining at 48hpi showing CICs anchored with host cells and spread out as spindle morphology in a hatching blastocyst. Red, native fluorescence of CICs, unstained. Green, CDX2 trophectoderm. White, ZO1 tight junction. Blue, DAPI.

SUMMARY

Biological activities and functional potential of adult cardiac interstitial cells continue to elude simple characterization despite decades of investigation and detailed characterization. We undertook this study to discover phenotypic properties of c-Kit[+] adult cardiac interstitial cells (cCICs) in the context of a cardiogenic environment and to understand the interaction between adoptively introduced cells and the host myocardial environment. Novel findings of long-term cCIC persistence in fetal and neonatal hearts stand in stark contrast to typical findings involving delivery to adult myocardium, and cCIC possess unanticipated capability to contribute to trophectoderm in early embryonic blastocyst development. Following the fate of cCICs in these various developmental stages reveals previously unappreciated aspects of cCIC biology and contributes to resolution of longstanding debates regarding inherent properties of in vitro-expanded cCICs. Collectively, our findings shed important insight into cCIC biology and adaptability as influenced by distinct cardiogenic environments. Given recent increased interest in cell treatment for congenital and pediatric cardiomyopathic conditions, this is the first study to our knowledge to incorporate cardiogenic environmental studies at the embryonic, fetal, and neonatal stage.

Chapter 2, in full, is has been submitted for publication of the material as it may appear in publication. Adaptation Within Embryonic and Neonatal Heart Environment Reveals Alternative Fates for Adult c-Kit[+] Cardiac Interstitial Cells. Bingyan J. Wang, Roberto Alvarez Jr., Alvin Muliono, Sharon Sengphanith, Megan M. Monsanto, Joi Weeks, Roberto Sacripanti, and Mark A. Sussman. The dissertation author was the primary author and investigator of this manuscript [2].

CHAPTER 3

Characterization and Validation of Transgenic Triple Color Reporter Mouse as a

Valuable Lineage Tracing and Cell Fate Model for Cardiomyocytes, Endothelial Cells,

and Smooth Muscle Cells

INTRODUCTION

Cell based therapy has drawn increasing attention in alleviating the effects of cardiac repair. Specifically, transplanted cells as a therapeutic approach has gained beneficial results and became the focus of many scientific endeavors[183–189]. This persistence, along with improved function gives hope to the use of c-Kit+ adult CPCs as a viable therapeutic approach to alleviating the damage caused by myocardial infarction (MI) and rebuilding the myocardium. However, minimal myocardial regeneration, albeit with improved function adds conjecture to adoptive transfer studies involving the use of c-Kit+ CPCs [190]. Although preliminary studies have paved the groundwork and proved these cells valuable, many important basic biology questions still remain regarding c-Kit+ CPCs if they are to be used as a worthwhile source for therapy [171,172,188,191,192].

As understanding CPC fate remains important, technical limitations still remain in current lineage tracking or cell tracking models. Tracking endogenous cell fate requires use of tissue specific promoters to delineate progeny as they commit to cardiogenic lineages. Models for tracking CPC fate typically involve complex breeding schemes where markers are excised or expressed via Cre/FLP recombination with contrasting results. Such models require crosses of two or three multiple mouse strains and administration of recombination reagent with timing restrictions to delimit promoter activity [107,171,172131,193,194]. Therefore, the promoter activity and recombination efficiency are often underestimated, resulting in an oversight of insufficient cell tracing [109]. On the other hand, tracking exogenous cell fate following transplantation requires engineering donor cells

81

with markers for their donor identity. For example, donor cells were often engineered to express fluorophores prior to transplantation (see Chapter 2). Another commonly used technique is to deliver male donor cells into a female recipient, and use the Y chromosome as the unique donor identifier [129,155]. In both methods, donor cells require additional genetic engineering *in vitro* prior to cell transplant. Additionally, cell tracking is limited to the presence of the donor cells, with the lineage adoption of donor cells requiring additional investigation such as immunohistochemistry of cell lineage markers.

To circumvent such limitation, a triple color reporter (TCR) mouse model was created by utilizing three promoters simultaneously that express in adult differentiated cardiac cell types, particularly, cardiomyocytes, smooth muscle cells and endothelial cells. The chosen promoters, alpha myosin heavy chain (αMHC)[42,195,196], smooth muscle myosin heavy chain (SMMHC) [197,198], and Tie2 [199–202] were validated in embryonic and adult tissues with true expression patterns consistent with their endogenous protein counterparts. Each promoter drives a unique fluorophore with a corresponding epitope tag in a promoter-fluorophore-epitope tag combination, providing a unique identifier for each tissue specific lineage. In particular, αMHC promoter drives Venus-HA as a cardiomyocyte reporter, Tie2 drives Cerulean-Myc as an endothelial lineage reporter, and SMMHC drives tdTomato-Flag as a smooth muscle cell specific reporter (Figure 3.1a). The three fluorophores were designed to span the spectra with non-overlapping excitation/emission frequencies, making it possible to screen all three fluorophores simultaneously *in situ.* More importantly, the fluorophore not only indicates the presence of donor cells, but provides a direct and concurrent read-out of the specific lineage

(cardiomyocyte, endothelial cell, or smooth muscle cell) that the donor cell has committed to.

In this Chapter, we report the generation and thorough characterization of transgenic TCR (Tg:TCR) mouse *in vivo* and *in vitro*. The extensive validation provided in this Chapter demonstrates that the Tg:TCR mouse is a valuable platform to study cell lineage and cardiogenesis, as well as a versatile primary cell source for committed tissue specific cell types and uncommitted progenitor cells with cardiomyocyte, endothelial cell, and smooth muscle cell lineage potential.

All animal protocols and studies were approved by the review board of the Institutional Animal Care and Use Committee at San Diego State University.

Tricolor plasmids

For endothelial cell lineage: DNA encoding Cerulean fluorescent protein (Roger Tsien lab, UCSD) was subcloned into pCFP-C1 (Clontech) plasmid in place of CFP through NheI and XhoI sites resulting in CMV-Cerulean-C1. Myc epitope tag DNA was fused immediately downstream of cerulean at the encoded C' terminal to create CMV-Cerulean-3XMyc. For endothelial cell specificity, Tie2 promoter was amplified using PCR and subcloned into CMV-Cerulean-Myc construct in place of CMV promoter, resulting in Tie2-Cerulean-Myc construct (Fig 3.1a)

For smooth muscle cell lineage: The tandem dimer tomato fluorescent protein DNA from pRSETb-td-Tomato (Roger Tsien lab, UCSD) was amplified using PCR to alter the 5' and 3' ends for subcloning; placed into pEGFP-C1 (Clontech) vector in place of EGPF using NheI and XhoI sites, resulting in CMV-tdTomato-C1. Flag epitope tag DNA was fused immediately downstream of tdTomato between XhoI and HindIII sites to create CMV-tdTomato-3XFlag construct. The smooth muscle myosin heavy chain 11 (SMMHC) promoter was amplified using PCR and subcloned in place of CMV promoter to create SMMHC-tdTomato-Flag construct (Fig 3.1a).

For cardiomyocyte lineage: Venus fluorescent protein DNA was placed into pYFP-C1 (Clontech) in place of YFP DNA, resulting in CMV-Venus-C1. A hemagglutinin (HA) epitope tag DNA was fused downstream of venus to create CMV-Venus-3XHA. The

Venus-HA fusion was digested using NheI and HindIII and subcloned downstream of alpha myosin heavy chain promoter (αMHC, a kind gift from Dr. Jeff Robbins, Cincinnati Children's Hospital) to create αMHC-Venus-HA (Fig 3.1a).

The three reporter constructs were individually transfected into HEK293 cells to confirm fluorescent protein/tag fusion by visualization of fluorescence via confocal microscopy (data not shown) and detectability of epitope tag via immunoblotting (used as molecular size controls in immunoblotting in this Chapter).

Molecular cloning and plasmid construction/verification used in this Chapter were completed by Dr. Roberto Alvarez, Jr.

Transgenic mouse generation and genotyping

Each reporter construct was linearized and purified. Fragments containing Tie2-Cerulean-Myc, SMMHC-tdTomato-Flag, and CMV-Venus-HA were mixed at 1:1:1 molar ratio and injected into 0.5dpc embryos and transplanted to pseudopregnant females. Live born pups were genotyped for the presence of all 3 transgenes with forward primer and reverse primer spanning the fusion of promoter and fluorescence protein. Tie2-Cerulean was confirmed by 5' GCC CTG CTG ATA CCA AGT GCC TT 3'(Fw) and 5' TCA GGG TCA GCT TGC CGT AG 3' (Rv); SMMHC-tdTmt was confirmed by 5' GGG TGG TGG TGG TAC ATG CCT G 3' (Fw) and 5' CAT GCC CCA GGA ACA GGT CGT 3' (Rv); αMHC-Venus was confirmed by 5' GAA TCA CAC CTG GGG TTC CC 3' (Fw) and 5' TCA GGG TCA GCT TGC CGT AG 3' (Rv). oIMR8744 5' AAA TGT TGC TTG TCT GGT G 3' and oIMR8745 5' GTC AGT CGA GTG CAC AGT TT 3' (Jackson Laboratory) were used as internal positive control (IPC) for integrity of mouse genomic DNA. Founder line 7 was

confirmed to express all three transgenes and was backcrossed to FVB wild type mouse for ten generations (7N10) to confirm stable transgene expression in germ line.

Pronuclear microinjection, founder screening, and generation of 7N10 Tg:TCR mouse were completed by Dr. Roberto Alvarez, Jr.

Immunoblotting

Mice were heparinized (Sigma-Aldrich H3393) by intraperitoneal injection (10Unit/g) and euthanized at harvest time points. For animals younger than 14 days, euthanasia was carried out by anesthetization on ice followed by decapitation. For animals at 14 days and older, euthanasia was carried out by isoflurane overdose followed by cervical dislocation. Organs were collected and immediately snap frozen in liquid nitrogen. Next, frozen tissues were homogenized in 10μL/mg RIPA lysis buffer (ThermoFisher, 89901) with freshly added proteinase inhibitor and phosphatase inhibitor cocktails (Sigma P0044, P8340, P5726) for 30min on ice with intermittent vortexing. Cell lysates were then centrifuged for 10min at 11 000g at 4°C to remove insoluble debris. Supernatants were quantified with Bradford assay (ThermoFisher, 23236) and 20μg lysates were run on 4-12% Bis-Tris protein gels (Invitrogen, NP0335BOX) and transferred onto PVDF membrane (Millipore, IPFL00010), followed by blocking in Odyssey Blocking Buffer in TBS (LI-COR, 927-50000) for 1 hour at RT. Antibodies were diluted in Blocking buffer supplemented with 0.2% Tween-20 to increase specificity. Primary antibodies (anti-Myc tag, ThermoFisher A21281, 1:500; anti-Flag tag M2, Sigma F1804, 1:1,000; anti-HA tag, Santa Cruz Biotechnology sc7392, 1:500; anti-vinculin, Sigma V9131, 1:2,000; anti-GFP, Rockland 600-101-215, 1:500; anti-Hsp60 N20, Santa Cruz Biotechnology sc-1052

1:500;) were incubated overnight at 4ºC and secondary antibodies (1:1,000) for 90min at RT. Immunoblots were scanned with LI-COR Odyssey Clx system.

Immunofluorescence staining

Animals were euthanized as described above followed by brief perfusion with PBS and 1% paraformaldehyde (PFA) (ThermoFisher, 28908) before organ removal. Tissues were fixed in 1% PFA immersion for 2 hours at RT and dehydrated in 30% sucrose in PBS overnight at 4ºC, then in OCT+30% Sucrose mix at 1:1 ratio, before mounting in NEG50 and frozen on dry ice. Frozen sections were cut at 12-16μm thickness and collected onto Superfrost glass slides. Sections were allowed to dry for 48 hours prior to storage at -20ºC. Following equilibrium at RT for 5min and brief rehydration in PBS, frozen tissue sections were incubated in permeabilization solution (0.1% Triton X-100, 0.1M Glycine, 1% BSA in PBS) for 30 minutes at RT, then blocked in blocking solution [10% Donkey Serum (Millipore, S30-100mL), 0.1M Glycine, 1% BSA in PBS] for 1 hour at RT. Antibodies were diluted in blocking solution.

For paraffin sections, tissues were perfused with PBS and 10% formalin (Sigma, HT501128-4L) before organ removal. Tissues were fixed in 10% formalin overnight at RT and processed for paraffin embedding. Paraffin sections were cut at 5μm thickness. Following deparaffinization and antigen retrieval, tissue slides were blocked in TNB solution (Perkin Elmer, FP1012) for 1 hour at RT. Antibodies were diluted in TNB solution.

Cells cultured on chamber slides were fixed in 1% PFA for 20min at RT, permeabilized for 15 minutes and blocked in blocking solution (10% Donkey Serum, 0.1M

Glycine, 1% BSA in PBS) for 1 hour prior to antibody staining. Antibodies were diluted in blocking solution.

Following blocking, samples were incubated overnight in primary antibodies at 4ºC (anti-Flag tag, Cell Signaling, 14793S, D6W5B, 1:100; anti-HA tag, Santa Cruz Biotech, sc7392. 1:100; anti-Myc tag, Thermo Fisher, A21281, 1:100; anti-GFP, Rockland, 600-101-215, 1:100; anti-Cyan/eCFP/GFP, TaKaRa Living colors, JL-8, 632381, 1:50; anti-tdTomato, Sicgen, Ab8181-200, 1:100; anti-CD31, Abcam ab28364, 1:50; anti-cTnT, Thermo Fisher, MA5-12960, 1:100; anti-Desmin, Abcam, ab15200, 1:100; anti-SM22α, Abcam, ab14106, 1:100; anti-Vimentin, ThermoFisher, PA 1-16759, 1:200), washed in PBS (frozen section, chamber slides) or TN (paraffin sections), and incubated in secondary antibodies (1:100) for 90 minutes at RT. DAPI (Sigma-Aldrich D9542, 0.1μg/mL), To-pro3 (ThermoFisher T3605, 0.1μM), Draq5 (Abcam ab108410, 1:100), or Draq7 (Abcam, ab109202, 1:100) were used as nuclear staining at the choice of various wavelength compatibility. Slides were mounted in 70% Glycerol in PBS and imaged by Leica SP8 confocal microscopy.

Neonatal mouse ventricular cardiomyocytes isolation

Neonatal cardiomyocytes were isolated as previously described with modification [203]. Briefly, a total of 6 P2 hearts were excised and atria removed, pooled, and incubated in 20mM 2,3-Butanedione monoxime (BDM, Sigma B0753, in PBS) with 0.125% trypsin/EDTA (ThermoFisher 25200056) overnight at 4ºC. After 16-20 hrs, hearts were digested in 7-10mg Collagenase II/Dispase (Sigma 10269638001) at 37ºC for 20min in 80rpm shaker. Next, ventricles were triturated 20 times and allowed to settle by gravity.

Supernatant was passed through a 70μm strainer, while the undigested tissue debris was mechanically minced, and digested again in Collagenase II/Dispase at 37ºC for additional 15min in 80rpm shaker. Dissociated cells were pelleted by centrifugation at 100g for 5min and plated in plating medium (5% Fetal Bovine Serum (FBS), 10% Horse Serum (HS), 19% M-199 media, 1X Pen/Strep, in 1X DMEM) on tissue culture plate, incubated at 37°C, 5% CO2 for three hours to remove non-cardiomyocytes. Supernatant containing cardiomyocytes was plated onto laminin coated 35mm glass bottom tissue culture dishes or 2-well chamber slides in plating media overnight to allow attachment. Next day, media was changed to maintenance medium (4% HS, 17% M-199 media, 1X Pen/Strep in 1X DMEM) for further incubation.

Adult cardiomyocytes and CICs isolation

Cardiomyocytes and CICs were simultaneously isolated as described in Chapter 2. Briefly, adult Tg:TCR hearts were enzymatically digested on a Langendorff system (Radnoti) with Collagenase type II (Worthington, LS004147, 230Unit/mL), minced and triturated, and filtered through 100μm cell strainer and separated from non-myocytes by gravity sedimentation. Cardiomyocyte and non-myocyte fractions were serially collected from three subsequent digestions, sedimentation, and filtration. Cardiomyocytes were plated on Laminin coated glass dish for 2 hours and rinsed briefly in PBS before imaging. Non-myocyte fraction was further filtered through 40μm and 30μm cell strainer, then sorted for Lineage depleted, CD45 depleted, and CD117+ CICs by MACS (magnetic-activated cell sorting) following manufacturer's protocol (Miltenyi, #130-110-470, #130-052-301, #130-091-224).

CICs growth and differentiation

Lin⁻CD45⁻CD117⁺ CICs were cultured in growth medium (DMEM, 10% embryonic stem cells FBS, 1% insulin-transferrin-selenium, leukemia inhibitory factor [10 ng/mL], basic fibroblast growth factor [10 ng/ml], epidermal growth factor [20 ng/mL], L-glutamine [0.07mg/mL], 1% penicillin-streptomycin-glutamine). For further expansion, adherent cells were passaged and expanded when 40% confluency was reached. For cell aggregation, 2.75×10^6 CICs were plated in 5mL EB medium [KnockOut DMEM (Gibco 10829-018) supplemented with 15% KnockOut Serum Replacement (Gibco 10828-028), 0.1mM MEM Non-Essential Amino Acids Solution (Gibco 11140-050), 1X GlutaMAX-I (Gibco 35050-079)] in low-attachment petri-dish for 4 days. For mesoderm induction, CIC-EBs were transferred to AF (ThermoFisher, S006100) coated tissue culture dish or chamber slides in EB medium supplemented with 10% ES-FBS to allow attachment overnight, followed by mesodermal induction media [IMDM (Gibco, 31980030) and Ham's F12 (HyClone, SH30026.01) supplemented with 5ng/mL Activin A (Peprotech, 120-14E), 0.5ng/mL BMP4 (Peprotech, 120-05ET), 5ng/mL human VEGF (Peprotech, 100-20) and 1X Pen/Strep (Gibco, 15140163)] for 24 hours, cardiac induction media [StemPro-34 SFM medium (Gibco, 10639011) supplemented with 2mM L-glutamine (Gibco, 25030081), 0.5mM Ascorbic acid (Sigma-Aldrich, A4403-100MG), 5ng/mL human VEGF, 10ng/mL human basic FGF, and 50ng/mL human FGF10 (Peprotech, 100-26)] for 7-21 days. All culturing conditions were kept in humidified incubator at 37°C with 5% CO_2. Subsequently, cells were washed twice in cold PBS and fixed in 1% PFA for immunocytochemistry.

Matrigel tube formation

Growth factor reduced Matrigel (Corning, 356231) was used to coat an 8-well glass chamber slide (150μL/well) and incubated for 30min at 37°C. CICs were plated in duplicate at 7,500 cells/well suspended in 100μL EBM-2 basal medium (Lonza, CC3156) supplemented with human vascular endothelial growth factor (hVEGF) (Peprotech, 100-20, 5ng/mL) and incubated on a stage-top incubator (Oto, 5% CO_2, 37°C) for time lapse recording for 24 hours. At the end of recording, Matrigel was dissolved in cold PBS/EDTA and differentiated cells was collected by centrifugation. Cell pellets were then processed for protein lysis and immunoblotting.

Smooth muscle cell isolation

Vascular smooth muscle cells (VSMCs) were isolated as previously described with modification [204]. Briefly, following euthanasia, the 1-2cm of inferior vena cava (IVC) was excised and adventitia was dissected and discarded. The smooth tube of IVC was then minced into 1-2mm pieces and digested in 200μL collagenase type II (230Unit/mL) for 4 hours at 37°C. Cell pellet was collected by centrifugation at 300g for 5min. All cells were resuspended and plated in SMC media (DMEM, 10% FBS, 1X PSG, 1X Fungizone).

Fluorescence activated cell sorting (FACS)

Single cell resuspension was analyzed using BD FACSMelody cell sorter. Cells isolated from non-transgenic littermate were used to exclude auto-fluorescence disturbance, and cultured HEK293 cells transfected with injection construct (expressing single fluorescence) were used as positive gating to establish fluorescence levels.

RESULTS

Generation and native fluorescence expression of Tg:TCR mouse

Three plasmid constructs were engineered to express a unique fluorophore and epitope tag under each tissue specific promoter for lineage tracing. For endothelial cell lineage, the expressions of cerulean fluorescence and Myc tag are driven by Tie2 promoter [199–202]. For smooth muscle lineage, the expressions of tdTomato (tdTmt) fluorescence and Flag tag are driven by smooth muscle myosin heavy chain 11 (SMMHC) promoter [197,198]. For cardiomyocyte lineage, the expression of venus fluorescence and HA tag are driven by α-myosin heavy chain (αMHC) promoter [42,195,196] (Figure 3.1a). Three linearized transgene constructs, Tie2-Cerulean-Myc, SMMHC-tdTomato-Flag, and αMHC-Venus-HA were co-injected into 0.5 days post coitum (dpc) FVB/NJ embryos at 1:1:1 molar ratio and uterine transferred to pseudo-pregnant females (Figure 3.1a). Germline transmission was verified by backcrossing potential founders that are positive of all three transgenes to FVB/NJ non-transgenic mice. Founder line 7 was selected as it faithfully carries all three transgenes in a co-segregation fashion. After 10 generations of backcrossing, Transgenic Tricolor (Tg:TCR) mouse line (7N10) was established and used in experimental procedures. The three transgene expressions were confirmed by PCR and immunoblotting (Figure 3.1b-c). Cardiomyocyte specific venus-HA expresses robustly in the heart and weak expression was detected in the lung as previously reported [205]. Endothelial reporter cerulean-Myc and smooth muscle reporter tdTmt-Flag were detected in heart, lung, and stomach (Figure 3.1c). The three fluorescence signals were designed to span spectra without overlapping in excitation/emission (Ex/Em), allowing

concurrent detection of all three transgenes. Confocal microscopy confirmed native

fluorescent expression in frozen cardiac tissue, in which cerulean (Ex433/Em475, cyan),

venus (Ex515/Em528, blue), and tdTmt (Ex554/Em581, red) were sequentially scanned

and verified (Figure 3.1d-e). Additionally, each fluorophore expression was exclusive to

its own lineage (Figure 3.1e). Cerulean, as endothelial reporter, was found in vascular

endothelium and capillary vessels (Figure 3.1e'). Venus, as cardiomyocyte reporter,

expresses exclusive to cardiomyocyte (Figure 3.1e''). tdTmt, as smooth muscle cell

reporter, was detected in vascular smooth muscle layer (Figure 3.1e'''). To further

examine if TCR expression is exclusive to lineage specificity, serial frozen heart sections

were co-stained with antibodies against each epitope tag, fluorophore, and lineage

specific marker to confirm co-expression *in situ* (Figure 3.1f-h). Indeed, Flag tag, tdTmt,

and smooth muscle 22-α (Sm22α) were only detected in smooth muscle cells (Figure

3.1f-f'''). HA tag, venus (stained by anti-GFP antibody), and cardiomyocyte marker

cardiac troponin T (cTnT) were only detected in cardiomyocytes (Figure 3.1g-g'''). Myc

tag, cerulean, and endothelial marker CD31 were only detected in vascular endothelium

and capillary vessels (Figure 3.1h-h''').

Immunochemistry on paraffin sections further verified the tissue-specific transgene

expression. As native fluorescence is lost after tissue processing, paraffin sections allow

the feasibility of three or more antibodies to be applied on the same section as a more

stringent colocalization determination. Immunostaining of HA, Myc, and Flag tags was

consistent as seen in native fluorescence, whereas HA tag was specific to

cardiomyocytes, Flag tag was expressed in vasculature, and Myc tag was found in

vascular endothelium (Figure 3.2a-a'''). Lineage specific staining further confirmed transgene expression is exclusive to each promoter specificity (Figure 3.2b-d).

Collectively, Tg:TCR allows direct visualization of tri-lineage tracing *in vivo* through direct simultaneous detection of cerulean, tdTmt, and venus with their representative tissue specificity.

Tricolor expression in non-cardiac organs

Endothelial and smooth muscle cells locate in various organs in addition to the heart. We next examined if TCR expression can be detected in non-cardiac organs. Indeed, Myc tag was detected in medulla and cortex regions in kidney (Figure 3.3a). Native fluorescence cerulean and tdTmt were expressed in kidney vasculature (Figure 3.3b). Although αMHC is predominantly used as cardiomyocyte specific marker in the heart, it has been reported to be expressed in the thick wall of the pulmonary veins of the lung [205]. All three native fluorescence signals were detected in the lung, whereas venus expression was restricted to pulmonary veins, while tdTmt was expressed in pulmonary arteries. Cerulean was detected in all vascular endothelial linings (Figure 3.3c-c'''). Bladder as a smooth muscle cell-rich organ [206], displayed robust tdTmt expression but not venus or cerulean (Figure 3.3d-d'''). Collectively, these data demonstrate that Tg:TCR transgenes are expressed in endothelium, αMHC positive tissues, and smooth muscle cells not only in the heart, but also in non-cardiac organs.

Tg:TCR serves as a cell lineage reporter during development

Developing heart is composed of premature cardiomyocytes and non-myocytes (including progenitor or precursor cells) during heart formation. Recent study reported

that the non-myocyte to cardiomyocyte segregation occurs between E10.5 and E11.5, and no αMHC expression was detected prior to E12.5 [131]. To provide a direct visual tracing of mature cardiomyocytes during cardiogenesis, E10.5 Tg:TCR embryos were collected and examined for native fluorescence (Figure 3.4a,d). To our surprise, venus was detected in the developing atria region (Figure 3.4b-c). Upon closer examination, venus positive cardiomyocytes exist in the developing myocardium in E10.5 heart (Figure 3.4e-e'''). This finding advanced the early onset of αMHC for 2 days, indicating that Tg:TCR is a more direct and a more sensitive reporter model for cardiomyogenesis and lineage tracing studies.

αMHC as a mature cardiomyocyte marker, is commonly believed to become predominant during early postnatal development [207]. We compared P3 and P7 postnatal hearts for their native venus expression. Consistent with previous reports, venus was restricted to atrial area in P3 heart and only sparsely expressed in ventricular and apex region (Figure 3.4e). By P7, venus expression became predominant in ventricle and apex, while atrial expression was maintained (Figure 3.4f). These data prove that Tg:TCR is a faithful reporter model for studies in postnatal heart maturation.

Tg:TCR provides concurrent primary cell source for lineage specific cell types

To continue validating Tg:TCR reporter *in vitro*, native fluorescence was examined in cardiomyocytes and vascular smooth muscle cells. Venus fluorescence was visible in some but not all neonatal cardiomyocytes isolated from P2 hearts (Figure 3.5a-a'''), consistent with the observation *in vivo* as shown in Figure 3.4. Interestingly, tdTmt signal was observed in neonatal cardiomyocyte, suggesting a role of SMMHC activity may exist

in myocyte maturation (e.g. myofibroblast transdifferentiation) or during βMHC to αMHC conversion (Figure 3.5a-a'''). In adult cardiomyocytes, almost all disassembled adult cardiomyocytes expressed venus fluorescence (Figure 3.5b-c), demonstrating the specificity and sensitivity of this reporter line. tdTmt fluorescence was expressed in 12.2% of vascular cells isolated from *inferior vena cava* (IVC) and was maintained in culture condition (Figure 3.5d-e). Therefore, Tg:TCR reporter provides a platform for simultaneous multi-lineage primary cell studies *in vitro*.

TCR fluorescence as a direct read-out for in vitro lineage differentiation

Conventional *in vitro* differentiation verification relies upon immunostaining of lineage specific marker, which requires termination of differentiation process and lineage immunostaining of cells. Tg:TCR reporter provides direct visualization of cell lineage adoption as a surrogate of promoter activity, therefore it can be used as a versatile cell source to study uncommitted stem cell fates *in vitro.* As such, we hypothesized that if differentiated cells begin to turn on promoter activity, then the tricolor reporter fluorescence should become visible during differentiation.

To test if native fluorescence would become positive upon differentiation, CICs[TCR] were subjected to various lineage differentiation *in vivo.* First, CICs[TCR] were plated on Matrigel to induce endothelial tube network formation and recorded cerulean emergence via live imaging. Prior to the induction, CICs[TCR] were negative of any fluorescence (Figure 3.6a). Within 24 hours of induction, CICs[TCR] formed vasculature in Matrigel, demonstrating their endothelial lineage potential (Figure 3.6b, Supplemental Video 3.1). More importantly, cerulean became visible at 16-24 hours (Figure 3.6c, Supplemental

Video 3.2). To exclude the possibility of Matrigel autofluorescence, differentiated CICs^{TCR} were harvested for immunoblotting analysis. Both Myc tag and cerulean transgenes (probed by anti-GFP antibody) were expressed after 24 hours differentiation (EnM) whereas both levels before differentiation were undetectable (GM) (Figure 3.6d). Next, CICs^{TCR} were induced to form embryoid bodies (EB) and cultured in mesoderm induction media. Differentiated cells became round and flat, reassembling the typical morphology of smooth muscle cell, drastically different than the skinny/spindly morphology before differentiation (Figure 3.7a-c). As expected, tdTmt expression became detectable at 14 days after differentiation (Figure 3.7d-e). Immunocytochemistry further confirmed that differentiated CICs^{TCR} expressed smooth muscle cell marker SM22α and fibroblast marker vimentin (Figure 3.7f-g). Third, we examined cardiogenic potential of CICs^{TCR} *in vitro.* We were unable to detect native venus expression *in vitro*, probably because αMHC activity was too weak to drive transgene expression in culture, or the inherent difficulties of cardiomyocyte differentiation *in vitro.* However, we were able to detect HA expression as a surrogate of αMHC activity and native venus fluorescence despite the rarity of such event (Figure 3.8). Together, these findings validate Tg:TCR reporter *in vitro* and suggest that TCR fluorescence can be used as a direct read-out for *in vitro* lineage differentiation.

97

DISCUSSION

Current studies fail to track the fate of progenitor cells as they differentiate into mature cardiac cell types, and there is little understanding of how the process is regulated. Use of tissue-specific promoter driven fluorophores allows us to track commitment of stem cells in the heart during development. In an effort to understand the distribution of various lineages within the myocardium, we generated the Tg:TCR mouse model, and extensively characterized and validated the faithful labeling of three cardiogenic lineages by three tissue specific promoter, αMHC (cardiomyocyte), SMMHC (smooth muscle cell), and Tie2 (endothelial cell). Each promoter successfully drives a unique fluorophore with minimal overlapping with the other two on the spectra, allowing simultaneous detection of all three lineages *in situ*. Additionally, each promoter also drives a unique epitope tag, providing an alternative surrogate read-out by immunoblotting or immunostaining.

Tg:TCR mouse is a straightforward lineage tracing tool during early cardiogenesis. By far, most genetic lineage tracing or fate mapping models require recombination of two or more strains [53,107,109,171,172,208]. Limitations exist in such models including timing and efficiency of recombination, therefore this may result in oversight of temporal or rare events. Tg:TCR model as a transgenic mouse line, can perfectly bypass this limitation and provide direct read-out of lineage adaptation by fluorophore expression (Figure 3.1-Figure 3.5). For example, postnatal cardiomyocyte maturation from P3 to P7 shown by Tg:TCR, is consistent with previous studies that the βMHC to αMHC switch occurs during early postnatal development [209]. However, we were able to detect αMHC activity (venus+) in embryonic hearts as early as prenatal E10.5 (Figure 3.4), greatly advancing the

98

previously reported E12.5 timing for 48 hours [131]. Hence, Tg:TCR mouse can be used as a valuable lineage tracing model especially during embryogenesis.

The validation of Tg:TCR mouse opens up limitless possibilities for future investigation that are not restricted in lineage tracing with the advantage of three simultaneous reporters. One of such possibilities is to use Tg:TCR as a model for cardiomyocyte differentiation, transdifferentiation, or dedifferentiation. If terminally differentiated adult cardiomyocytes can re-enter the cell cycle remains unclear. A recent study presented an *in vitro* live imaging system to follow adult cardiomyocytes (ACM) in culture, and reported that ACM is capable of dedifferentiating as characterized by morphological means such as disassembly of sarcomeric structure [210]. Now with the Tg:TCR model, such a system can be improved by hosting two intrinsic fluorophores as dedifferentiation or transdifferentiation markers as shown in Figure 3.5a. For example, if a dedifferentiated ACM adopts smooth muscle cell lineage in culture, the cell would lose venus expression and gain tdTmt. Alternatively, if a cultured myofibroblast were able to transdifferentiate into αMHC+ myocyte, the cell would switch color from tdTmt to venus during live imaging recording. Further understanding on ACM dedifferentiation and transdifferentiation can provide valuable insights on mammalian heart regeneration mechanisms, as such evidences are essential steps towards regeneration in vertebrate hearts yet remains missing in mammalian hearts (see Chapter 1).

Cardiomyocyte differentiation *in vitro* is challenging not only because of its complicated and time consuming nature, but also because the procedure requires stringent cardiogenecity of cardiac stem cells (Figure 3.8). Although capable of

differentiating into endothelial and smooth muscle cell lineages (Figure 3.6-Figure 3.7), the cardiogenecity of cCICs remains controversial in part due to the heterogeneous nature of CIC population [107,171,172]. In this study, we were unable to induce direct venus expression possibly due to a combination of reasons from both cell source and culturing conditions (Figure 3.8). However, *in vitro* cardiomyocyte conversion from ESCs or induced pluripotent cells (iPSCs) to cardiomyocytes has become an established protocol and has widely been used in drug screening for cardiovascular diseases [211–213]. As an alternative approach, the future steps are to generate Tg:TCR iPSCs and subsequently convert iPSCs into beating cardiomyocytes directly expressing venus (αMHC+) *in vitro*. As a proof of concept, we have successfully differentiated ESCs into beating EBs (data not shown). Mouse embryonic fibroblasts (MEF) were isolated from E13.5 Tg:TCR embryos and are currently being reprogrammed into iPSCs^{TCR} (data not shown). Achieving iPSC^{TCR} in culture would provide a convenient *in vitro* system for further investigations on cardiomyocyte lineage commitment.

Although the TCR mouse was originally designed to trace cardiogenic lineages, its lineage tracing potential is not limited to just cardiac cell types. As shown in Figure 3.3, αMHC activity and venus expression is detected in lung, combined vascular smooth muscle and endothelial expressions are detected in kidney, lung, and bladder. Therefore, Tg:TCR mouse effectively demonstrates lineage commitment in an organismal context. Collectively, Tg:TCR mouse not only provides a genetically and spectrally distinct addition to lineage tracing and fate mapping models, but by virtue of its spectral capabilities it

provides a platform for straightforward spatiotemporal lineage reporter and serves as a

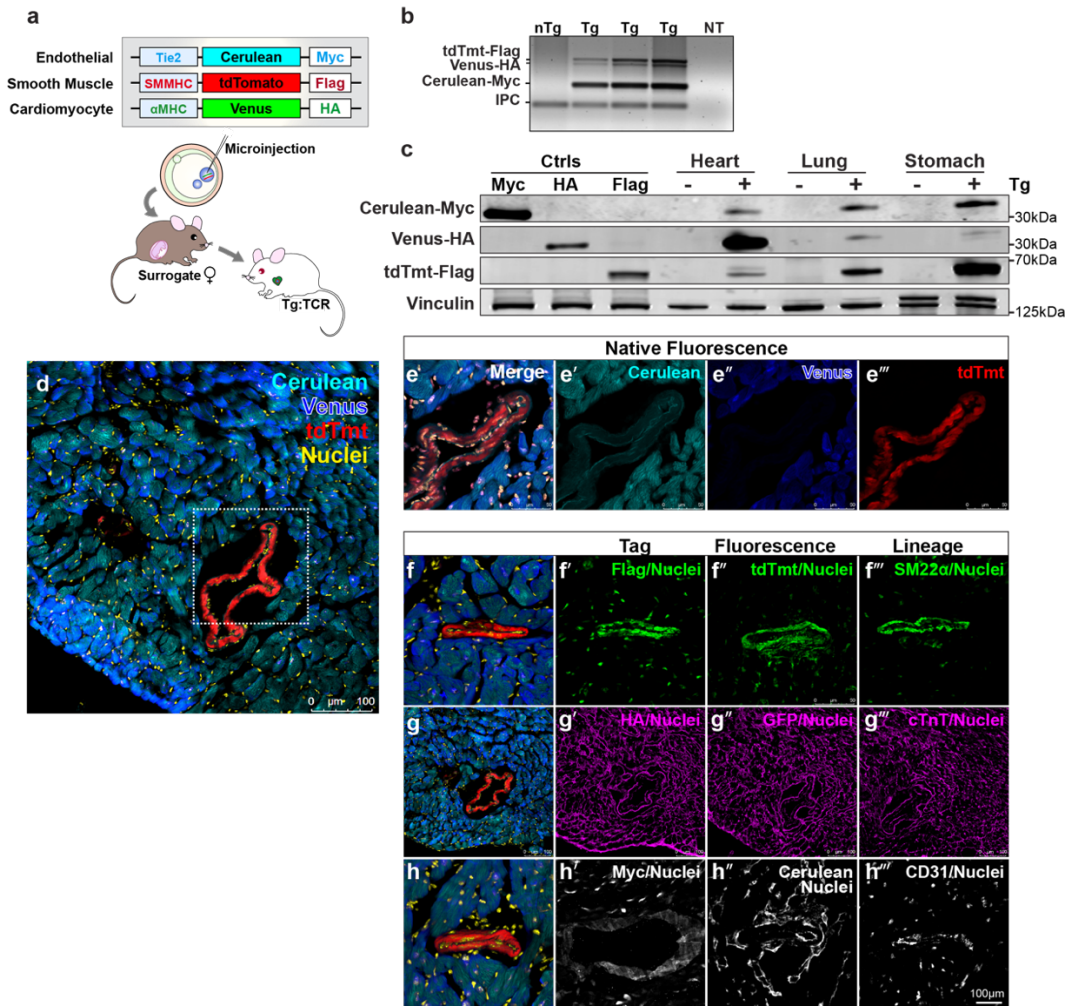source for fluorophore tagged derivation of cell lines.

Figure 3.1 Generation of Tg:TCR mouse

(a) Schematic of transgenic mouse production. Cerulean, cyan. tdTomato, red. Venus, green. (b) PCR genotyping confirms all three transgenes integration in genomic DNA. Tg, transgenic. nTg, non-transgenic. NT, no template. IPC, internal positive control. (c) Immunoblot analysis of organ proteins from adult Tg:TCR mouse demonstrating tissue specificity of transgene expression. Ctrls: HEK293 cells transfected with plasmid DNA of individual transgene. (d) Representative images of native fluorescence from frozen section of adult Tg:TCR heart. (e-e''') high magnification and single channel view of boxed area in (d). (f-h) Immunohistochemistry of serial frozen sections showing triple-expression of molecular tags, fluorophores, or lineage specific markers at the same region. (f-f''') Smooth muscle lineage. (g-g''') Cardiomyocyte lineage. (h-h''') Endothelial lineage. (f,g,h) Overlay of native fluorescence. SM22α, smooth muscle cell marker. cTnT, cardiomyocyte marker. CD31, endothelial marker. Cerulean, cyan. tdTmt, red. Venus, blue. Scale bar, 100μm.
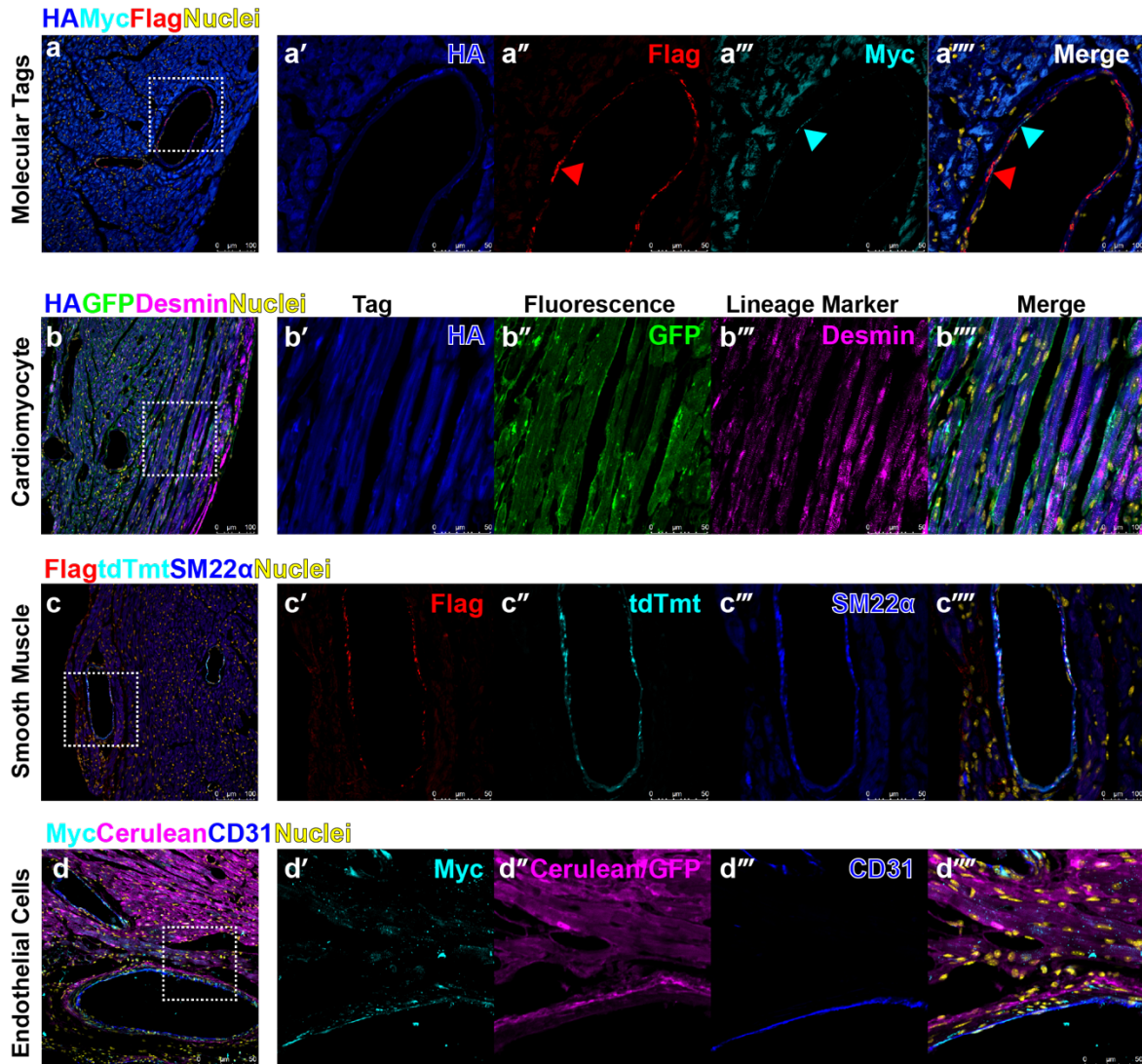
Figure 3.2 Co-visualization of fluorescent proteins, epitope tags, and lineage markers in Tg:TCR mouse heart

(a) Immunohistochemistry on paraffin sections showing expressions of three molecular tags in the heart. HA tag, cardiomyocyte lineage, blue. Myc tag, endothelial cell lineage, cyan. Flag tag, smooth muscle lineage, red. Nuclei, yellow. Boxed area is magnified in a'-a''''. Arrowheads pointing at expression of vascular smooth muscle cells (Flag tag, red, a'') and endothelial lining (Myc tag, cyan, a'''). (b-d) Immunohistochemistry showing colocalization of molecular tag, fluorescence, and lineage marker of cardiomyocyte (b), smooth muscle cells (c), and endothelial cell lineage (d). (b'-b'''') boxed area in (b). HA tag, blue. Venus (stained by anti-GFP antibody), green. Desmin, magenta. (c'-c'''') boxed area in (c). Flag tag, red. tdTmt (stained by anti-tdTmt antibody), cyan. SM22α, blue. (d'-d'''') boxed area in (d). Myc tag, cyan. Cerulean (stained by anti-GFP antibody), magenta. CD31, blue. Scale bar, 50µm.
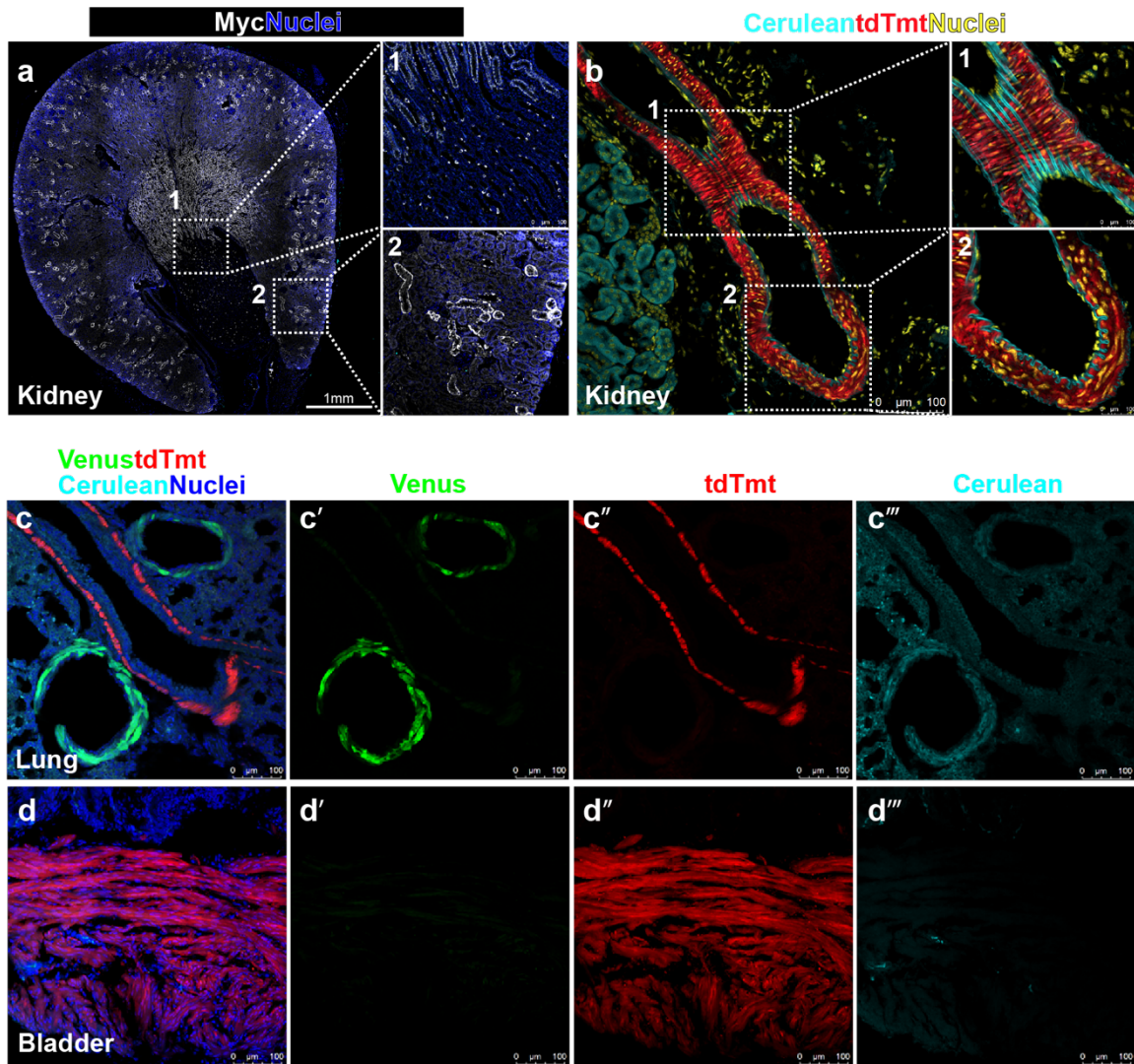
Figure 3.3 Tricolor expression in non-cardiac organs

(a) Tilescan of a transverse paraffin section of kidney showing expressions of Myc tag in medulla and cortex regions. Myc tag, white. Nuclei, blue. (b) Representative of native fluorescence (cryosection) atrenal vascular region of kidney. Cerulean, cyan. tdTmt, red. Nuclei, yellow. (c-c''') Representative confocal images of native fluorescence in lung. Venus, green. tdTmt, red. Cerulean, cyan. Nuclei, blue. (d-d''') Representative confocal images of tdTmt fluorescence expression in bladder. tdTmt, red. Nuclei, blue. Scale bar, 1mm in (a), 100μm in (b-d).
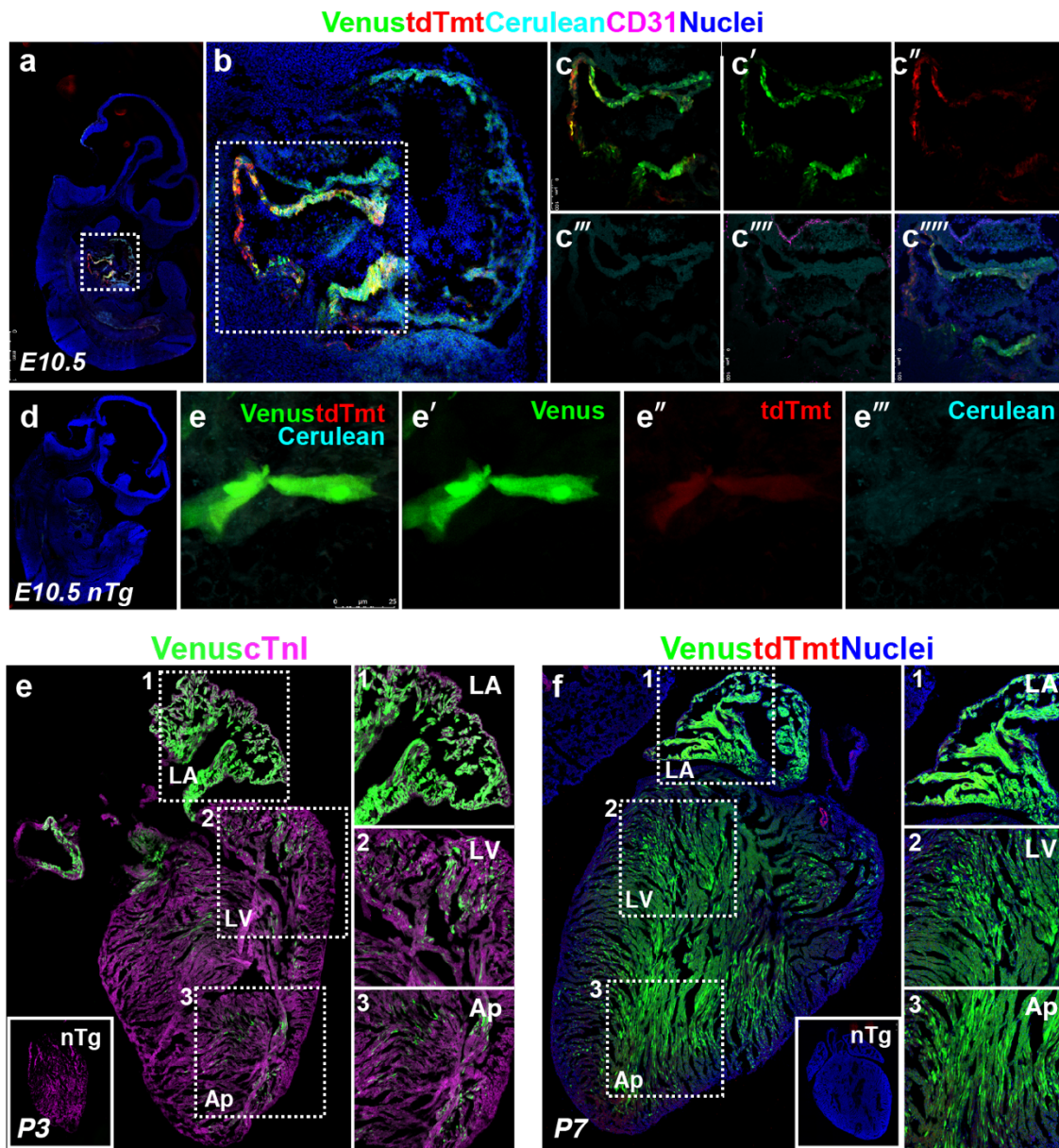
Figure 3.4 Tg:TCR serves as a cell lineage reporter during development

(a) Three transgene expressions in an embryonic heart at E10.5. Non-transgenic littermate control is shown in (d). Boxed area in (a) is shown in (b). Boxed area in (b) is shown in (c-c''''''). (c''''-c'''''') Immunostaining of CD31 (magenta) colocalizing with cerulean fluorescence. (e-e''') Ventricular cardiomyocytes expressing native venus fluorescence as early as E10.5. Venus, green. tdTmt, red. Cerulean, cyan. Nuclei, blue. (e) Tilescan of a P3 heart showing majority αMHC⁺ (venus) myocytes localize at atrial region but not at ventricular or apex region. Venus, green. cTnI, magenta. (f) Tilescan of a sagittal section of a P7 heart showing αMHC⁺ (venus) myocytes all over the heart. Venus, green. tdTmt, red. Nuclei, blue. nTg, non-transgenic.

105
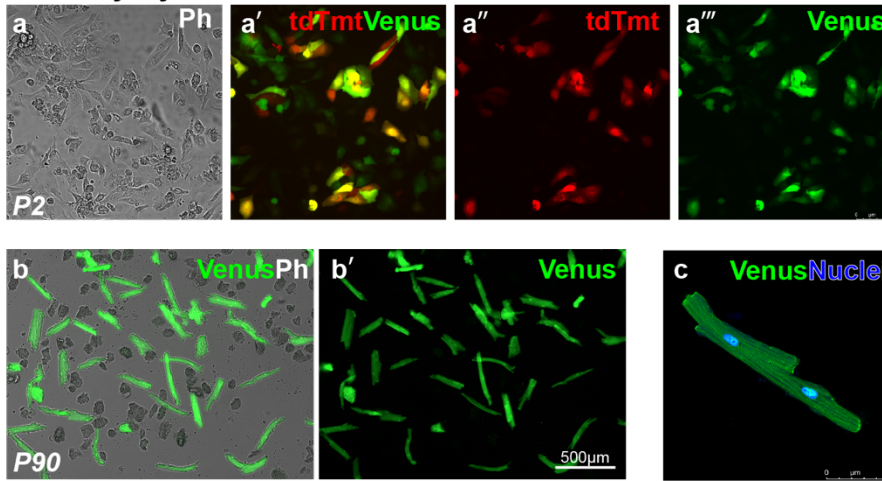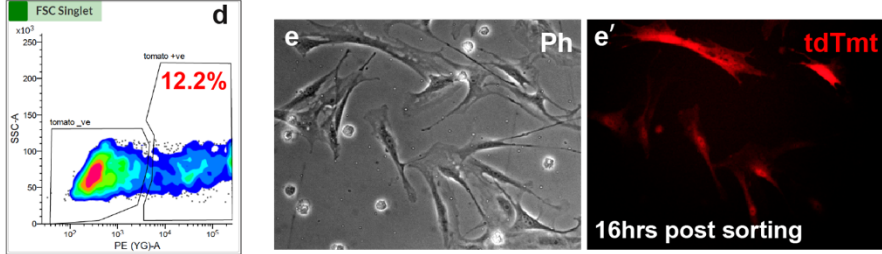
Figure 3.5 Tg:TCR provides concurrent primary cell source for lineage specific cell types

(a) Representative images of isolated P2 neonatal cardiomyocyte expressing venus (green) and tdTmt (red) fluorescence. Scale bar 100μm. (b) Representative images of isolated adult P90 cardiomyocyte expressing venus fluorescence (green) only. Scale bar 500μm. (c) higher magnification of a single adult cardiomyocyte with visible sarcomeric structure and native venus expression. Nuclei, blue. (d) Flow cytometry plots of tdTmt$^+$ cells isolated from inferior vena cava, 12.2% of all population are positive of tdTmt. (e) tdTmt native fluorescence is maintained in culture 16hrs post sorting. tdTmt, red. Ph, phase contrast.
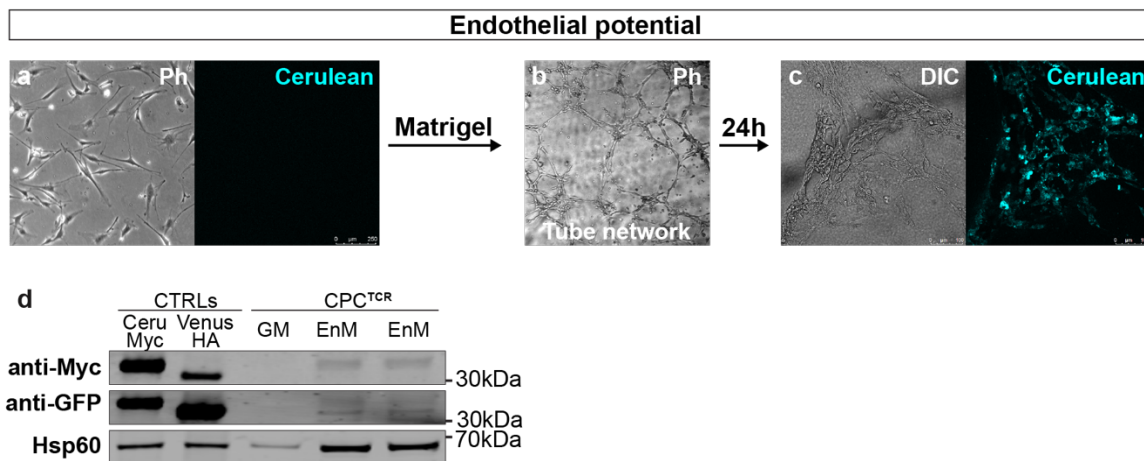
Figure 3.6 Native cerulean expression as a direct read-out of endothelial commitment

(a) CIC^{TCR} in growth media is negative of cerulean expression before differentiation. (b) CIC^{TCR} form tubular network upon culturing in Matrigel. (c) 24hrs after induction of endothelial differentiation, differentiated CIC^{TCR} begin to express native cerulean (cyan) fluorescence. (d) Immunoblotting analysis confirms Myc tag and cerulean expression after differentiation. Ph, phase contrast. DIC, differential interference contrast. GM, growth medium. EnM, endothelial media on Matrigel. Hsp60, heat shock protein 60, loading control.
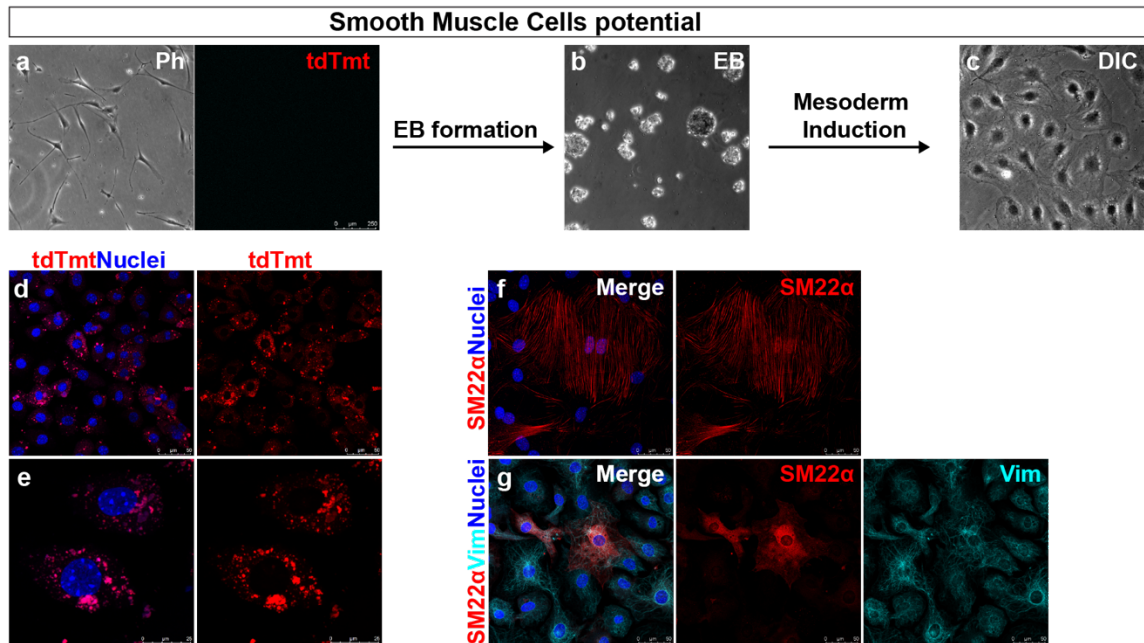
Figure 3.7 Native tdTmt expression as a direct read-out of smooth muscle lineage differentiation

(a) CIC[TCR] in growth media is negative of tdTmt expression before differentiation. Morphology of cells is thin and spindly. (b) Morphology of EBs formed by CIC[TCR] after 4 days culturing in suspension. (c) Morphology of differentiated CIC[TCR] 14 days after mesodermal induction, cells become flat and round. (d-e) native tdTmt expression (red) of differentiated CIC[TCR]. (f-g) immunostaining of differentiated tdTmt[+] CIC[TCR] showing expression of smooth muscle marker SM22α (red) and fibroblast marker vimentin (cyan), confirming *in vitro* commitment of smooth muscle lineage. Nuclei, blue. Ph, phase contrast. EB, embryoid body. DIC, differential interference contrast.
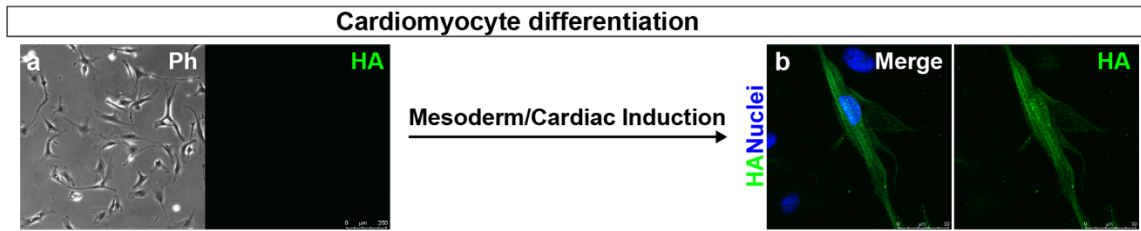
Figure 3.8 Transgene epitope tag HA as a surrogate of cardiomyocyte lineage marker

(a) CIC^{TCR} in growth media is negative of HA tag expression before differentiation. Morphology of cells is thin and spindly. (b) Differentiated CIC^{TCR} after mesoderm and cardiac induction expresses HA tag (green). HA tag is used as a surrogate of native Venus. Nuclei, blue. Ph, phase contrast.

Chapter 3, is presented in this dissertation as an alternative model and primary cell source for cardiac interstitial cell fate study of Chapter 2. I would like to acknowledge Dr. Roberto Alvarez Jr. for his extensive work in designing and establishing the Tg:TCR mouse line. Chapter 3, in full, will be prepared for submission. (Tentative title) Transgenic Triple Color Reporter Mouse as a Valuable Lineage Tracing and Cell Fate Model for Cardiomyocytes, Endothelial Cells, and Smooth Muscle Cells. Bingyan J. Wang, Roberto Alvarez Jr., Sharon Sengphanith, Alvin Muliono, David Ebeid, Carolina Esquer, and Mark A. Sussman. The dissertation author is the primary author and investigator of this manuscript as of December 2019.

SUPPLEMENTAL VIDEOS

Supplemental Video 3.1 Time lapse of CIC^{TCR} tube network formation on Matrigel, bright field.

Time lapse video of 24 hours of CIC^{TCR} forming tube network on Matrigel. Native cerulean become visible as the tube forms, starting from 16 hours. Video showing overlay of bright field and native cerulean, cyan.

Supplemental Video 3.2 Time lapse of CIC^{TCR} tube network formation on Matrigel, cerulean only.

Time lapse video of 24 hours of CIC^{TCR} forming tube network on Matrigel. Native cerulean become visible as the tube forms, starting from 16 hours. Video showing only cerulean (cyan) fluorescence for visualization.

REFERENCES

1.   Broughton KM, Wang BJ, Firouzi F, Khalafalla F, Dimmeler S, Fernandez-Aviles F, Sussman MA. Mechanisms of Cardiac Repair and Regeneration. *Circulation research*. 2018;122(8):1151–1163.

2.   Wang BJ, Alvarez R, Muliono A, Sengphanith S, Monsanto MM, Weeks J, Sacripanti R, Sussman MA. Adaptation Within Embryonic and Neonatal Heart Environment Reveals Alternative Fates for Adult c-Kit+ Cardiac Interstitial Cells. *bioRxiv*. 2019.

3.   Hu N, Sedmera D, Yost HJ, Clark EB. Structure and function of the developing zebrafish heart. *Anatomical Record*. 2000;260(2):148–157.

4.   Poss KD, Wilson LG, Keating MT. Heart Regeneration in Zebrafish. *Science*. 2002;298(5601):2188–2190.

5.   Lepilina A, Coon AN, Kikuchi K, Holdway JE, Roberts RW, Burns CG, Poss KD. A Dynamic Epicardial Injury Response Supports Progenitor Cell Activity during Zebrafish Heart Regeneration. *Cell*. 2006;127(3):607–619.

6.   Kikuchi K, Poss KD. Cardiac Regenerative Capacity and Mechanisms. *Annual Review of Cell and Developmental Biology*. 2012;28:719–41.

7.   González-Rosa JM, Mercader N. Cryoinjury as a myocardial infarction model for the study of cardiac regeneration in the zebrafish. *Nature Protocols*. 2012;7(4):782–788.

8.   González-Rosa JM, Martín V, Peralta M, Torres M, Mercader N. Extensive scar formation and regression during heart regeneration after cryoinjury in zebrafish. *Development*. 2011;138(9):1663–1674.

9.   Wang J, Panáková D, Kikuchi K, Holdway JE, Gemberling M, Burris JS, Singh SP, Dickson AL, Lin YF, Khaled Sabeh M, Werdich AA, Yelon D, MacRae CA, Poss KD. The regenerative capacity of zebrafish reverses cardiac failure caused by genetic cardiomyocyte depletion. *Development*. 2011;138(16):3421–3430.

10.   Jopling C, Suñé G, Faucherre A, Fabregat C, Izpisua Belmonte JC. Hypoxia induces myocardial regeneration in zebrafish. *Circulation*. 2012;126(25):3017–3027.

11.   Parente V, Balasso S, Pompilio G, Verduci L, Colombo GI, Milano G, Guerrini U, Squadroni L, Cotelli F, Pozzoli O, Capogrossi MC. Hypoxia/Reoxygenation Cardiac Injury and Regeneration in Zebrafish Adult Heart. Salloum FN, ed. *PLoS ONE*. 2013;8(1):e53748.

12. Lafontant PJ, Burns AR, Grivas JA, Lesch MA, Lala TD, Reuter SP, Field LJ, Frounfelter TD. The Giant Danio (D. Aequipinnatus) as A Model of Cardiac Remodeling and Regeneration. *Anatomical Record*. 2012;295(2):234–248.

13. Grivas J, Haag M, Johnson A, Manalo T, Roell J, Das TL, Brown E, Burns AR, Lafontant PJ. Cardiac repair and regenerative potential in the goldfish (Carassius auratus) heart. In: *Comparative Biochemistry and Physiology Part - C: Toxicology and Pharmacology.*Vol 163.; 2014:14–23.

14. Ito K, Morioka M, Kimura S, Tasaki M, Inohaya K, Kudo A. Differential reparative phenotypes between zebrafish and medaka after cardiac injury. *Developmental Dynamics*. 2014;243(9):1106–1115.

15. Harvey RP. Patterning the vertebrate heart. *Nature reviews. Genetics*. 2002;3(7):544–56.

16. Poss KD. *Getting to the heart of regeneration in zebrafish.*; 2007:36–45.

17. Drenckhahn JD, Schwarz QP, Gray S, Laskowski A, Kiriazis H, Ming Z, Harvey RP, Du XJ, Thorburn DR, Cox TC. Compensatory Growth of Healthy Cardiac Cells in the Presence of Diseased Cells Restores Tissue Homeostasis during Heart Development. *Developmental Cell*. 2008;15(4):521–533.

18. Mahmoud AI, Kocabas F, Muralidhar SA, Kimura W, Koura AS, Thet S, Porrello ER, Sadek HA. Meis1 regulates postnatal cardiomyocyte cell cycle arrest. *Nature*. 2013;497(7448):249–253.

19. Notari M, Ventura-Rubio A, Bedford-Guaus SJ, Jorba I, Mulero L, Navajas D, Martí M, Raya Á. The local microenvironment limits the regenerative potential of the mouse neonatal heart. *Science advances*. 2018;4(5):eaao5553.

20. Porrello ER, Olson EN. A neonatal blueprint for cardiac regeneration. *Stem Cell Research*. 2014;13(3):556–570.

21. Uygur A, Lee RT. Mechanisms of Cardiac Regeneration. *Developmental Cell*. 2016;36(4):362–374.

22. Muralidhar SA, Mahmoud AI, Canseco D, Xiao F, Sadek HA. Harnessing the power of dividing cardiomyocytes. *Global Cardiology Science and Practice*. 2013;2013(3):29.

23. Porrello ER, Mahmoud AI, Simpson E, Hill JA, Richardson JA, Olson EN, Sadek HA. Transient regenerative potential of of the Neonatal Mouse Heart. *Science*. 2011;331(February):1078–1081.

24. Porrello ER, Mahmoud AI, Simpson E, Hill JA, Richardson JA, Olson EN, Sadek

HA. Transient regenerative potential of the neonatal mouse heart. *Science*. 2011;331(6020):1078–80.

25. Soonpaa MH, Kim KK, Pajak L, Frnaklin M, Field LJ. Cardiomyocyte DNA synthesis and multinucleation during murine development. *Am.J.Physiol.* 1996;271:H2183–H2189.

26. Porrello ER, Mahmoud AI, Simpson E, Johnson BA, Grinsfelder D, Canseco D, Mammen PP, Rothermel BA, Olson EN, Sadek HA. Regulation of neonatal and adult mammalian heart regeneration by the miR-15 family. *PNAS*. 2013;110(1):187–192.

27. Jesty SA, Steffey MA, Lee FK, Breitbach M, Hesse M, Reining S, Lee JC, Doran RM, Nikitin AY, Fleischmann BK, Kotlikoff MI. C-kit + precursors support postinfarction myogenesis in the neonatal, but not adult, heart. *PNAS*. 2012;109(33):13380–5.

28. Haubner BJ, Adamowicz-Brice M, Khadayate S, Tiefenthaler V, Metzler B, Aitman T, Penninger JM. Complete cardiac regeneration in a mouse model of myocardial infarction. *Aging*. 2012;4(12):966–977.

29. Robledo M. Myocardial Regeneration in Young Rats. *The American journal of pathology*. 1956;32(6):1215–1239.

30. Haubner BJ, Schneider J, Schweigmann U, Schuetz T, Dichtl W, Velik-Salchner C, Stein JI, Penninger JM. Functional Recovery of a Human Neonatal Heart after Severe Myocardial Infarction. *Circulation Research*. 2016;118(2):216–221.

31. Fratz S, Hager A, Schreiber C, Schwaiger M, Hess J, Stern HC. Long-term myocardial scarring after operation for anomalous left coronary artery from the pulmonary artery. *Annals of Thoracic Surgery*. 2011;92(5):1761–1765.

32. Schmid G, Pfitzer P. Mitoses and binucleated cells in perinatal human hearts. *Virchows Archiv B Cell Pathology Including Molecular Pathology*. 1985;48(1):59–67.

33. Rupp S, Schranz D. Cardiac Regeneration in Children. *Pediatric Cardiology*. 2015;36(4):713–718.

34. Laflamme MA, Murry CE. Regenerating the heart. *Nature Biotechnology*. 2005;23(7):845–856.

35. Weisman HF, Bush DE, Mannisi JA, Bulkley BH. Global cardiac remodeling after acute myocardial infarction: A study in the rat model. *Journal of the American College of Cardiology*. 1985;5(6):1355–1362.

36. Pantely GA, Malone SA, Rhen WS, Anselone CG, Arai A, Bristow J, Bristow JD. Regeneration of myocardial phosphocreatine in pigs despite continued moderate ischemia. *Circulation Research*. 1990;67(6):1481–1493.

37. Hu X, Xu Y, Zhong Z, Wu Y, Zhao J, Wang Y, Cheng H, Kong M, Zhang F, Chen Q, Sun J, Li Q, Jin J, Li Q, Chen L, et al. A large-scale investigation of hypoxia-preconditioned allogeneic mesenchymal stem cells for myocardial repair in nonhuman primates: Paracrine activity without remuscularization. *Circulation Research*. 2016;118(6):970–983.

38. Van Amerongen MJ, Engel FB. Features of cardiomyocyte proliferation and its potential for cardiac regeneration: Stem Cells Review Series. *Journal of Cellular and Molecular Medicine*. 2008;12(6A):2233–2244.

39. Zak R. Cell proliferation during cardiac growth. *Am J Cardiol*. 1973;31(2):211–219.

40. Xiao Q, Zhang G, Wang H, Chen L, Lu S, Pan D, Liu G, Yang Z. A p53-based genetic tracing system to follow postnatal cardiomyocyte expansion in heart regeneration. *Development*. 2017;144(4):580–589.

41. Mollova M, Bersell K, Walsh S, Savla J, Das LT, Park S-YY, Silberstein LE, Dos Remedios CG, Graham D, Colan S, Kühn B. Cardiomyocyte proliferation contributes to heart growth in young humans. *PNAS*. 2013;110(4):1446–51.

42. Alvarez R, Wang BJ, Quijada PJ, Avitabile D, Ho T, Shaitrit M, Chavarria M, Firouzi F, Ebeid D, Monsanto MM, Navarrete N, Moshref M, Siddiqi S, Broughton KM, Bailey BA, et al. Cardiomyocyte cell cycle dynamics and proliferation revealed through cardiac-specific transgenesis of fluorescent ubiquitinated cell cycle indicator (FUCCI). *Journal of molecular and cellular cardiology*. 2019;127:154–164.

43. Naqvi N, Li M, Calvert JW, Tejada T, Lambert JP, Wu J, Kesteven SH, Holman SR, Matsuda T, Lovelock JD, Howard WW, Iismaa SE, Chan AY, Crawford BH, Wagner MB, et al. A proliferative burst during preadolescence establishes the final cardiomyocyte number. *Cell*. 2014;157(4):795–807.

44. Hesse M, Fleischmann BK, Kotlikoff MI. *Concise review: The role of C-kit expressing cells in heart repair at the neonatal and adult stage.*; 2014:1701–1712.

45. Bergmann O, Bhardwaj RD, Bernard S, Zdunek S, Barnabé-Heider F, Walsh S, Zupicich J, Alkass K, Buchholz BA, Druid H, Jovinge S, Frisén J, Barnabé-Heide F, Walsh S, Zupicich J, et al. Evidence for cardiomyocyte renewal in humans. *Science*. 2009;324(5923):98–102.

46. Ali SR, Hippenmeyer S, Saadat L V., Luo L, Weissman IL, Ardehali R. Existing cardiomyocytes generate cardiomyocytes at a low rate after birth in mice. *PNAS*. 2014;111(24):8850–8855.

47. Jopling C, Sleep E, Raya M, Martí M, Raya A, Belmonte JCI. Zebrafish heart regeneration occurs by cardiomyocyte dedifferentiation and proliferation. *Nature*. 2010;464(7288):606–609.

48. Kikuchi K, Holdway JE, Werdich AA, Anderson RM, Fang Y, Egnaczyk GF, Evans T, Macrae CA, Stainier DYR, Poss KD. Primary contribution to zebrafish heart regeneration by gata4(+) cardiomyocytes. *Nature*. 2010;464(7288):601–5.

49. Hatzistergos KE, Hare JM. Murine Models Demonstrate Distinct Vasculogenic and Cardiomyogenic cKit+ Lineages in the Heart. *Circulation research*. 2016;118(3):382–7.

50. Alkass K, Panula J, Westman M, Wu T Di, Guerquin-Kern JL, Bergmann O. No Evidence for Cardiomyocyte Number Expansion in Preadolescent Mice. *Cell*. 2015;163(4):1026–1036.

51. Senyo SE, Steinhauser ML, Pizzimenti CL, Yang VK, Cai L, Wang M, Wu T Di, Guerquin-Kern J-LL, Lechene CP, Lee RT, Guerquin-Kern J-LL, Lechene CP, Lee RT. Mammalian heart renewal by pre-existing cardiomyocytes. *Nature*. 2013;493(7432):433–436.

52. Senyo SE, Lee RT, Kühn B. Cardiac regeneration based on mechanisms of cardiomyocyte proliferation and differentiation. *Stem Cell Research*. 2014;13(3):532–541.

53. Liu Q, Yang R, Huang X, Zhang H, He L, Zhang L, Tian X, Nie Y, Hu S, Yan Y, Zhang L, Qiao Z, Wang Q-D, Lui KO, Zhou B. Genetic lineage tracing identifies in situ Kit-expressing cardiomyocytes. *Cell Research*. 2015;26(1):119–130.

54. Kikuchi K, Holdway JE, Werdich AA, Anderson RM, Fang Y, Egnaczyk GF, Evans T, MacRae CA, Stainier DYR, Poss KD. Primary contribution to zebrafish heart regeneration by gata4+ cardiomyocytes. *Nature*. 2010;464(7288):601–605.

55. Bettencourt-Dias M, Mittnacht S, Brockes JP. Heterogeneous proliferative potential in regenerative adult newt cardiomyocytes. *Journal of Cell Science*. 2003;116(19):4001–4009.

56. Ausma J, Litjens N, Lenders MH, Duimel H, Mast F, Wouters L, Ramaekers F, Allessie M, Borgers M. Time course of atrial fibrillation-induced cellular structural remodeling in atria of the goat. *J Mol Cell Cardiol*. 2001;33(12):2083–2094.

57. Weil BR, Ozcan C. Cardiomyocyte Remodeling in Atrial Fibrillation and Hibernating Myocardium: Shared Pathophysiologic Traits Identify Novel Treatment Strategies? *BioMed research international*. 2015;2015(Figure 2):587361.

58. Zhang Y, Zhong JF, Qiu H, MacLellan WR, Marbán E, Wang C. Epigenomic

Reprogramming of Adult Cardiomyocyte-Derived Cardiac Progenitor Cells. *Scientific Reports*. 2015;5:1–15.

59. Kubin T, Pöling J, Kostin S, Gajawada P, Hein S, Rees W, Wietelmann A, Tanaka M, Lörchner H, Schimanski S, Szibor M, Warnecke H, Braun T. Oncostatin M is a major mediator of cardiomyocyte dedifferentiation and remodeling. *Cell stem cell*. 2011;9(5):420–32.

60. Sdek P, Zhao P, Wang Y, Huang CJ, Ko CY, Butler PC, Weiss JN, MacLellan WR. Rb and p130 control cell cycle gene silencing to maintain the postmitotic phenotype in cardiac myocytes. *Journal of Cell Biology*. 2011;194(3):407–423.

61. Bearzi C, Rota M, Hosoda T, Tillmanns J, Nascimbene A, De Angelis A, Yasuzawa-Amano S, Trofimova I, Siggins RW, LeCapitaine N, Cascapera S, Beltrami AP, D 'alessandro DA, Zias E, Quaini F, et al. Human cardiac stem cells. *PNAS*. 2007;104(35):14068–14073.

62. Beltrami AP, Barlucchi L, Torella D, Baker M, Limana F, Chimenti S, Kasahara H, Rota M, Musso E, Urbanek K, Leri A, Kajstura J, Nadal-Ginard B, Anversa P. Adult cardiac stem cells are multipotent and support myocardial regeneration. *Cell*. 2003;114(6):763–76.

63. Bolli R, Chugh AR, D'Amario D, Loughran JH, Stoddard MF, Ikram S, Beache GM, Wagner SG, Leri A, Hosoda T, Sanada F, Elmore JB, Goichberg P, Cappetta D, Solankhi NK, et al. Cardiac stem cells in patients with ischaemic cardiomyopathy (SCIPIO): Initial results of a randomised phase 1 trial. *Lancet*. 2011;378(9806):1847–1857.

64. Linke A, Muller P, Nurzynska D, Casarsa C, Torella D, Nascimbene A, Castaldo C, Cascapera S, Bohm M, Quaini F, Urbanek K, Leri A, Hintze TH, Kajstura J, Anversa P. Stem cells in the dog heart are self-renewing, clonogenic, and multipotent and regenerate infarcted myocardium, improving cardiac function. *PNAS*. 2005;102(25):8966–8971.

65. Bolli R, Tang X-LX, Sanganalmath SK, Rimoldi O, Mosna F, Abdel-latif A, Jneid H, Rota M, Leri A, Kajstura J, Cardiomyopathy I, Bolli R, Tang X-LX, Sanganalmath SK, Rimoldi O, et al. Intracoronary Delivery of Autologous Cardiac Stem Cells Improves Cardiac Function in a Porcine Model of Chronic Ischemic Cardiomyopathy. *Circulation*. 2013;128(2):122–131.

66. Tang X-LXLX-L, Rokosh G, Sanganalmath SK, Yuan F, Sato H, Mu J, Dai S, Li C, Chen N, Peng Y, Dawn B, Hunt G, Leri A, Kajstura J, Tiwari S, et al. Intracoronary administration of cardiac progenitor cells alleviates left ventricular dysfunction in rats with a 30-day-old infarction. *Circulation*. 2010;121(2):293–305.

67. Dawn B, Stein AB, Urbanek K, Rota M, Whang B, Rastaldo R, Torella D, Tang X-

LX-L, Rezazadeh A, Kajstura J, Leri A, Hunt G, Varma J, Prabhu SD, Anversa P, et al. Cardiac stem cells delivered intravascularly traverse the vessel barrier, regenerate infarcted myocardium, and improve cardiac function. *PNAS*. 2005;102(10):3766–3771.

68.   Ellison GM, Vicinanza C, Smith AJ, Aquila I, Leone A, Waring CD, Henning BJ, Stirparo GG, Papait R, Scarfò M, Agosti V, Viglietto G, Condorelli G, Indolfi C, Ottolenghi S, et al. Adult c-kit(pos) cardiac stem cells are necessary and sufficient for functional cardiac regeneration and repair. *Cell*. 2013;154(4):827–42.

69.   Vicinanza C, Aquila I, Scalise M, Cristiano F, Marino F, Cianflone E, Mancuso T, Marotta P, Sacco W, Lewis FC, Couch L, Shone V, Gritti G, Torella A, Smith AJ, et al. Adult cardiac stem cells are multipotent and robustly myogenic: c-kit expression is necessary but not sufficient for their identification. *Cell Death and Differentiation*. 2017;24(12):2101–2116.

70.   Leri A, Rota M, Pasqualini FS, Goichberg P, Anversa P. Origin of cardiomyocytes in the adult heart. *Circ Res*. 2015;116(1):150–166.

71.   Urbanek K, Cesselli D, Rota M, Nascimbene A, De Angelis A, Hosoda T, Bearzi C, Boni A, Bolli R, Kajstura J, Anversa P, Leri A. Stem cell niches in the adult mouse heart. *PNAS*. 2006;103(24):9226–9231.

72.   Urbanek K, Cabral-Da-Silva MC, Ide-Iwata N, Maestroni S, Delucchi F, Zheng H, Ferreira-Martins J, Ogórek B, D'Amario D, Bauer M, Zerbini G, Rota M, Hosoda T, Liao R, Anversa P, et al. Inhibition of Notch1-dependent cardiomyogenesis leads to a dilated myopathy in the neonatal heart. *Circ Res*. 2010;107(3):429–441.

73.   Vassort G. Adenosine 5'-Triphosphate: a P2-Purinergic Agonist in the Myocardium. *Physiological Reviews*. 2001;81(2):767–806.

74.   Orlic D, Kajstura J, Chimenti S, Limana F, Jakoniuk I, Quaini F, Nadal-Ginard B, Bodine DM, Leri A, Anversa P. Mobilized bone marrow cells repair the infarcted heart, improving function and survival. *PNAS*. 2001;98(18):10344–10349.

75.   Orlic D, Kajstura J, Chimenti S, Jakoniuk I, Anderson SM, Li B, Pickel J, McKay R, Nadal-Ginard B, Bodine DM, Leri A, Anversa P. Bone marrow cells regenerate infarcted myocardium. *Nature*. 2001;410(6829):701–705.

76.   Kuramochi Y, Fukazawa R, Migita M, Hayakawa J, Hayashida M, Uchikoba Y, Fukumi D, Shimada T, Ogawa S. Cardiomyocyte regeneration from circulating bone marrow cells in mice. *Pediatric Research*. 2003;54(3):319–325.

77.   Kajstura J, Rota M, Whang B, Cascapera S, Hosoda T, Bearzi C, Nurzynska D, Kasahara H, Zias E, Bonaf?? M, Nadal-Ginard B, Torella D, Nascimbene A, Quaini F, Urbanek K, et al. Bone marrow cells differentiate in cardiac cell lineages after

infarction independently of cell fusion. *Circ Res*. 2005;96(1):127–137.

78. Rota M, Kajstura J, Hosoda T, Bearzi C, Vitale S, Esposito G, Iaffaldano G, Padin-Iruegas ME, Gonzalez A, Rizzi R, Small N, Muraski J, Alvarez R, Chen X, Urbanek K, et al. Bone marrow cells adopt the cardiomyogenic fate in vivo. *PNAS*. 2007;104(45):17783–17788.

79. Hare JM, Fishman JE, Gerstenblith G, DiFede Velazquez DL, Zambrano JP, Suncion VY, Tracy M, Ghersin E, Johnston P V., Brinker JA, Breton E, Davis-Sproul J, Byrnes J, George R, Lardo A, et al. Comparison of Allogeneic vs Autologous Bone Marrow–Derived Mesenchymal Stem Cells Delivered by Transendocardial Injection in Patients With Ischemic Cardiomyopathy. *Jama*. 2012;308(22):2369.

80. Strauer BE, Brehm M, Zeus T, Köstering M, Hernandez A, Sorg R V., Kögler G, Wernet P. Repair of infarcted myocardium by autologous intracoronary mononuclear bone marrow cell transplantation in humans. *Circulation*. 2002;106(15):1913–1918.

81. Janssens S, Dubois C, Bogaert J, Theunissen K, Deroose C, Desmet W, Kalantzi M, Herbots L, Sinnaeve P, Dens J, Maertens J, Rademakers F, Dymarkowski S, Gheysens O, Van Cleemput J, et al. Autologous bone marrow-derived stem-cell transfer in patients with ST-segment elevation myocardial infarction: Double-blind, randomised controlled trial. *Lancet*. 2006;367(9505):113–121.

82. Alfaro MP, Vincent A, Saraswati S, Thorne CA, Hong CC, Lee E, Young PP. sFRP2 Suppression of Bone Morphogenic Protein (BMP) and Wnt Signaling Mediates Mesenchymal Stem Cell (MSC) Self-renewal Promoting Engraftment and Myocardial Repair. *Journal of Biological Chemistry*. 2010;285(46):35645–35653.

83. Hung S-C, Pochampally RR, Chen S-C, Hsu S-C, Prockop DJ. Angiogenic Effects of Human Multipotent Stromal Cell Conditioned Medium Activate the PI3K-Akt Pathway in Hypoxic Endothelial Cells to Inhibit Apoptosis, Increase Survival, and Stimulate Angiogenesis. *STEM CELLS*. 2007.

84. Quaini F, Urbanek K, Beltrami AP, Finato N, Beltrami CA, Nadal-Ginard B, Kajstura J, Leri A, Anversa P. Chimerism of the transplanted heart. *The New England journal of medicine*. 2002;346(1):5–15.

85. Heallen T, Zhang M, Wang J, Bonilla-Claudio M, Klysik E, Johnson RL, Martin JF. Hippo pathway inhibits Wnt signaling to restrain cardiomyocyte proliferation and heart size. *Science*. 2011;332(6028):458–61.

86. Zhou Q, Li L, Zhao B, Guan K. The hippo pathway in heart development, regeneration, and diseases. *Circ Res*. 2015;116(8):1431–47.

87. Lin Z, von Gise A, Zhou P, Gu F, Ma Q, Jiang J, Yau AL, Buck JN, Gouin KA, van

119

Gorp PRR, Zhou B, Chen J, Seidman JG, Wang D-Z, Pu WT. Cardiac-Specific YAP Activation Improves Cardiac Function and Survival in an Experimental Murine MI Model. *Circulation Research*. 2014;115(3):354–363.

88. Xin M, Kim Y, Sutherland LB, Murakami M, Qi X, McAnally J, Porrello ER, Mahmoud AI, Tan W, Shelton JM, Richardson JA, Sadek HA, Bassel-Duby R, Olson EN. Hippo pathway effector Yap promotes cardiac regeneration. *PNAS*. 2013;110(34):13839–13844.

89. Azcoitia V, Aracil M, Martinez-A C, Miguel Torres. The homeodomain protein Meis1 is essential for definitive hematopoiesis and vascular patterning in the mouse embryo. *Developmental Biology*. 2005;280:307–320.

90. Bersell K, Arab S, Haring B, Kühn B. Neuregulin1/ErbB4 signaling induces cardiomyocyte proliferation and repair of heart injury. *Cell*. 2009;138(2):257–70.

91. Wadugu B, Kühn B. The role of neuregulin/ErbB2/ErbB4 signaling in the heart with special focus on effects on cardiomyocyte proliferation. *American journal of physiology. Heart and circulatory physiology*. 2012;302(11):H2139-47.

92. Gemberling M, Karra R, Dickson AL, Poss KD. Nrg1 is an injury-induced cardiomyocyte mitogen for the endogenous heart regeneration program in zebrafish. *eLife*. 2015;2015(4):1–17.

93. Polizzotti BD, Ganapathy B, Walsh S, Choudhury S, Ammanamanchi N, Bennett DG, dos Remedios CG, Haubner BJ, Penninger JM, Kühn B. Neuregulin stimulation of cardiomyocyte regeneration in mice and human myocardium reveals a therapeutic window. *Science Translational Medicine*. 2015;7(281):281ra45.

94. Engel FB, Hsieh PCH, Lee RT, Keating MT. FGF1/p38 MAP kinase inhibitor therapy induces cardiomyocyte mitosis, reduces scarring, and rescues function after myocardial infarction. *PNAS*. 2006;103(42):15546–15551.

95. Engel FB. p38 MAP kinase inhibition enables proliferation of adult mammalian cardiomyocytes. *Genes Dev*. 2005;19(10):1175–1187.

96. Chattergoon NN, Giraud GD, Louey S, Stork P, Fowden AL, Thornburg KL. Thyroid hormone drives fetal cardiomyocyte maturation. *FASEB journal*. 2012;26(1):397–408.

97. Chattergoon NN, Giraud GD, Thornburg KL. Thyroid hormone inhibits proliferation of fetal cardiac myocytes in vitro. *Journal of Endocrinology*. 2007;192(2):R1–R8.

98. Chen W, Frangogiannis NG. Fibroblasts in post-infarction inflammation and cardiac repair. *Biochim Biophys Acta.* 2013;1833(4):945–53.

99. Murry CE, Kay MA, Bartosek T, Hauschka SD, Schwartz SM. Muscle differentiation during repair of myocardial necrosis in rats via gene transfer with MyoD. *Journal of Clinical Investigation*. 1996;98(10):2209–2217.

100. Ieda M, Fu JD, Delgado-Olguin P, Vedantham V, Hayashi Y, Bruneau BG, Srivastava D. Direct reprogramming of fibroblasts into functional cardiomyocytes by defined factors. *Cell*. 2010;142(3):375–386.

101. Efe JA, Hilcove S, Kim J, Zhou H, Ouyang K, Wang G, Chen J, Ding S. Conversion of mouse fibroblasts into cardiomyocytes using a direct reprogramming strategy. *Nature Cell Biology*. 2011;13(3):215–222.

102. Lalit PA, Salick MR, Nelson DO, Squirrell JM, Shafer CM, Patel NG, Saeed I, Schmuck EG, Markandeya YS, Wong R, Lea MR, Eliceiri KW, Hacker TA, Crone WC, Kyba M, et al. Lineage Reprogramming of Fibroblasts into Proliferative Induced Cardiac Progenitor Cells by Defined Factors. *Cell Stem Cell*. 2016;18(3):354–67.

103. Zebrowski DC, Vergarajauregui S, Wu CC, Piatkowski T, Becker R, Leone M, Hirth S, Ricciardi F, Falk N, Giessl A, Just S, Braun T, Weidinger G, Engel FB. Developmental alterations in centrosome integrity contribute to the post-mitotic state of mammalian cardiomyocytes. *eLife*. 2015;4(AUGUST2015):1–16.

104. Poss KD, Nechiporuk A, Hillam AM, Johnson SL, Keating MT. Mps1 defines a proximal blastemal proliferative compartment essential for zebrafish fin regeneration. *Development*. 2002;129(22):5141–9.

105. Seki A, Coppinger JA, Jang C, Yates JR, Fang G. Bora and the kinase Aurora a cooperatively activate the kinase Plk1 and control mitotic entry. *Science*. 2008;320(5883):1655–8.

106. Crippa S, Nemir M, Ounzain S, Ibberson M, Berthonneche C, Sarre A, Boisset G, Maison D, Harshman K, Xenarios I, Diviani D, Schorderet D, Pedrazzini T. Comparative transcriptome profiling of the injured zebrafish and mouse hearts identifies miRNA-dependent repair pathways. *Cardiovascular Research*. 2016;110(1):73–84.

107. Hatzistergos KE, Takeuchi LM, Saur D, Seidler B, Dymecki SM, Mai JJ, White IA, Balkan W, Kanashiro-Takeuchi RM, Schally A V., Hare JM. cKit+ cardiac progenitors of neural crest origin. *PNAS*. 2015;112(42):13051–6.

108. Gude NA, Broughton KM, Firouzi F, Sussman MA. Cardiac ageing: extrinsic and intrinsic factors in cellular renewal and senescence. *Nature Reviews Cardiology*. 2018;15(9):523–542.

109. Gude NA, Firouzi F, Broughton KM, Ilves K, Nguyen KP, Payne CR, Sacchi V,

Monsanto MM, Casillas AR, Khalafalla FG, Wang BJ, Ebeid DE, Alvarez R, Dembitsky WP, Bailey BA, et al. Cardiac c-Kit Biology Revealed by Inducible Transgenesis. *Circulation research*. 2018;123(1):57–72.

110. Kanisicak O, Khalil H, Ivey MJ, Karch J, Maliken BD, Correll RN, Brody MJ, Lin SCJ, Aronow BJ, Tallquist MD, Molkentin JD. Genetic lineage tracing defines myofibroblast origin and function in the injured heart. *Nature Communications*. 2016;7:12260.

111. Yu J, Seldin MM, Fu K, Li S, Lam L, Wang P, Wang Y, Huang D, Nguyen TL, Wei B, Kulkarni RP, Di Carlo D, Teitell M, Pellegrini M, Lusis AJ, et al. Topological Arrangement of Cardiac Fibroblasts Regulates Cellular Plasticity. *Circulation research*. 2018;123(1):73–85.

112. Furtado MB, Costa MW, Pranoto EA, Salimova E, Pinto AR, Lam NT, Park A, Snider P, Chandran A, Harvey RP, Boyd R, Conway SJ, Pearson J, Kaye DM, Rosenthal NA. Cardiogenic genes expressed in cardiac fibroblasts contribute to heart development and repair. *Circulation Research*. 2014;114(9):1422–1434.

113. Quijada P, Hariharan N, Cubillo JD, Bala KM, Emathinger JM, Wang BJ, Ormachea L, Bers DM, Sussman MA, Poizat C. Nuclear calcium/calmodulin-dependent protein kinase II signaling enhances cardiac progenitor cell survival and cardiac lineage commitment. *J Biol Chem*. 2015;290(42):25411–25426.

114. Natsumeda M, Florea V, Rieger AC, Tompkins BA, Banerjee MN, Golpanian S, Fritsch J, Landin AM, Kashikar ND, Karantalis V, Loescher VY, Hatzistergos KE, Bagno L, Sanina C, Mushtaq M, et al. A Combination of Allogeneic Stem Cells Promotes Cardiac Regeneration. *Journal of the American College of Cardiology*. 2017.

115. Koudstaal S, Jansen of Lorkeers SJ, Gaetani R, Gho JMIH, van Slochteren FJ, Sluijter JPG, Doevendans PA, Ellison GM, Chamuleau SAJ. Concise Review: Heart Regeneration and the Role of Cardiac Stem Cells. *STEM CELLS Translational Medicine*. 2013;2(6):434–443.

116. Tallquist MD, Molkentin JD. Redefining the identity of cardiac fibroblasts. *Nature Reviews Cardiology*. 2017;14(8):484–491.

117. Frangogiannis NG. *Cardiac fibrosis: Cell biological mechanisms, molecular pathways and therapeutic opportunities*.; 2019:70–99.

118. Nadal-Ginard B, Ellison GM, Torella D. The cardiac stem cell compartment is indispensable for myocardial cell homeostasis, repair and regeneration in the adult. *Stem cell research*. 2014;13(3 Pt B):615–30.

119. Oh H, Bradfute SB, Gallardo TD, Nakamura T, Gaussin V, Mishina Y, Pocius J,

Michael LH, Behringer RR, Garry DJ, Entman ML, Schneider MD. Cardiac progenitor cells from adult myocardium: Homing, differentiation, and fusion after infarction. *PNAS*. 2003;100(21):12313–12318.

120. Günter J, Wolint P, Bopp A, Steiger J, Cambria E, Hoerstrup SP, Emmert MY. Microtissues in Cardiovascular Medicine: Regenerative Potential Based on a 3D Microenvironment. *Stem Cells International*. 2016;2016:1–20.

121. Mohsin S, Khan M, Toko H, Bailey B, Cottage CT, Wallach K, Nag D, Lee A, Siddiqi S, Lan F, Fischer KM, Gude N, Quijada P, Avitabile D, Truffa S, et al. Human cardiac progenitor cells engineered with Pim-I kinase enhance myocardial repair. *JACC*. 2012;60(14):1278–1287.

122. Korski KI, Kubli DA, Wang BJ, Khalafalla FG, Monsanto MM, Firouzi F, Echeagaray OH, Kim T, Adamson RM, Dembitsky WP, Gustafsson ÅB, Sussman MA. Hypoxia Prevents Mitochondrial Dysfunction and Senescence in Human c-Kit + Cardiac Progenitor Cells. *Stem Cells*. 2019;37(4):555–567.

123. Quijada P, Salunga HT, Hariharan N, Cubillo JD, El-Sayed FG, Moshref M, Bala KM, Emathinger JM, De La Torre A, Ormachea L, Alvarez R, Gude NA, Sussman MA. Cardiac stem cell hybrids enhance myocardial repair. *Circulation Research*. 2015;117(8):695–706.

124. Gaetani R, Feyen DAM, Doevendans PA, Gremmels H, Forte E, Fledderus JO, Ramjankhan FZ, Messina E, Sussman MA, Giacomello A, Sluijter JPG. Different types of cultured human adult Cardiac Progenitor Cells have a high degree of transcriptome similarity. *Journal of Cellular and Molecular Medicine*. 2014;18(11):2147–2151.

125. Kim T, Echeagaray OH, Wang BJ, Casillas A, Broughton KM, Kim B-H, Sussman MA. In situ transcriptome characteristics are lost following culture adaptation of adult cardiac stem cells. *Scientific reports*. 2018;8(1):12060.

126. Broughton KM, Khieu T, Nguyen N, Rosa M, Mohsin S, Quijada P, Wang BJ, Echeagaray OH, Kubli DA, Kim T, Firouzi F, Monsanto MM, Gude NA, Adamson RM, Dembitsky WP, et al. Cardiac interstitial tetraploid cells can escape replicative senescence in rodents but not large mammals. *Communications Biology*. 2019;2(1):205.

127. Zhu K, Wu Q, Ni C, Zhang P, Zhong Z, Wu Y, Wang Y, Xu Y, Kong M, Cheng H, Tao Z, Yang Q, Liang H, Jiang Y, Li Q, et al. Lack of Remuscularization Following Transplantation of Human Embryonic Stem Cell-Derived Cardiovascular Progenitor Cells in Infarcted Nonhuman Primates. *Circulation Research*. 2018;122(7):958–969.

128. Hong KU, Li Q-H, Guo Y, Patton NS, Moktar A, Bhatnagar A, Bolli R. A highly sensitive and accurate method to quantify absolute numbers of c-kit+ cardiac stem

cells following transplantation in mice. *Basic research in cardiology*. 2013;108(3):346.

129. Tang XL, Li Q, Rokosh G, Sanganalmath SK, Chen N, Ou Q, Stowers H, Hunt G, Bolli R. Long-Term Outcome of Administration of c-kitPOS Cardiac Progenitor Cells after Acute Myocardial Infarction: Transplanted Cells Do not Become Cardiomyocytes, but Structural and Functional Improvement and Proliferation of Endogenous Cells Persist for at Lea. *Circulation Research*. 2016;118(7):1091–1105.

130. Hong KU, Guo Y, Li QH, Cao P, Al-Maqtari T, Vajravelu BN, Du J, Book MJ, Zhu X, Nong Y, Bhatnagar A, Bolli R. C-Kit+ Cardiac Stem Cells Alleviate Post-Myocardial Infarction Left Ventricular Dysfunction Despite Poor Engraftment and Negligible Retention in the Recipient Heart. *PLoS ONE*. 2014;9(5):1–7.

131. Li Y, Lv Z, He L, Huang X, Zhang S, Zhao H, Pu W, Li Y, Yu W, Zhang L, Liu X, Liu K, Tang J, Tian X, Wang Q-D, et al. Genetic Tracing Identifies Early Segregation of the Cardiomyocyte and Nonmyocyte Lineages. *Circulation Research*. 2019;125(3):343–355.

132. Sakaue-Sawano A, Kurokawa H, Morimura T, Hanyu A, Hama H, Osawa H, Kashiwagi S, Fukami K, Miyata T, Miyoshi H, Imamura T, Ogawa M, Masai H, Miyawaki A. Visualizing Spatiotemporal Dynamics of Multicellular Cell-Cycle Progression. *Cell*. 2008;132(3):487–498.

133. Gao E, Lei YH, Shang X, Huang ZM, Zuo L, Boucher M, Fan Q, Chuprun JK, Ma XL, Koch WJ. A novel and efficient model of coronary artery ligation and myocardial infarction in the mouse. *Circulation research*. 2010;107(12):1445–53.

134. Ackers-Johnson M, Li PY, Holmes AP, O'Brien SM, Pavlovic D, Foo RS. A Simplified, Langendorff-Free Method for Concomitant Isolation of Viable Cardiac Myocytes and Nonmyocytes from the Adult Mouse Heart. *Circulation Research*. 2016;119(8):909–920.

135. Monsanto MM, White KS, Kim T, Wang BJ, Fisher K, Ilves K, Khalafalla FG, Casillas A, Broughton K, Mohsin S, Dembitsky WP, Sussman MA. Concurrent Isolation of 3 Distinct Cardiac Stem Cell Populations from a Single Human Heart Biopsy. *Circ Res*. 2017;121(2):113–124.

136. Torella D, Ellison GM, Nadal-Ginard B, Indolfi C. Cardiac stem and progenitor cell biology for regenerative medicine. *Trends in cardiovascular medicine*. 2005;15(6):229–36.

137. Wobus AM, Holzhausen H, Jakel P, Schoneich J. Characterization of a pluripotent stem cell line derived from a mouse embryo. *Experimental cell research*. 1984;152(1):212–219.

138. Kang L, Gao S. Pluripotency of induced pluripotent stem cells. *Journal of animal science and biotechnology*. 2012;3(1):5.

139. Keene CD, Ortiz-Gonzalez XR, Jiang Y, Largaespada DA, Verfaillie CM, Low WC. Neural differentiation and incorporation of bone marrow-derived multipotent adult progenitor cells after single cell transplantation into blastocyst stage mouse embryos. *Cell transplantation*. 2003;12(3):201–13.

140. Clarke DL, Johansson CB, Wilbertz J, Veress B, Nilsson E, Karlström H, Lendahl U, Frisén J. Generalized potential of adult neural stem cells. *Science*. 2000;288(5471):1660–3.

141. Jiang Y, Jahagirdar BN, Reinhardt RL, Schwartz RE, Keene CD, Ortiz-Gonzalez XR, Reyes M, Lenvik T, Lund T, Blackstad M, Du J, Aldrich S, Lisberg A, Low WC, Largaespada DA, et al. Pluripotency of mesenchymal stem cells derived from adult marrow. *Nature*. 2002;418(6893):41–9.

142. Mascetti VL, Pedersen RA. Human-Mouse Chimerism Validates Human Stem Cell Pluripotency. *Cell stem cell*. 2016;18(1):67–72.

143. Cohen MA, Markoulaki S, Jaenisch R. Matched Developmental Timing of Donor Cells with the Host Is Crucial for Chimera Formation. *Stem cell reports*. 2018;10(5):1445–1452.

144. De Los Angeles A, Pho N, Redmond DE. Generating human organs via interspecies chimera formation: Advances and barriers. *Yale Journal of Biology and Medicine*. 2018;91(3):333–342.

145. Tarkowski AK, Witkowska A, Opas J. Development of cytochalasin in B-induced tetraploid and diploid/tetraploid mosaic mouse embryos. *Journal of embryology and experimental morphology*. 1977;41:47–64.

146. MacKay GE, West JD. Fate of tetraploid cells in 4n↔2n chimeric mouse blastocysts. *Mechanisms of Development*. 2005.

147. Kulandavelu S, Karantalis V, Fritsch J, Hatzistergos KE, Loescher VY, McCall F, Wang B, Bagno L, Golpanian S, Wolf A, Grenet J, Williams A, Kupin A, Rosenfeld A, Mohsin S, et al. Pim1 Kinase Overexpression Enhances ckit+ Cardiac Stem Cell Cardiac Repair Following Myocardial Infarction in Swine. *Journal of the American College of Cardiology*. 2016;68(22):2454–2464.

148. Mohsin S, Khan M, Nguyen J, Alkatib M, Siddiqi S, Hariharan N, Wallach K, Monsanto M, Gude N, Dembitsky W, Sussman MA. Rejuvenation of human cardiac progenitor cells with Pim-1 kinase. *Circulation research*. 2013;113(10):1169–79.

149. Cohen MA, Wert KJ, Goldmann J, Markoulaki S, Buganim Y, Fu D, Jaenisch R.

Human neural crest cells contribute to coat pigmentation in interspecies chimeras after in utero injection into mouse embryos. *PNAS*. 2016;113(6):1570–1575.

150. Leong YY, Ng WH, Ellison-Hughes GM, Tan JJ. Cardiac Stem Cells for Myocardial Regeneration: They Are Not Alone. *Frontiers in cardiovascular medicine*. 2017;4:47.

151. Sussman MA. Cardiac nonmyocyte subpopulations: a secular congregation. *Regenerative medicine*. 2019;14(6):489–494.

152. Hariharan N, Quijada P, Mohsin S, Joyo A, Samse K, Monsanto M, De La Torre A, Avitabile D, Ormachea L, McGregor MJ, Tsai EJ, Sussman MA. Nucleostemin rejuvenates cardiac progenitor cells and antagonizes myocardial aging. *JACC*. 2015;65(2):133–147.

153. Yanamandala M, Zhu W, Garry DJ, Kamp TJ, Hare JM, Jun H wook, Yoon Y sup, Bursac N, Prabhu SD, Dorn GW, Bolli R, Kitsis RN, Zhang J. Overcoming the Roadblocks to Cardiac Cell Therapy Using Tissue Engineering. *Journal of the American College of Cardiology*. 2017;70(6):766–775.

154. Karantalis V, Suncion-Loescher VY, Bagno L, Golpanian S, Wolf A, Sanina C, Premer C, Kanelidis AJ, McCall F, Wang B, Balkan W, Rodriguez J, Rosado M, Morales A, Hatzistergos K, et al. Synergistic effects of combined cell therapy for chronic ischemic cardiomyopathy. *Journal of the American College of Cardiology*. 2015.

155. Tokita Y, Tang X-LL, Li Q, Wysoczynski M, Hong KU, Nakamura S, Wu W-JJ, Xie W, Li D, Hunt G, Ou Q, Stowers H, Bolli R. Repeated Administrations of Cardiac Progenitor Cells Are Markedly More Effective Than a Single Administration: A New Paradigm in Cell Therapy. *Circulation research*. 2016;119(5):635–51.

156. Epstein SE, Lipinski MJ, Luger D. Persistent Inflammation, Stem Cell–Induced Systemic Anti-Inflammatory Effects, and Need for Repeated Stem Cell Injections: Critical Concepts Influencing Optimal Stem Cell Strategies for Treating Acute Myocardial Infarction and Heart Failure. *Journal of the American Heart Association*. 2018;7(4):e008524.

157. Kuhn EN, Wu SM. Origin of cardiac progenitor cells in the developing and postnatal heart. *Journal of Cellular Physiology*. 2010;225(2):321–325.

158. Quijada P, Sussman MA. Making it stick: Chasing the optimal stem cells for cardiac regeneration. *Expert Review of Cardiovascular Therapy*. 2014.

159. Wu J, Platero-Luengo A, Sakurai M, Sugawara A, Gil MA, Yamauchi T, Suzuki K, Bogliotti YS, Cuello C, Morales Valencia M, Okumura D, Luo J, Vilariño M, Parrilla I, Soto DA, et al. Interspecies Chimerism with Mammalian Pluripotent Stem Cells. *Cell*. 2017;168(3):473-486.e15.

160. Bressan M, Liu G, Mikawa T. Early mesodermal cues assign avian cardiac pacemaker fate potential in a tertiary heart field. *Science*. 2013;340(6133):744–8.

161. Eisenberg LM, Kubalak SW, Eisenberg CA. Stem cells and the formation of the myocardium in the vertebrate embryo. *The anatomical record. Part A, Discoveries in molecular, cellular, and evolutionary biology*. 2004;276(1):2–12.

162. Do JT, Choi HW, Choi Y, Schöler HR. Pluripotent Hybrid Cells Contribute to Extraembryonic as well as Embryonic Tissues. *Stem Cells and Development*. 2011;20(6):1063–1069.

163. Kruglova AA, Kizilova EA, Zhelezova AI, Gridina MM, Golubitsa AN, Serov OL. Embryonic stem cell/fibroblast hybrid cells with near-tetraploid karyotype provide high yield of chimeras. *Cell and Tissue Research*. 2008;334(3):371–380.

164. Ying QL, Nichols J, Evans EP, Smith AG. Changing potency by spontaneous fusion. *Nature*. 2002;416(6880):545–548.

165. Bertin E, Piccoli M, Franzin C, Spiro G, Donà S, Dedja A, Schiavi F, Taschin E, Bonaldo P, Braghetta P, De Coppi P, Pozzobon M. First steps to define murine amniotic fluid stem cell microenvironment. *Scientific Reports*. 2016;6:1–12.

166. Wang X, Li T, Cui T, Yu D, Liu C, Jiang L, Feng G, Wang L, Fu R, Zhang X, Hao J, Wang Y, Wang L, Zhou Q, Li W, et al. Human embryonic stem cells contribute to embryonic and extraembryonic lineages in mouse embryos upon inhibition of apoptosis. *Cell research*. 2018;28(1):126–129.

167. Li G, Chen J, Zhang X, He G, Tan W, Wu H, Li R, Chen Y, Gu R, Xie J, Xu B. Cardiac repair in a mouse model of acute myocardial infarction with trophoblast stem cells. *Scientific reports*. 2017;7(1):44376.

168. Chimenti I, Smith RR, Li T-S, Gerstenblith G, Messina E, Giacomello A, Marbán E. Relative roles of direct regeneration versus paracrine effects of human cardiosphere-derived cells transplanted into infarcted mice. *Circulation research*. 2010;106(5):971–80.

169. Jackson R, Tilokee EL, Latham N, Mount S, Rafatian G, Strydhorst J, Ye B, Boodhwani M, Chan V, Ruel M, Ruddy TD, Suuronen EJ, Stewart DJ, Davis DR. Paracrine Engineering of Human Cardiac Stem Cells With Insulin-Like Growth Factor 1 Enhances Myocardial Repair. *Journal of the American Heart Association*. 2015;4(9):e002104.

170. Tufan H, Zhang XHX-H, Haghshenas N, Sussman MAA, Cleemann L, Morad M. Cardiac progenitor cells engineered with Pim-1 (CPCeP) develop cardiac phenotypic electrophysiological properties as they are co-cultured with neonatal myocytes. *Journal of molecular and cellular cardiology*. 2012;53(5):695–706.

171. van Berlo JH, Kanisicak O, Maillet M, Vagnozzi RJ, Karch J, Lin S-CJ, Middleton RC, Marbán E, Molkentin JD. c-kit+ cells minimally contribute cardiomyocytes to the heart. *Nature*. 2014;509(7500):337–41.

172. Sultana N, Zhang L, Yan J, Chen J, Cai W, Razzaque S, Jeong D, Sheng W, Bu L, Xu M, Huang G-Y, Hajjar RJ, Zhou B, Moon A, Cai C-L. Resident c-kit(+) cells in the heart are not cardiac stem cells. *Nature communications*. 2015;6:8701.

173. Lam NT, Sadek HA. Neonatal Heart Regeneration. *Circulation*. 2018;138(4):412–423.

174. Franz M, Jung C, Lauten A, Figulla HR, Berndt A. Tenascin-C in cardiovascular remodeling: potential impact for diagnosis, prognosis estimation and targeted therapy. *Cell adhesion & migration*. 2015;9(1–2):90–5.

175. Song L, Wang L, Li F, Yukht A, Qin M, Ruther H, Yang M, Chaux A, Shah PK, Sharifi BG. Bone Marrow-Derived Tenascin-C Attenuates Cardiac Hypertrophy by Controlling Inflammation. *Journal of the American College of Cardiology*. 2017;70(13):1601–1615.

176. Grumet M, Milev P, Sakurai T, Karthikeyan L, Bourdon M, Margolis RK, Margolis RU. Interactions with tenascin and differential effects on cell adhesion of neurocan and phosphacan, two major chondroitin sulfate proteoglycans of nervous tissue. *The Journal of biological chemistry*. 1994;269(16):12142–6.

177. Tian S, X. Ma P, Wang Z, Liu Q, Gnatovskiy L. Heart Regeneration with Embryonic Cardiac Progenitor Cells and Cardiac Tissue Engineering. *Journal of Stem Cell and Transplantation Biology*. 2015;01(01):1–12.

178. Ruggiero A, Thorek DLJ, Guenoun J, Krestin GP, Bernsen MR. Cell tracking in cardiac repair: what to image and how to image. *European radiology*. 2012;22(1):189–204.

179. Rupp S, Jux C. Advances in heart failure therapy in pediatric patients with dilated cardiomyopathy. *Heart Failure Reviews*. 2018;23(4):555–562.

180. Rupp S, Bauer J, Tonn T, Schächinger V, Dimmeler S, Zeiher AM, Schranz D. Intracoronary administration of autologous bone marrow-derived progenitor cells in a critically ill two-yr-old child with dilated cardiomyopathy. *Pediatric Transplantation*. 2009;13(5):620–623.

181. Selem SM, Kaushal S, Hare JM. Stem cell therapy for pediatric dilated cardiomyopathy. *Current Cardiology Reports*. 2013.

182. Zeinaloo AA, Zanjani KS, Khosroshahi AG. Further follow up of the cardiomyopathic patient treated by intracoronary administration of autologous mesenchymal stem

cells. *Pediatric Transplantation*. 2011.

183. de Almeida PE, van Rappard JRM, Wu JC. In vivo bioluminescence for tracking cell fate and function. *American Journal of Physiology-Heart and Circulatory Physiology*. 2011;301(3):H663–H671.

184. Zhang S, Zhao L, Shen L, Xu D, Huang B, Wang Q, Lin J, Zou Y, Ge J. Comparison of various niches for endothelial progenitor cell therapy on ischemic myocardial repair: Coexistence of host collateralization and Akt-mediated angiogenesis produces a superior microenvironment. *Arteriosclerosis, Thrombosis, and Vascular Biology*. 2012.

185. Singh MK, Epstein JA. Epicardium-derived cardiac mesenchymal stem cells expanding the outer limit of heart repair. *Circulation Research*. 2012.

186. Fadini GP, Losordo D, Dimmeler S. Critical reevaluation of endothelial progenitor cell phenotypes for therapeutic and diagnostic use. *Circ Res*. 2012;110(4):624–637.

187. Schuh A, Kroh A, Konschalla S, Liehn EA, Sobota RM, Biessen E Al, Bot I, Tolga Taha S, Schober A, Marx N, Weber C, Sasse A. Myocardial regeneration by transplantation of modified endothelial progenitor cells expressing SDF-1 in a rat model. *Journal of Cellular and Molecular Medicine*. 2012.

188. Solheim S, Seljeflot I, Lunde K, Bratseth V, Aakhus S, Forfang K, Arnesen H. The influence of intracoronary injection of bone marrow cells on prothrombotic markers in patients with acute myocardial infarction. *Thrombosis Research*. 2012.

189. Katare R, Riu F, Mitchell K, Gubernator M, Campagnolo P, Cui Y, Fortunato O, Avolio E, Cesselli D, Beltrami AP, Angelini G, Emanueli C, Madeddu P. Transplantation of human pericyte progenitor cells improves the repair of infarcted heart through activation of an angiogenic program involving micro-RNA-132. *Circ Res*. 2011;109(8):894–906.

190. Fischer KM, Cottage CT, Wu W, Din S, Gude NA, Avitabile D, Quijada P, Collins BL, Fransioli J, Sussman MA. Enhancement of myocardial regeneration through genetic engineering of cardiac progenitor cells expressing pim-1 kinase. *Circulation*. 2009;120(21):2077–2087.

191. Nadal-Ginard B, Ellison GM, Torella D. Absence of Evidence Is Not Evidence of Absence. *Circulation Research*. 2014;115(4):415–418.

192. Vicinanza C, Aquila I, Cianflone E, Scalise M, Marino F, Mancuso T, Fumagalli F, Giovannone ED, Cristiano F, Iaccino E, Marotta P, Torella A, Latini R, Agosti V, Veltri P, et al. Kitcre knock-in mice fail to fate-map cardiac stem cells. *Nature*. 2018;555(7697):E1–E5.

193. Liu Q, Yang R, Huang X, Zhang H, He L, Zhang L, Tian X, Nie Y, Hu S, Yan Y, Zhang L, Qiao Z, Wang QD, Lui KO, Zhou B. Genetic lineage tracing identifies in situ Kit-expressing cardiomyocytes. *Cell Research*. 2016;26(1):119–130.

194. Zhang L, Tian X, Li Y, He L, Zhang H, Huang X, Liu Q, Pu W, Zhang L, Li Y, Zhao H, Wang Z, Zhu J, Nie Y, Hu S, et al. Identification of a hybrid myocardial zone in the mammalian heart after birth. *Nature Communications*. 2017;8(1).

195. Gulick J, Subramaniam A, Neumann J, Robbins J. Isolation and characterization of the mouse cardiac myosin heavy chain genes. *Journal of Biological Chemistry*. 1991;266(14):9180–9185.

196. Krenz M, Sanbe A, Bouyer-Dalloz F, Gulick J, Klevitsky R, Hewett TE, Osinska HE, Lorenz JN, Brosseau C, Federico A, Alpert NR, Warshaw DM, Perryman MB, Helmke SM, Robbins J. Analysis of myosin heavy chain functionality in the heart. *Journal of Biological Chemistry*. 2003;278(19):17466–17474.

197. Miano JM, Cserjesi P, Ligon KL, Periasamy M, Olson EN. Smooth muscle myosin heavy chain exclusively marks the smooth muscle lineage during mouse embryogenesis. *Circulation Research*. 1994;75(5):803–812.

198. Miano JM, Olson EN. Erratum: Expression of the smooth muscle cell calponin gene marks the early cardiac and smooth muscle cell lineages during mouse embryogenesis (Journal of Biological Chemistry (1996) 271 (7095-7103)). *Journal of Biological Chemistry*. 1997;272(43):27492.

199. Sato TN, Qin Y, Kozak CA, Audus KL. Tie-1 and tie-2 define another class of putative receptor tyrosine kinase genes expressed in early embryonic vascular system. *PNAS*. 1993;90(20):9355–9358.

200. Suri C, Jones PF, Patan S, Bartunkova S, Maisonpierre PC, Davis S, Sato TN, Yancopoulos GD. Requisite role of angiopoietin-1, a ligand for the TIE2 receptor, during embryonic angiogenesis. *Cell*. 1996;87(7):1171–1180.

201. Maisonpierre PC, Suri C, Jones PF, Bartunkova S, Wiegand SJ, Radziejewski C, Compton D, McClain J, Aldrich TH, Papadopoulos N, Daly TJ, Davis S, Sato TN, Yancopoulos GD. Angiopoietin-2, a Natural Antagonist for Tie2 That Disrupts in vivo Angiogenesis. *Science*. 1997;277(5322):55–60.

202. Drake CJ, Fleming PA. Vasculogenesis in the day 6.5 to 9.5 mouse embryo. *Blood*. 2000;95(5):1671–1679.

203. Ehler E, Moore-Morris T, Lange S. Isolation and Culture of Neonatal Mouse Cardiomyocytes. *JoVE*. 2013;(79).

204. Ray JL, Leach R, Herbert JM, Benson M. Isolation of vascular smooth muscle cells

from a single murine aorta. *Methods in cell science : an official journal of the Society for In Vitro Biology*. 2001;23(4):185–8.

205. Subramaniam A, Jones WK, Gulick J, Wert S, Neumann J, Robbins J. Tissue-specific regulation of the alpha-myosin heavy chain gene promoter in transgenic mice. *The Journal of biological chemistry*. 1991;266(36):24613–20.

206. Karagiannis P, Babu GJ, Periasamy M, Brozovich F V. The smooth muscle myosin seven amino acid heavy chain insert's kinetic role in the crossbridge cycle for mouse bladder. *Journal of Physiology*. 2003;547(2):463–473.

207. Taegtmeyer H, Sen S, Vela D. Return to the fetal gene program: A suggested metabolic link to gene expression in the heart. In: *Annals of the New York Academy of Sciences*.; 2010.

208. He L, Li Y, Li Y, Pu W, Huang X, Tian X, Wang Y, Zhang H, Liu Q, Zhang L, Zhao H, Tang J, Ji H, Cai D, Han Z, et al. Enhancing the precision of genetic lineage tracing using dual recombinases. *Nature Medicine*. 2017;23(12):1488–1498.

209. Krenz M, Sadayappan S, Osinska HE, Henry JA, Beck S, Warshaw DM, Robbins J. Distribution and structure-function relationship of myosin heavy chain isoforms in the adult mouse heart. *Journal of Biological Chemistry*. 2007;282(33):24057–24064.

210. Wang WE, Li L, Xia X, Fu W, Liao Q, Lan C, Yang D, Chen H, Yue R, Zeng C, Zhou L, Zhou B, Duan DD, Chen X, Houser SR, et al. Dedifferentiation, proliferation, and redifferentiation of adult mammalian cardiomyocytes after ischemic injury. *Circulation*. 2017;136(9):834–848.

211. Kokkinopoulos I, Ishida H, Saba R, Coppen S, Suzuki K, Yashiro K. Cardiomyocyte differentiation from mouse embryonic stem cells using a simple and defined protocol. *Developmental Dynamics*. 2016.

212. Sharma A, Wu JC, Wu SM. Induced pluripotent stem cell-derived cardiomyocytes for cardiovascular disease modeling and drug screening. *Stem Cell Research and Therapy*. 2013;4(6).

213. Sharma A, McKeithan WL, Serrano R, Kitani T, Burridge PW, del Álamo JC, Mercola M, Wu JC. Use of human induced pluripotent stem cell–derived cardiomyocytes to assess drug cardiotoxicity. *Nature Protocols*. 2018;13(12):3018–3041.